PREPARATION OF PALLADIUM-BASED ELECTROCATALYSTS FOR DIRECT ETHANOL
FUEL CELLS

Mr. Thantakorn Nitaya

A Dissertation Submitted in Partial Fulfillment of the Requirements

for the Degree of Doctor of Philosophy in Chemical Technology

Department of Chemical Technology

Faculty of Science

Chulalongkorn University

Academic Year 2018

การเตรียมตัวเร่งปฏิกิริยาเชิงไฟฟ้าฐานแพลเลเดียมสำหรับเซลล์เชื้อเพลิงชนิดเอทานอลโดยตรง

นายธันฐกรณ์ นิตยะ

วิทยานิพนธ์นี้เป็นส่วนหนึ่งของการศึกษาตามหลักสูตรปริญญาวิทยาศาสตรดุษฎีบัณฑิต
สาขาวิชาเคมีเทคนิค ภาควิชาเคมีเทคนิค
คณะวิทยาศาสตร์ จุฬาลงกรณ์มหาวิทยาลัย
ปีการศึกษา 2561

Thesis Title	PREPARATION OF PALLADIUM-BASED ELECTROCATALYSTS FOR DIRECT ETHANOL FUEL CELLS
By	Mr. Thantakorn Nitaya
Field of Study	Chemical Technology
Thesis Advisor	Associate Professor KEJVALEE PRUKSATHORN, Dr. de L'INPT
Thesis Co Advisor	Assistant Professor Kunakorn Poochinda, Ph.D.
	Professor San Ping Jiang, Ph.D.

Accepted by the Faculty of Science, Chulalongkorn University in Partial Fulfillment of the Requirement for the Doctor of Philosophy

--- Dean of the Faculty of Science

(Professor Polkit Sangvanich, Ph.D.)

DISSERTATION COMMITTEE

--- Chairman

(Associate Professor Prasert Reubroycharoen, Ph.D.)

--- Thesis Advisor

(Associate Professor KEJVALEE PRUKSATHORN, Dr. de L'INPT)

--- Thesis Co-Advisor

(Assistant Professor Kunakorn Poochinda, Ph.D.)

--- Thesis Co-Advisor

(Professor San Ping Jiang, Ph.D.)

--- Examiner

(Professor Mali Hunsom, Ph.D., Dr. de L'INPT)

--- Examiner

(Associate Professor Nisit Tantavichet, Ph.D.)

--- External Examiner

(Assistant Professor Bussarin Ksapabutr, Ph.D.)

ธันฐกรณ์ นิตยะ : การเตรียมตัวเร่งปฏิกิริยาเชิงไฟฟ้าฐานแพลเลเดียมสำหรับเซลล์เชื้อเพลิง
ชนิดเอทานอลโดยตรง. (PREPARATION OF PALLADIUM-BASED
ELECTROCATALYSTS FOR DIRECT ETHANOL FUEL CELLS) อ.ที่ปรึกษาหลัก : รศ.
ดร.เก็จวลี พฤกษาทร, อ.ที่ปรึกษาร่วม : ผศ. ดร.คุณากร ภู่จินดา,ศ. ดร.ซาน ปิง เจียง

งานวิจัยนี้ศึกษาผลการเตรียมตัวเร่งปฏิกิริยาฐานแพลเลเดียมสำหรับเซลล์เชื้อเพลิงชนิดเอ
ทานอลโดยตรง ตัวแปรที่ศึกษา ได้แก่ ชนิดของโลหะตัวที่สอง (ทอง รูทีเนียม และทังสเตน) ชนิดของ
ตัวรองรับ (คาร์บอนวัลแคน และ ท่อนาโนคาร์บอน) และวิธีในการปรังปรุงพื้นผิวของตัวรองรับ และ
ศึกษากลไกการเกิดปฏิกิริยาออกซิเดชันของเอทานอลด้วยเทคนิคเคมีไฟฟ้า ในส่วนแรกพบว่า การใช้
โลหะผสมแพลเลเดียมและทังสเตนส่งผลอย่างมีนัยสำคัญในการเพิ่มกัมมันตภาพและเสถียรภาพของ
ตัวเร่งปฏิกิริยาสำหรับปฏิกิริยาออกซิเดชันของเอทานอลและเมทานอล อย่างไรก็ตามสำหรับกลีเซ
อรอลตัวเร่งปฏิกิริยาที่ให้สมรรถนะที่ดีคือโลหะผสมแพลเลเดียมและทอง ในขณะที่การปรับปรุงพื้นผิว
ของตัวรองรับท่อนาโนคาร์บอน พบว่าการปรับปรุงด้วยวิธีออกซิเดชันด้วยกรดให้สมรรถนะของตัวเร่ง
ปฏิกิริยาสำหรับเชื้อเพลิงเอทานอลต่ำกว่าการปรับปรุงด้วยพอลิเอทีลีนอิมีน อย่างไรก็ตามกัมมันต
ภาพและเสถียรภาพของตัวเร่งปฏิกิริยาดีขึ้นเมื่อใช้ตัวรองรับที่เตรียมด้วยวิธีการจัดวางโมเลกุลอย่าง
เป็นระเบียบได้ด้วยตนเองกับเฮเทอโรพอลิแอซิด ตัวเร่งปฏิกิริยาแพลเลเดียมที่ร้อยละ30 เป็นปริมาณที่
เหมาะสมสำหรับปฏิกิริยาเอทานอลออกซิเดชัน ในการศึกษาตัวรองรับที่ใช้อะตอมเดี่ยวของโลหะ
นิกเกิลบนตัวรองรับท่อนาโนคาร์บอน พบว่าตัวรองรับนี้สามารถเพิ่มสมรรถนะการเกิดปฏิกิริยา
แอลกอฮอล์ออกซิเดชันของตัวเร่งปฏิกิริยาแพลเลเดียมได้ดี การศึกษากลไกการเกิดปฏิกิริยา
ออกซิเดชันของเอทานอลพบว่าอะซิเตทไอออนเป็นผลิตภัณฑ์สุดท้าย ในขณะที่อะซีทาลดีไฮด์ยังเป็น
ผลิตภัณฑ์ระหว่างทางที่ยังมีความว่องไวอยู่ จึงอาจสรุปได้ว่าตัวเร่งปฏิกิริยาแพลเลเดียมจะไม่ไปตัด
โครงสร้างคาร์บอนของเอทานอล

สาขาวิชา	เคมีเทคนิค	ลายมือชื่อนิสิต ....
ปีการศึกษา	2561	ลายมือชื่อ อ.ที่ปรึกษาหลัก ....
		ลายมือชื่อ อ.ที่ปรึกษาร่วม ....
		ลายมือชื่อ อ.ที่ปรึกษาร่วม ....

5672905823 : MAJOR CHEMICAL TECHNOLOGY

KEYWORD: DIRECT ETHANOL FUEL CELL / PALLADIUM / ACTIVITY AND STABILITY /
ANODE CATALYST

Thantakorn Nitaya : PREPARATION OF PALLADIUM-BASED ELECTROCATALYSTS FOR DIRECT ETHANOL FUEL CELLS. Advisor: Assoc. Prof. KEJVALEE PRUKSATHORN, Dr. de L'INPT Co-advisor: Asst. Prof. Kunakorn Poochinda, Ph.D.,Prof. San Ping Jiang, Ph.D.

This research was to investigate the effect of palladium-based catalyst and supporting materials for direct ethanol fuel cell in alkaline media. The studied variables were the secondary metal (gold, ruthenium, and tungsten), types of support (carbon Vulcan, carbon nanotubes). Regarding the secondary metal incorporation, $Pd_{99}W_1/C$ resulted in a significant enhancement in activity and stability for ethanol and methanol electrooxidation. In contrast with glycerol oxidation, $Pd_{99}Au_1/C$ exhibited a better activity and stability than other catalysts. With the surface functionalization of carbon nanotube support, it was clear that the acid oxidation of carbon nanotube gave a poor palladium catalytic performance for ethanol oxidation compared with functionalized polyethyleneimine (PEI-CNT). Moreover, the activity and stability of the catalysts were improved by self-assembly PEI-CNT with phosphotungstic acid. For self-assembled PEI-CNT, 30% Pd was the most suitable loading of ethanol oxidation. Furthermore, the utilization of the nickel single atom catalyst as a new type of supporting material was performed. The results demonstrated that the use of this support can enhance the catalytic performance of palladium for alcohol oxidation. Finally, the study of the ethanol oxidation mechanism revealed that the acetate ion was the final product and acetaldehyde was still the active intermediate. It can be concluded that the catalytic activity of palladium did not cause the carbon session in ethanol structure.

Field of Study:	Chemical Technology	Student's Signature	
Academic Year:	2018	Advisor's Signature	
		Co-advisor's Signature	
		Co-advisor's Signature	

ACKNOWLEDGEMENTS

After an intensive of five years, today is the day: writing this note of many thanks is the finishing touch on my dissertation. It has been a period of intense learning for me, not only in the academic area, but also on a personal life. Doing this dissertation has had a massive impact on me. I would like to reflect on the people who have supported and helped me so much throughout this period

I would like to express my million thanks to my cherished mother for her love, endless support, wise counsel and the sympathetic ear. Hope she sees me from somewhere.

I would also like to express my deepest gratitude and sincere appreciation to my supervisors, Assoc. Prof. Dr. Kejvalee Pruksathorn, Asst. Prof. Dr. Kunakorn Poochinda, Prof. Dr. San Ping Jiang, Prof. Dr. Mali Hunsom, Dr. Yi Cheng and Prof. Dr. Shanfu Lu for encouraging guidance, provision and support thoughout this research. It is impossible to thank them enough for their time and effort. They always raise me up and respect me more than I respected myself. Without their trust, valuable advice, never-ending patience and seeming inexhaustible knowledge of scientific research, this dissertation would not have been successfully completed.

I would extend my appreciation to Assoc. Prof. Dr. Prasert Reubroycharoen, Assoc. Prof. Dr. Nisit Tantavichet and Asst. Prof. Dr. Bussarin Ksapabutr for serving as the chairman and members of the dissertation committee, and for their comments and suggestions.

Finally, I gratefully acknowledged the financial support from the Graduate School of Chulalongkorn University (Overseas Research Experience Scholarship for Graduate Student), the 90th Anniversary of Chulalongkorn University Scholarship, and the Thailand Research Fund.

Thantakorn Nitaya

TABLE OF CONTENTS

LIST OF TABLE

FIGURE CONTENT

CHAPTER I
INTRODUCTION

1.1 RATIONALES, THEORIES

Direct ethanol fuel cell (DEFC) has attracted much interest as a new energy conversion system since ethanol is an easier handle and has a lower toxicity than methanol. Unfortunately, the main obstacle for DEFC usage in daily life is cost because platinum (Pt) is used as the electrocatalyst. Besides, the ethanol oxidation reaction (EOR) in acid electrolyte, a common component in fuel cells, provides a lower activity and a higher fuel crossover than that in basic electrolyte. In this study, palladium (Pd) alloys are investigated as anode electrocatalysts, in order to replace Pt, in alkaline media. The ethanol electrooxidation activity of in basic solution demonstrated that Pd had a higher performance than Pt. Many researchers tried to enhance the performance of Pd catalyst by alloying with other metals with some success, but the EOR mechanisms of Pd and its alloys on different supports had not been clarified. Consequently, the challenges in direct ethanol fuel cells development are not only to reduce cost of production but also to enhance the catalyst activity for ethanol oxidation. The PdAu/C catalyst provided better stability but had lower activity than Pd/C. Moreover, it was demonstrated that adding of Ru, between 1 and 10% atomic, to form Pd_xRu_{1-x}/C, enhanced EOR activity, compared with Pd/C alone. Furthermore, palladium-nickel (PdNi) on Vulcan XC-72 provided both higher activity and stability for ethanol electrooxidation than Pd. In case of supported PdNi on carbon nanofiber (CNF), it was found that PdNi/CNF showed a higher activity than Pd/C. Recently, carbon nanotube (CNT) has been used as the catalyst support due to their outstanding electrical, thermal and mechanical properties. It was reported that PdSn, with the atomic ratio of 90:10, supported on multiwall carbon nanotubes (MWCNT) provided an enhanced electrocatalytic performance as well. However, the surface of MWCNT is very inert for metal deposition, so a surface functionalization is necessary. The acid treatment, with a mixture between nitric acid (HNO_3) and sulfuric acid (H_2SO_4), is a

typical method to generate anchor sites for metal deposition. Unfortunately, this method generated some surface defects and damaged CNT structure, resulting in some reduced electrical properties. Thus, functionalized CNT with non-covalent; such as polymer, surfactants and polyelectrolyte, will be investigated in this work in order to promote catalyst dispersion and uniformity, as well as to enhance the catalytic activity, without causing any major damage to the supports.

1.2 OBJECTIVES OF DISSERTATION

1. To study the effect of secondary metal for Pd-based catalyst on ethanol electrooxidation in alkaline media and its potential use for direct ethanol fuel cell.

2. To study the effect of functionalized supporting material with non-covalent species for Pd-based catalyst on ethanol electrooxidation in alkaline media.

3. To investigate the ethanol oxidation reaction (EOR) mechanism of Pd-based electrocatalyst in basic electrolyte.

1.3 RESEARCH METHODOLOGY AND EXPERIMENTAL PROCEDURES

1. Review basic principles and related literatures for alkaline electrolyte direct ethanol fuel cell

2. Prepare all of equipment tools and chemicals which required for the experiment.

3. Investigate the effect of studied parameters on ethanol electrooxidation in alkaline media, which composed of

   - type of secondary metal: Au, Ru, and W

   - type of supporting material: Vulcan XC-72 and carbon nanotube

   - type of functionalization method: Acid functionalization and non-covalent functionalization

4. Characterize the physical and chemical properties of electrocatalysts by XRD, EDX, SEM, TEM, XPS.

5. Study the electrooxidation toward alcohol; methanol, ethanol, and glycerol, in alkaline media

6. Investigate the ethanol electrooxidation mechanism in alkaline media by cyclic voltammetry technique.

7. Discuss and summarize the experimental results.

8. Write manuscript and dissertation.

CHAPTER II

THEORY AND LITERATURE REVIEWS

2.1 OVERVIEW OF FUEL CELLS

Fuel cell is an electrochemical device that produces electricity directly using electrochemical reaction between the fuel (hydrogen, methanol, ethanol, etc.) and oxidant (oxygen or air) without combustion process, resulting in the fuel cell's efficiency is higher than a combustion engine. Moreover, the usage of fuel cell for electrical generator is environmentally friendly since the by-product from fuel cell is obtained only water and heat [1-3].

The first fuel cell was introduced by William Grove in 1839, was called "Gaseous Voltaic Battery". This system showed the reaction of oxygen and hydrogen in water electrolysis that provides electricity, as represented in Figure 2.1. According to Grove's experiments, he found that the electricity generated was very small, as a result of the contact area of the electrode and the charge carrier in electrolyte is less. Moreover, the distance between the electrode and the electrolyte makes the large resistance in the flow of electrons. He improved by increasing the surface area of the platinum terminal.
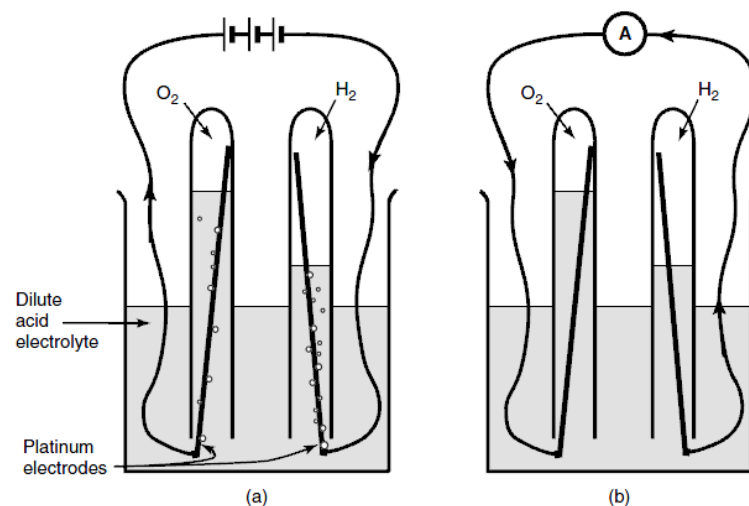
Figure 2.1 The gaseous voltaic battery proposed by William Grove. [1]

Successfully of hydrogen for fuel cells in 1889, Mond and Langer attempted to invent fuel cells using air and coal gas. In addition, William Jacques experimented with the process of producing electricity directly from coal. This device was called carbon battery. Later in 1921, Baur developed a high temperature cell using carbon as an anode while iron oxide was served as a cathode in Molten alkaline carbonate electrolyte fuel cell. This fuel cell operates at temperatures of around 1000 °C. However, there is still a problem with the fuel cell material failure due to the difficulty of the slag removal.

British researchers continually refined the fuel cells in the laboratory. Until 1932. Bacon and his-workers from Cambridge University announced that they could improve and build a new type of fuel cell which used alkaline electrolyte and nickel metal as catalyst. In 1959, he and his team made a patent for a fuel cell with a capacity of 6 kilowatts, which is sufficient to drive the forklift.

Figure 2. 2 A 6-kW fuel cell developed by Francis Bacon in 1959. [2]

Furthermore in the 1960s, the National Aeronautics and Space Administration (NASA) has spent a great deal of money for developing a fuel for the Apollo project under collaborated with United Technologies Corporation (UTC), which uses the fuel cell for produce electricity and drinking water.

Figure 2. 3 Alkaline fuel cell system for Apollo spacecraft developed by United Technologies Corp. (UTC). [2]

In the 1980s and 1990s, Ballard Power System Inc. introduced Nafion; a polymeric material, that was quite cheap and durable as an electrolyte. Meanwhile, the catalyst research was focused on reduces the number of precious metal catalysts, such as platinum, to solve cost problem.

2.2 TYPE OF FUEL CELLS

For the classification of the fuel cell, they can be classified in accordance with the type of fuel, the operating temperature range or the type of electrolytes. Herein, this section is displayed the classification of fuel cells by the type of electrolytes that it is commonly used to classify the fuel cells [2, 4].

2.2.1 ALKALINE FUEL CELL (AFC)

The alkaline fuel cell was the first fuel cell which developed by UTC in the early 1960s. The objective of the development was to serve as a source of electricity in aerospace, especially Apollo spacecraft. At that time, the alkaline fuel cells performed a better performance than another fuel cell since cathode was more active to oxygen

reduction reaction due to the facility of hydroxyl charge carrier (OH⁻). In the case of electrocatalysts, it is also possible to use a variety of metal, either platinum (Pt) or nickel (Ni), from equation (2.1) (2.2) and Figure 2.4. is illustrated each half-cell reaction and working principle of this type of fuel cell.
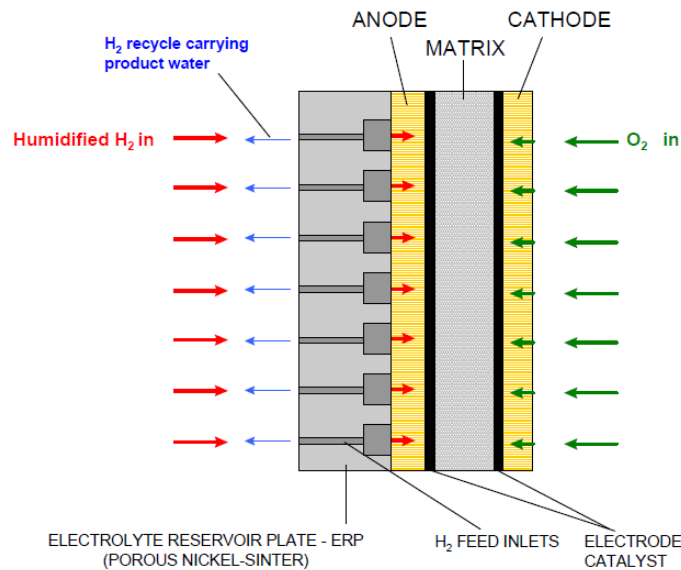
Figure 2. 4 The principle of Alkaline Fuel Cells. [3]

Anode: $$H_{2(g)} + 2OH^- \rightarrow 2\,H_2O_{(l)} + 2e^-$$ (2.1)

Cathode: $$\frac{1}{2}O_{2(g)} + H_2O_{(l)} + 2e^- \rightarrow 2OH^-$$ (2.2)

Overall reaction: $$H_{2(g)} + \frac{1}{2}O_{2(g)} \rightarrow H_2O_{(l)}$$ (2.3)
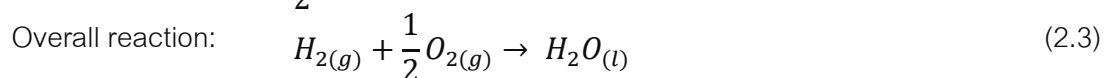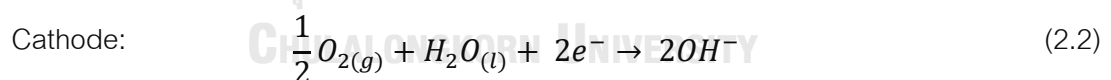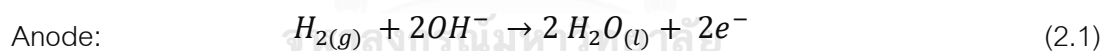
The most commonly used alkali electrolyte is alkaline earth metal hydroxide which potassium hydroxide (KOH) has the highest potential for charge carrier compared with another alkaline group. The amount of potassium hydroxide for using this application in the range of about 30% to 50% and the temperature of the cell is about 120-260 $^{\circ}$C. Unfortunately, this type of fuel cell has very easy for contaminating, such as carbon monoxide (CO), carbon dioxide (CO_2), that reacted with alkaline ions to form carbonated

sludge. Therefore, only pure hydrogen and oxygen are required. Because of this, the cost is very high. It is not popular in the market.

2.2.2 PHOSPHORIC ACID FUEL CELL (PAFC)

PAFC is more tolerance to contaminated gases; e.g. CO, CO_2, than AFC. It still uses the same fuel and oxidation. For electrolyte, phosphoric acid is used as electrolyte. The operating temperature is in the range around 170-200 ^{o}C. PAFC is operated at high temperature, thus it takes a long time to start-up. However, this type of fuel cell is suitable for use in small power stations and is currently commercially available. It has about 200 kW of electricity. The electrochemical reaction and basic operating of PAFC is shown in equations (2.4) to (2.6), respectively.

Anode: $$H_{2(g)} \rightarrow 2\,H^+ + 2e^-$$ (2.4)

Cathode: $$\frac{1}{2}O_{2(g)} + 2\,H^+ + 2e^- \rightarrow H_2O_{(l)}$$ (2.5)

Overall reaction: $$H_{2(g)} + \frac{1}{2}O_{2(g)} \rightarrow H_2O_{(l)}$$ (2.6)
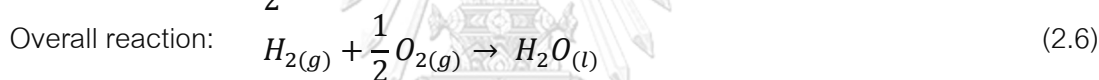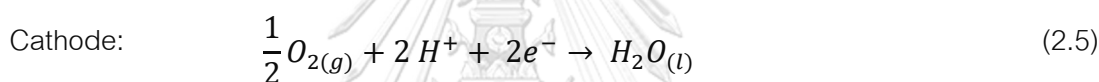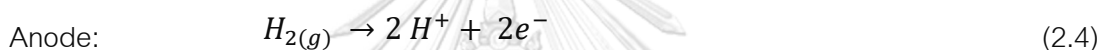
The advantage of PAFC is chemically and thermally stable. Nevertheless, the electrocatalysts both anode and cathode still need precious metal; such as platinum, Thus, the high cost production is considered for commercially.

2.2.3 MOLTEN CARBONATE FUEL CELL (MCFC)

MCFC has a high operating temperature about 650 ^{o}C. It also reduces costs due to this fuel cell can use the non-noble metal as an electrochemical catalyst, both oxidation and reduction. Molten carbonate fuel cells are developed for use natural gas or coal in power plants application. In addition to using at high temperature and high pressure provided a high pressure steam, hence MCFC can be connected to the power system, is called "co-Generation system". For the basic operation are illustrated in equations (2.7-2.9) and Figure 2.5.

Anode: $$H_{2(g)} + CO_3^{2-} \rightarrow CO_{2(g)} + H_2O_{(l)} + 2e^-$$ (2.7)

Cathode: $$\frac{1}{2}O_{2(g)} + CO_{2(g)} + 2e^- \rightarrow CO_3^{2-}$$ (2.8)

Overall reaction: $$H_{2(g)} + \frac{1}{2}O_{2(g)} \rightarrow H_2O_{(l)}$$ (2.9)
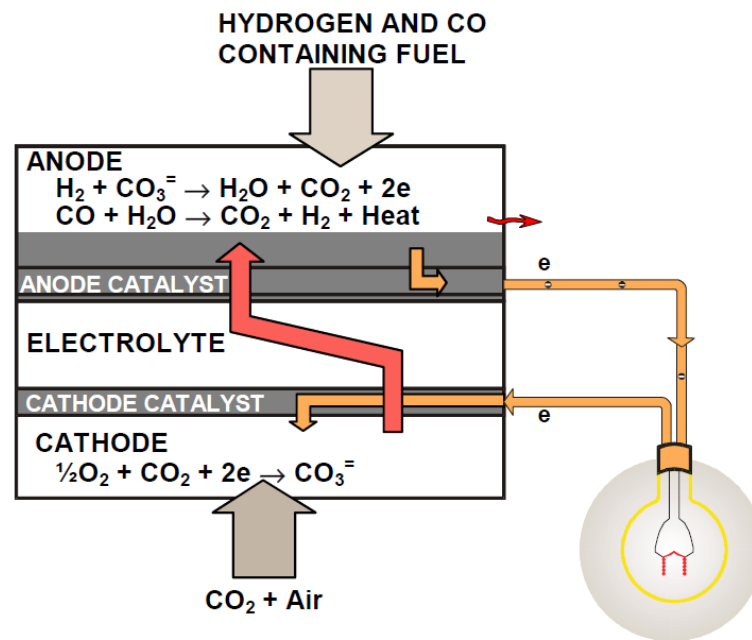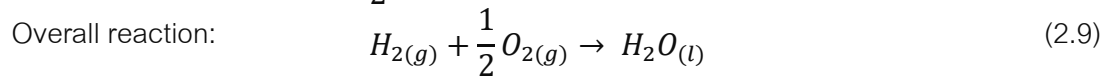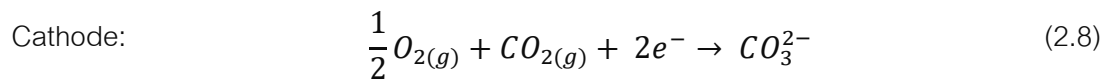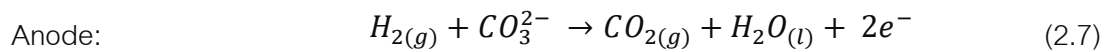
Figure 2. 5 The basic operation of MCFC. [3]

As mention above, MCFC can be operated at high temperature. It is not necessary to use the noble metal as an electrocatalyst. Owning to this type of fuel cell is resistant to carbon monoxide and carbon dioxide, it is also considerate for used as fuel. For this reason, this fuel cell can use coal-based fuels or natural gas. It is also more resistant to contaminants than other types of fuel cells. However, the disadvantage of MCFC is durability cause from working at high temperature operation leading to the corrosion problem.

2.2.4 SOLID OXIDE FUEL CELL (SOFC)

The basic operation of SOFC were illustrated in Figure 2.6 and equations 2.10 to 2.12. The non-porous ceramic compound; for example, Y_2O_3-stabilized ZrO_2, was served

as electrolyte in SOFC. This type of cell operates at high temperature approximately 600-1,000 °C. It is suitable for use as a large power station because it can produce a lot of electricity. Therefore, this generated heat, which caused by side-product, can be used to rotate the steam turbine to produce electricity in the system (co-generator). For using the co-generator system can increase the efficiency of electrical generator. SOFC operate at high temperatures, hence they have not required the use of noble metal catalysts. Moreover, it is also resistant to various impurities; e.g. sulfate compounds, carbon monoxide even carbon dioxide, as same as molten carbonate fuel cells. On the other hand, high temperature operation is also a disadvantage for this type of fuel cell. It takes a long time to start-up or shut-down. Besides, the high operating temperature needs for excellent cover materials to prevent heat loss and protect workers. In the research and development of this type of fuel cell must consider factors of cost reduction and increase the durability is important too.

Anode:
$$H_{2(g)} + O^{2-} \rightarrow H_2O_{(l)} + 2e^-$$
(2.10)

Cathode:
$$\frac{1}{2}O_{2(g)} + 2e^- \rightarrow O^{2-}$$
(2.11)

Overall reaction:
$$H_{2(g)} + \frac{1}{2}O_{2(g)} \rightarrow H_2O_{(l)}$$
(2.12)
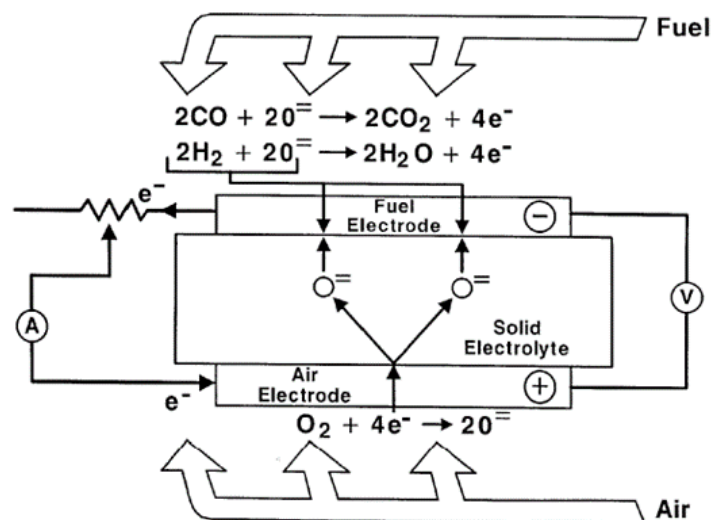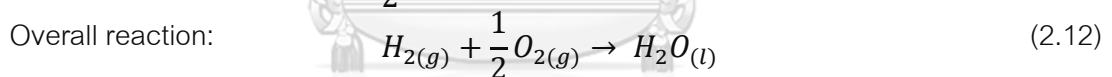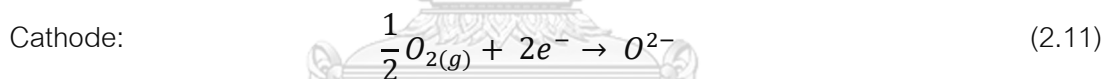
Figure 2. 6 Illustration of operation of SOFC. [3]

2.2.5 POLYMER ELECTROLYTE MEMBRANE FUEL CELL (PEMFC)

PEM fuel is suite for use in mobile or vehicle applications because it is lightweight, take a short time to start up/shut down and the temperature is quite low compared with other fuel cells. The temperature and pressure in the range of about 60 to 100 $^\circ$C and 1-2 atm, respectively. The principle of operation of the PEM fuel cell is shown in Figure 2.7. Hydrogen is fed into the anode side. When the hydrogen gas is exposed to the catalyst layer, it is produced a protons and electrons by hydrogen oxidation reaction (HOR), as shown in equation (2.13). The protons move through the membrane from the anode side to the cathode side. At the same time, the electrons move to the outer circuit. Both the proton and the electron are combined with the oxygen that is fed into the cathode. The water and heat is obtained as a side-product by oxygen reduction reaction (ORR) described in equation (2.14)

Anode: $$H_{2(g)} \rightarrow 2\,H^+ + \,2e^-$$ (2.13)

Cathode: $$\frac{1}{2}O_{2(g)} + 2\,H^+ + \,2e^- \rightarrow H_2O_{(l)}$$ (2.14)

Overall reaction: $$H_{2(g)} + \frac{1}{2}O_{2(g)} \rightarrow H_2O_{(l)}$$ (2.15)
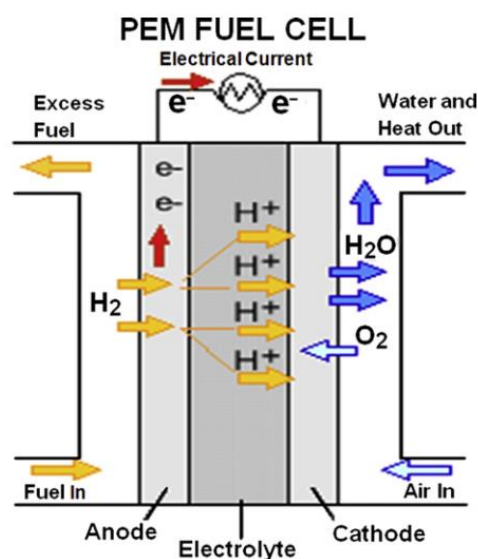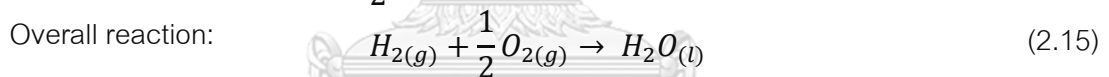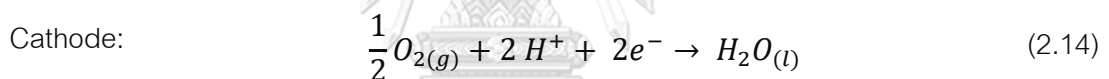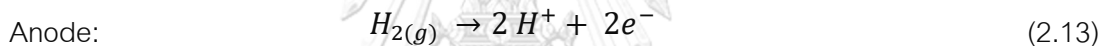
Figure 2.7 Schematic of PEMFC. [5]

As mentioned, PEM fuel cells operate at low temperatures hence the warm-up time is quicker than other fuel cells. The components part is simple and easier to fabricate than other types of fuel cells. Additionally, this type of fuel cell has a long life. Nevertheless, this fuel cell needs a noble metal, which is expensive as a catalyst. In general, platinum metal is used as an electrochemical catalyst. Moreover, the catalyst is seriously sensitive to carbon monoxide (CO) contamination in hydrogen fuel from fuel processor. Generally, hydrogen gas is derived from the reforming process of hydrocarbons such as alcohol or natural gas which may be contaminated by carbon monoxide. One of the challenges of developing this fuel cell is to develop a catalyst that is resistant to carbon monoxide. At present, the catalyst used is the alloy of platinum-ruthenium.

In summary for fuel cell classification, the type of fuel cell is divided by the type of electrolyte. The different types of fuel cells focus on different applications since the operating conditions, temperature, fuel type and different efficiency. Table 2.1 summarizes the different types of fuel cells.

Table 2.1 Type of fuel cells [2]

Type of fuel cell	Electrolyte	Charge carrier	Operating temperature ($^{\circ}$C)	Fuel	Performance (%)	Application
AFC	KOH	OH$^-$	~60-200	High purity H_2	35-55	Aerospace
PAFC	H_3PO_4	H$^+$	~ 220	H_2 High purity H_2	40	Small power plant (200 kW)
SOFC	yttria, zirconia	O^{2-}	~1000	H_2, CO, CO_2 CH_4	> 50	Middle to large power plant
MCFC	Lithium & potassium carbonate	CO$_3^{2-}$	~650	H_2, CO, CO_2 CH_4	> 50	Middle to large power plant
PEMFC	Polymer (e.g. Nafion®)	H$^+$	50-100	High purity H_2, or alcohol	35-45	Vechicles or portables

2.3 ALKALINE FUEL CELL (AFC) AND ALKALINE ELECTROLYTE MEMBRANE FUEL CELL (AEMFCS)

Before discussing the utilization of aqueous alkaline and alkaline electrolyte membrane (AEM) for fuel cell. It should be remark that the acid electrolyte; e.g. sulfuric acid or phosphoric acid, is commonly used in low- or middle-temperature fuel cell. As mention in section 2.2, AFC is required high purity oxygen or air because it is sensitive for CO_2. In contrast with acid electrolyte, they are not only stable in contaminated ambient air but also high charge conductivity. Furthermore with using solid electrolyte, the Nafion® membrane is served as solid electrolyte. Normally, the expected properties of the membrane for fuel cells should be a good proton conductivity and serve as an electrical insulator that is to prevent the electrons from anode travel to the cathode side. When considering the structure of the membrane, it can be seen that the backbone (main chain) is a Polytetrafluoroethylene (PTFE) in the structure provided the membrane to have good mechanical properties and good chemical stability. However, the disadvantage of this type of membrane is expensive and the operating temperature is limited to approximately 150 $^\circ$C [6-8].

The operating system between acid and alkaline electrolyte are compared and displayed in Figure 2.8. In the case of acidic (H^+) condition from Figure 2.8 (a), similar to Grove's experiment, which commonly used phosphoric acid or proton exchange membrane fuel for PAFC and PEMFC, respectively. The acid fuel cell can be explained with hydrogen gas splitting toward protons and electrons. The protons moved through the electrolyte, which saturated humidity water molecules, by electro-osmotic drag, while the electrons travel out through an external circuit. The protons and electrons meet at the cathode where they were oxidized upon reaction with oxygen reduction reaction to obtain water as by-product. For alkaline electrolyte from Figure 2.8 and Figure 2.9, hydrogen and hydroxide ions (OH^-) from the electrolyte react to create water and electrons. The electrons move through the external circuit with the same in acid electrolyte; meanwhile, they react with oxygen and water to generate the OH^- which transported through the electrolyte to the anode. The operating diagram for alkaline fuel cell; where water is produced and used, was interesting both water balance and transport, especially at high currents, that carry over to the AEMFC. In contrast with acid fuel cells, the main obstruct is flooding at the cathode but in alkaline systems the flooding only occurred at anode side.

Furthermore, this system is necessary to force the water from anode move back to cathode for the oxygen reduction reaction.
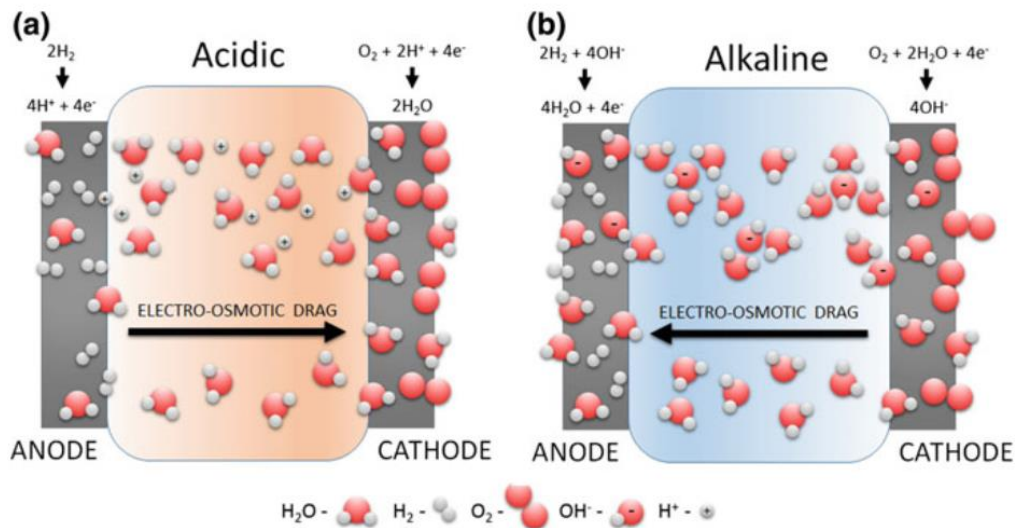
Figure 2.8 The operation of acid (a) and alkaline (b) electrolyte fuel cell. [6]
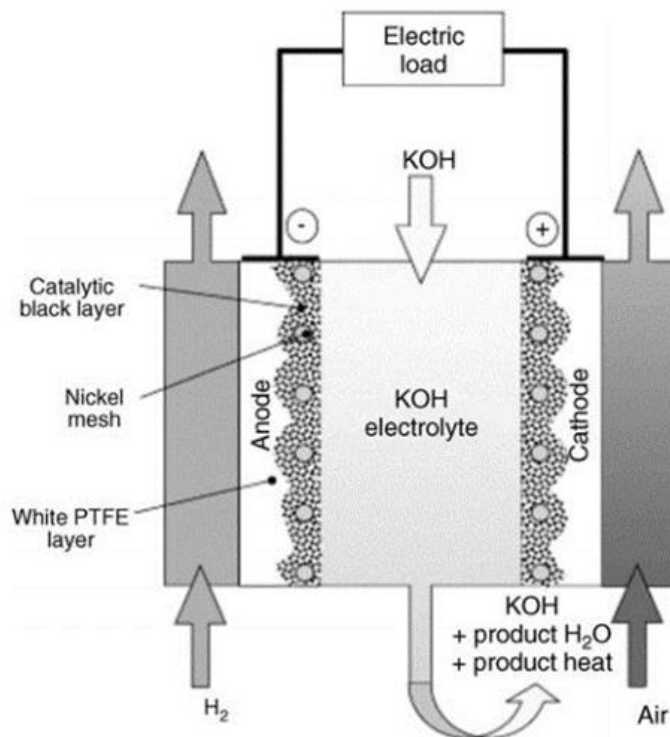
Figure 2.9 Diagram for the aqueous electrolyte for alkaline fuel cell [7]

Another interesting issue between acid and alkaline are relating to the ion carrier (protons and hydroxide anions) and electro-osmosis drag. The acid environment is proton-rich and its move through anode to cathode that led to decrease cell performance cause from fuel crossover. On the other hand from acid fuel cell, the electro-osmosis drag of AFC move from cathode to anode, thus AFC would prevent fuel crossover. As we know that the AFC is sensitive with contaminated species (especially carbon dioxide; CO_2) from ambient air which is necessary to used practically and commercially in fuel cells. CO_2 rapidly reacts with the OH^- in the electrolyte to form bicarbonate and carbonate anions, then carbonate species and potassium cations are interacting to form potassium carbonate (K_2CO_3); which will block the hydroxyl group for charge carrier, as displayed in Equation 2.16 to 2.18.

$$CO_2 + OH^- \leftrightarrow HCO_3^- \tag{2.16}$$

$$HCO_3^- + OH^- \leftrightarrow CO_3^{2-} + H_2O \tag{2.17}$$

$$CO_3^- + K^+ \leftrightarrow K_2CO_{3(s)} \tag{2.18}$$
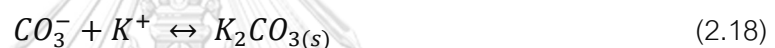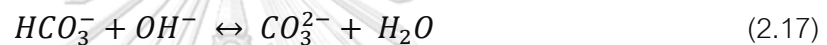
From above reactions, it seems like potassium carbonate solids are the one of important role for reducing performance in AFC. Herein, precipitated potassium carbonate solids are formed on the cathode electrode that leads to dead cell performance by electrode blockage. This effect of carbonation formation should be managed by pre-treatment the ambient air to remove CO_2 before feed to cathode or periodically change the electrolyte, but this method is complicated. The one of way to solve this problem is using the solid electrolyte, especially polymer material, called alkaline electrolyte membrane (AEM), represented in Figure 2.10. Even though the utilization of AEM still obtain the bicarbonate and carbonate ions from the reaction between CO_2 and hydroxide ions, AEM is stationary and these anions can be transferred independently within electrolyte solid membrane. Therefore, this electrolyte cannot blockage with precipitated carbonate species. However, it is not guaranteed that CO_2 will not damage the fuel cell when using AEM. The observation for AEM is a formation of carbonate species cause from speedy reaction between anion and contaminated CO_2. Moreover, the ions exchangeability will decrease; even if, carbonates is not solid form. The tiny CO_2 contamination still is dropped the cell performance by membrane conductivity destruction.
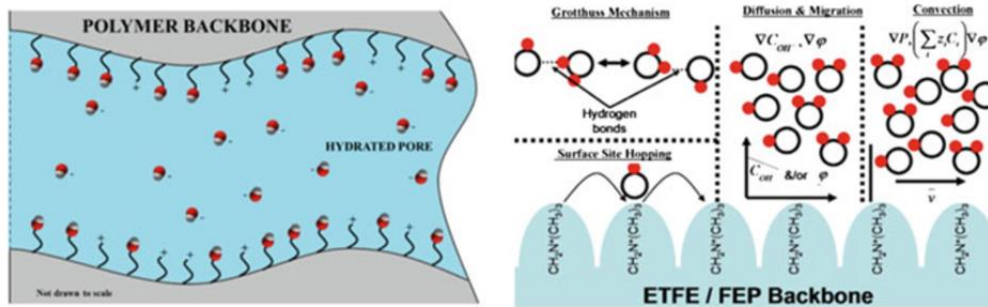
Figure 2.10 Transportation of hydroxide anion in AEM [6]

2.4 DIRECT ETHANOL FUEL CELLS (DEFC)
2.4.1 BACKGROUND OF DIRECT ETHANOL FUEL CELL

Increasing of the portable electronics markets such as mobile phones and tablets, lead to the essential of accessory devices, which are used for storage or generate electrical energy. Batteries are well-known as backup energy storage; however, these devices have many limitations. Especially, they always need time in order to collect power. In addition, most batteries usage in daily life are non-rechargeable, thus the problem of overflowing city garbage is increased. Thus, the polymer electrolyte fuel cells (PEMFCs) is expecting as a generator the electricity for this power-hungry device. Hydrogen is well-known as a fuel in PEMFCs application due to rapid oxidation reaction while water is obtained as a by-product. Thus, the electricity generated by the PEM fuel cell is environmentally friendly. Unfortunately, it has many problematics; such as manufacture process, conveyance, storage, health safety etc., for using gaseous fuel. Moreover, the infrastructure for using energy is familiar with a liquid phase as results of that liquid alcohol should be used as fuel for solving this problem; is called direct liquid fuel cells (DLFCs) [6, 7, 9, 10]. Table 2.2 represent some candidate alcohol for DLFCs application. Among of them, ethanol has potential for transportation application because of low toxic, easy to handle, high energy efficiency. In addition, ethanol can be produced from agricultural product through fermentation process from cellulose-based raw material [11]. It is a sharp contrast with hydrogen. For this reason, ethanol is the outstanding and promising renewable bio-fuel resource when compared with the other alcohols. Recently, DEFC can be categorized into two class that depended on the type of electrolyte; PEM or AEM.

Table 2.2 Thermodynamics data of electrooxidation reaction for some alcohols with standard conditions [7, 11]

Fuel	N_e	E_{oxd}^{o} / V vs. SHE	E_{cell}^{o} / V	W_e / kWhkg^{-1}	Efficiency at 25 ^{o}C (%)	Safety property
Hydrogen	2	0	1.23	32.8 (	83	Flammable
Methanol	6	0.016	1.21	6.1	96.7	High Toxicity
Ethanol	12	0.084	1.15	8.0	96.9	Non-toxic
Glycerol	14	-0.01	1.22	5.0	99.3	Non-toxic

Figure 2.11 and equation 2.19 to 2.21 are illustrated the schematic of direct ethanol fuel cell and half-reaction when operating with PEM electrolyte. Instead of hydrogen, ethanol is fed at the anode side while oxygen or ambient air is supplied at the cathode side. The water, heat and very small amount of CO_2 are obtained as by-product. The electricity is generated from electrooxidation toward ethanol where the transportation of electrons was moving through external circuit from anode to cathode.
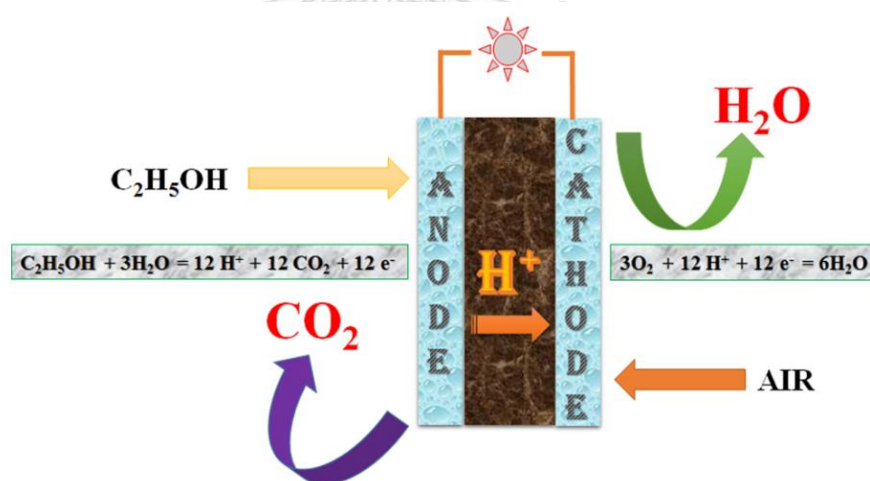
Figure 2. 11 Illustration of direct ethanol fuel cell using PEM as electrolyte. [10]

Anode: $C_2H_5OH + 3H_2O \leftrightarrow 12H^+ + 2CO_2 + 12e^-$ (2.19)

Cathode: $3O_2 + 12H^+ + 12e^- \leftrightarrow 6H_2O$ (2.20)

Overall reaction: $C_2H_5OH + 3O_2 \leftrightarrow 2CO_2 + 3H_2O$ (2.21)
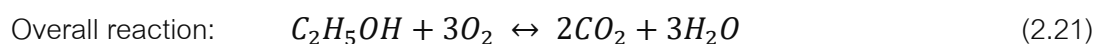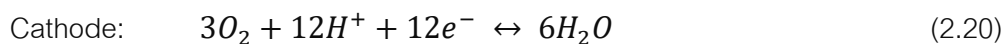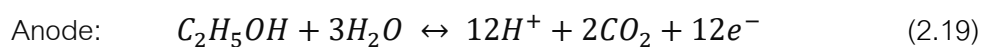
From equation 2.19 to 2.21 assume that the EOR is complete reaction that ethanol molecule is breaking C-C bond to obtain CO_2. For EOR mechanism will be discussed in the anode catalyst for EOR. The challenge for DEFC using PEM is a sluggish both anodic and cathodic reaction for EOR and ORR, respectively. Consequently, many researcher and developer try to develop DEFC utilized with alkaline or AEM.

In the case of alkaline or AEM for DEFC, the operating system is represented in Figure 2.12. From schematic for alkaline or AEM, it seems like the operation similar with acid electrolyte. The ethanol is fed at the anode side and react with hydroxyl ion to obtain CO_2 water and electrons. Electron travel to external circuit from anode to cathode, then they meet together with oxidant (oxygen or air) for oxygen reduction reaction and generate hydroxyl ions. The half-cell reactions for each side are displayed in equation 2.22 to 2.24.
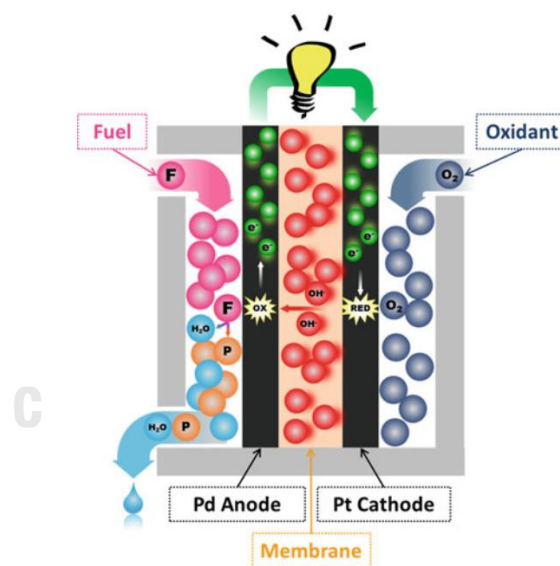
Figure 2.12 schematic of AEM fuel cell using various fuels. [6]

The initial development of direct ethanol fuel cell in alkaline media was investigated more than 10 years ago that was interested in the use of various less noble metal catalyst since this system not only provided higher kinetic activity but also the high-cost production can be illuminated as well. When compared with two categories of DEFCs, the problem

with AFC stability with ambient air was considerate as well as this issue is the main problem of membrane researcher to solve this problem.

2.4.2 ELECTROCATALYSTS FOR ETHANOL ELECTROOXIDATION REACTION IN ACID AND ALKALINE ELECTROLYTE

From the previous topic the author discussed the principle of direct ethanol fuel cell using two different electrolytes. Herein [6, 7, 10, 12-15], this topic is to talk about the basic knowledge for ethanol oxidation in both acid and alkaline media for using metal electrocatalysts. Firstly, the EOR normally depends on the type of electrolyte and type of metal catalysts. The electrochemical oxidation reaction toward ethanol leads to the formation of adsorbed intermediates which obtained from non-complete EOR, and by-products. The intermediates product plays a key role for performance because they were blocked the active site of catalyst lead to performance degradation of the fuel cell. Theoretically, the ethanol should be oxidized into 12 electrons per ethanol molecule followed "dual pathway", as shown in Figure 2.13. It can be observed that carbon monoxide is one of an intermediate product from ethanol oxidation reaction (EOR). As we know that the main barrier to DEFCs usage in daily life is cost since platinum (Pt) is required as the electrocatalyst. Moreover, this metal is extremely sensitive to contaminated carbon monoxide (CO) [16, 17]. Typically, carbon monoxide is one of an intermediate product from ethanol oxidation reaction (EOR). Figure 2.13 show well-known possibly mechanism of ethanol electrooxidation using Pt, which called "dual pathway" . For C_1 pathway, ethanol is completely oxidized to carbon dioxide (CO_2) by adsorbed CO (CO_{ads}) and provided 12 electrons. The acetate species are obtained from partial oxidation of ethanol by C_2 pathway without the cleavage of C-C bond and produced 4 electrons. However, EOR mechanism is still unclear that involved a complicated sequential and parallel reaction routes. The disruptions of acid electrolyte are provided both low activity and high fuel crossover with respect to basic electrolyte. Then Pt which is precious metal is required as electrocatalyst in acid media. Simões et al. [18] explored possible oxidation reactions mechanism of ethanol on PtSn electrocatalyst as shown in Figure 2.14. The electrochemical oxidation of ethanol in acid electrolyte requires Pt, which is primarily involved in two key steps occurring during the oxidation process. Firstly, dissociative adsorptions of ethanol are occurred and obtained acetaldehyde.

Subsequently, re-adsorbed acetaldehyde is reacted with adsorbed OH group to obtain acetic acid. For route 5, dehydrogenation of ethoxy species reacts with OH group to form acetic acid directly. It can be noted that CO is one of intermediate products of this ethanol oxidation mechanism. Furthermore, not only other products and by-products such as acetaldehyde and acetic acid will interrupt electrooxidation reaction but also CO_2 is the main intermediate product. The electrooxidation removal of carbonaceous species and the cleavage of the C–C bond are the two main obstacles and rate-determining steps. Thus, more active electrocatalysts for EOR are necessary to enhance ethanol electrooxidation at lower temperatures. Even though, there is some factor in the oxidation of low-molecular alcohols on Pt (e.g., CO is produced as intermediate), the best catalyst is not the same for all situations. The most common anode catalyst in acidic electrolyte is focused on binary (PtRu and PtSn) and ternary (PtRuSn) alloys. At this point, PtSn is considered as electrocatalyst in acid media. For using PtSn, the proposed mechanism for this catalyst are demonstrated in Figure 2.14. The role of Sn is served as promoter Pt in order to assist removal intermediate products by bifunctional effect and the electronic interaction between Pt and alloyed metals.
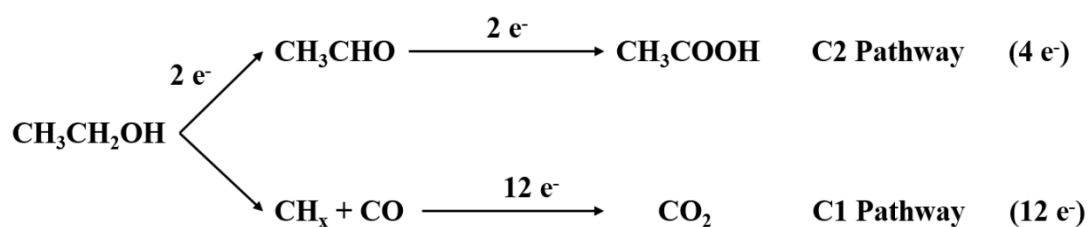
Figure 2.13 Parallel pathways of ethanol oxidation on Pt-based electrocatalyst in either acid or basic electrolyte. [15]
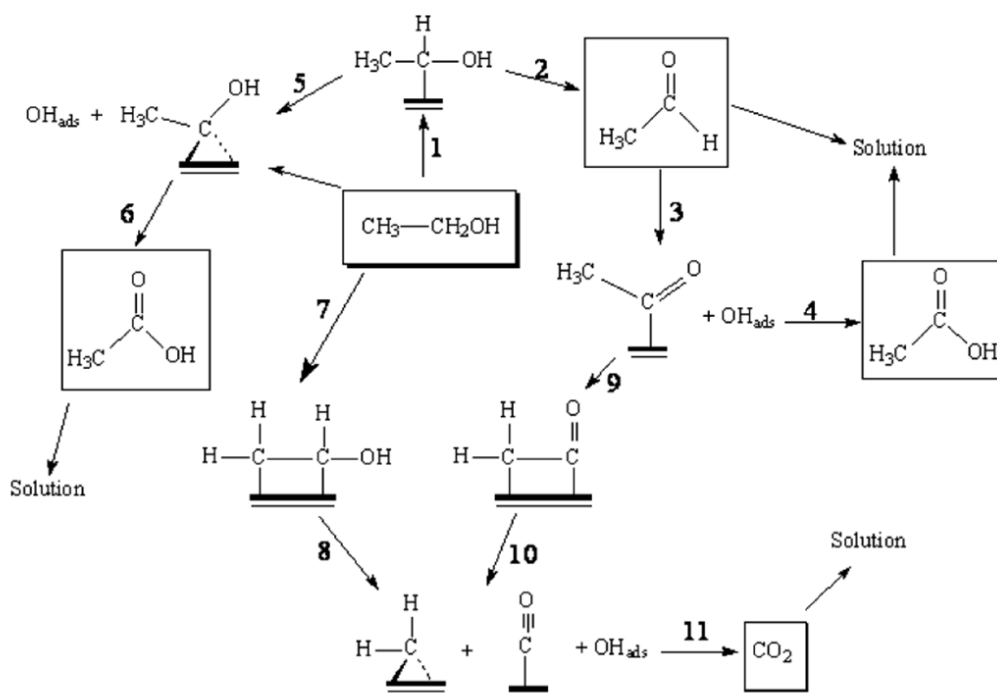
Figure 2.14 Ethanol electroxidation on PtSn catalyst in acid electrolyte. [18]

Although PtSn is the most expected for EOR catalysts, the exact ratio of Sn and Pt is still uncleared. It depends on catalyst preparation method, degree of alloying, and operating fuel cell temperature. The ternary catalyst PtSnRu is proposed to be the best alternative anode catalyst.

Because of the ethanol oxidation reaction (EOR) in acid electrolyte, a common component in fuel cells provides a lower activity and a higher fuel crossover than that in basic electrolyte. Palladium (Pd) is promised as an anode electrocatalyst, in order to replace Pt, in alkaline media. Due to Pd is lower price and higher activity in alkaline media than Pt. The ethanol oxidation on Pd is displayed in Figure 2.15. It seems that ethanol may be dehydrogenated to form acetyl rather than acetaldehyde, and then decomposed to form CO and CH_x by cleavage of the C-C bond. EOR mechanisms of Pd and its alloys on different supports had not been clarified because the complicate ethanol electrooxidation provided many intermediate products. According to Liang et al. work [14], they proposed the ethanol oxidation mechanism for Pd surfaces, followed the equations 2.22 to 2.26. Theoretically of ethanol electrooxidation mechanism, dual-pathway is always well-known for express phenomena on Pd surfaces, which are involved with and without C-C breaking in ethanol molecule. The Pd is absorbed OH⁻ from electrolyte while ethanol chemisorption

is occurred as well, follow reaction 2.22 and 2.23. Absorbed EtOH on Pd reacted with OH⁻ to obtain adsorbed ethoxy species. This species is strongly adsorbed on Pd surfaces. From reaction (2.25) is the slowest step, as well as the reaction (2.26), is very fast. In case of reaction (2.25), ethoxy species is strongly adsorbed on Pd surfaces which are playing an important role for reducing active site of Pd. Accordingly, the criteria of design electrocatalyst in order to improve electrooxidation activity toward ethanol should be promoted oxidation of ethoxy species, both bi-function effect and electronic effect, by adding other metals. Typically, to form adsorbed hydroxide surfaces species for oxidizing carbonaceous species are involve with bi-function effect. Moreover, when modifying of Pd with another material is provided a change of electronic structure resulting in binding adsorbed species weaklier and facility to remove. In this work, Au, Ru and W were selected which based on ability to adsorbed and desorbed OH⁻ species for enhancing oxidized ethoxy species on Pd surfaces.
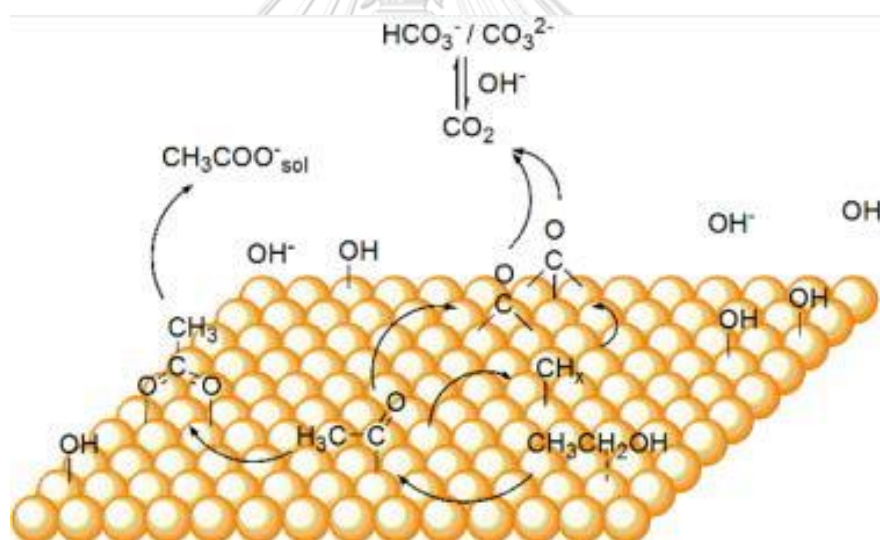
Figure 2.15 Ethanol electrooxidation (EOR) on Pd catalyst in basic electrolyte.[15]

$$Pd + OH^- \leftrightarrow Pd - (OH) + e^- \qquad (2.22)$$

$$Pd + C_2H_5OH \leftrightarrow Pd - C_2H_5OH \qquad (2.23)$$

$$Pd - C_2H_5OH + 3OH^- \rightarrow Pd - (C_2H_3O) + 3H_2O + 3e^- \qquad (2.24)$$

$$Pd - (C_2H_3O) + Pd - (OH) \xrightarrow{r.d.s.} Pd - (CH_3COOH) + Pd \qquad (2.25)$$

$$Pd - (CH_3COOH) + OH^- \rightarrow Pd + CH_3COO^- + H_2O \qquad (2.26)$$
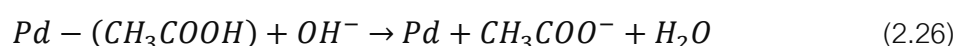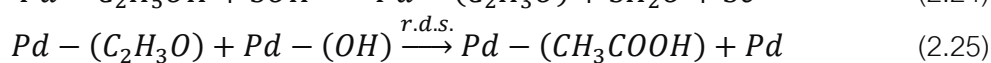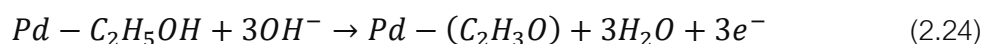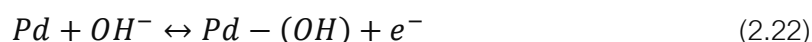
Consequently, many researchers tried to enhance the performance of Pd catalyst by alloying with other metals with some success, but the EOR mechanisms of Pd and its alloys on different supports had not been clarified. Furthermore, the challenges in direct ethanol fuel cells development are not only to reduce cost of production but also to enhance the catalyst activity for ethanol oxidation. Supporting material types and properties of catalyst are important parameter effect on catalyst performance. Thus, functionalized supporting materials will be investigated in this work in order to promote catalyst dispersion and uniformity, as well as to enhance the catalytic activity.

2.5 SUPPORTING MATERIAL FOR FUEL CELL CATALYST

In fuel cells electrocatalyst system, supporting materials is one of the main factors; which is used as metal accommodation to ensuring large electrochemical active surfaces, affect the catalyst performance. The supported catalyst system has been interested in nanostructured development since they can be offered faster electron transfer and high electrocatalytic activity. Generally, these may be classified into two main categories that included of carbon-based supports and non-carbonaceous supports. Herein, the carbon blacks (CBs) is recognized as the most famous material for used as support in fuel cell application due to its have many advantages followed below [7, 19, 20].

- good electrical conductivity and good corrosion resistance

- good metal and support interaction

- huge surface area

- enable the ionomer or electrolyte to take the nanoparticles near to the reactants

- easy to water management to prevent flooding

- less contamination and

- low price of cost production

Not only commercially CBs (represented in Table 2.3) but also the different types of carbon nanostructures are considered. For carbon nanostructures; such as carbon

nanotubes (CNTs), carbon nanofibers (CNFs), mesoporous carbons (MCs), or graphene are promised as new-class for nanostructured supporting material. Recently, there have been many reports about CNTs utilization as support and they provided an impressive catalytic performance. The advantage of CNT is provided a good electrical property and mechanical properties, as represented in Table 2.4. In order to promote the electrocatalytic reaction toward ethanol, the catalyst supported on carbon should be contributed to enhancing EOR performance by high specific surface area, good electric conductivity, appropriate pore size, and resistance with the corrosive condition.

Table 2.3 Physical properties of commercially carbon material [7, 19]

Commercialized carbon	Surface Area (m^2/g)	manufacture
Vulcan XC–72R	250	Cabot Corp
Shawinigan	80	Chevron
Black Pearl 2000 (BP2000)	1500	Cabot Corp
Ketjen Black (KB EC600JD	1270	Ketjen Black

Table 2.4 Some properties of CNTs compared with some metal [19]

Material	Current density (A/cm^2)	Mean free path (nm) at 300 K	Melting temperature (K)	Density (g/cm^3)	Tensile strength (GPa)	Thermal conductivity (x 10^3 W/m-K)	Temperature coefficient of resistance (x 10^{-3} /K)
Tungsten (W)	10^8	33	3695	19.25	1.51	0.173	4.5
Copper (Cu)	10^7	40	1375	8.94	0.22	0.385	4
SWCNT	>10^9	>10^3		1.3-1.4	22.2±2.2	1.75-5.8	<1.1
MWCNT	>10^9	2.5x10^4	3,800	1.75-2.1	11-63	3	-1.37

Carbon nanotube (CNT) was accidentally discovered by Iijima in 1991. The general idea for CNT fabrication is rolled graphene sheets and show both semiconducting

and metallic properties depending on their chirality. For CNT preparation, chemical vapor deposition (CVD), plasma-enhanced chemical vapor deposition (PECVD), laser ablation, arc discharge, etc. can be served for synthesis techniques. The conventional CNTs are made of seamless cylinders of hexagonal carbon networks with forms of single-wall (SWCNTs) or multiwall carbon nanotubes (MWCNTs). The SWCNT is a rolled of graphene sheet into cylindrical form. It can be metallic or semiconducting properties which depended on the chirality structure and can be categorized by three types; composed of armchair, zigzag, and (3) chiral (Figure 2.16).
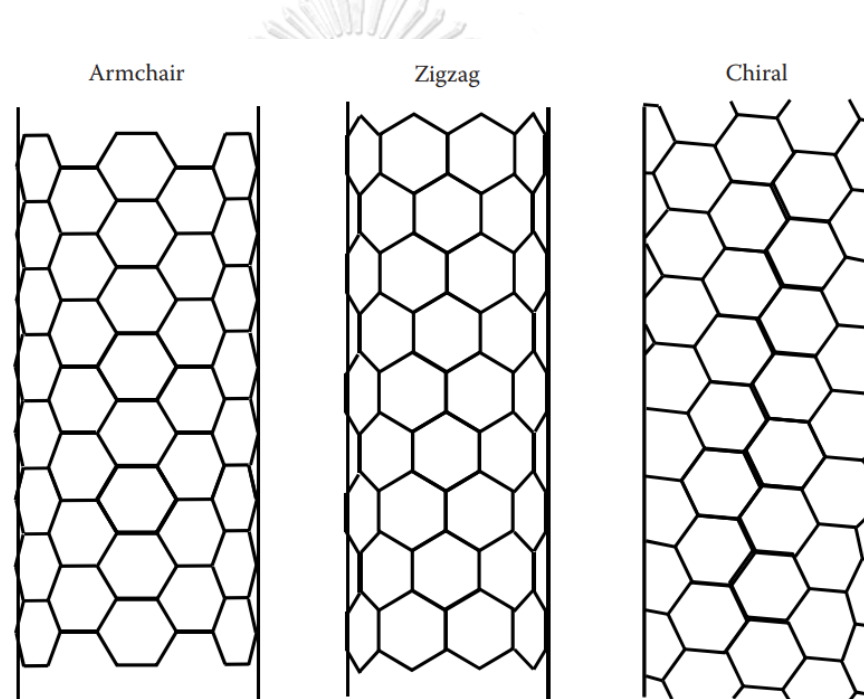
Figure 2.16 Type of SWCNT. [20]

For armchair structure is always metallic, while zigzag and chiral SWCNTs can be semiconducting or metallic form. Due to the metallically SWCNT has a long mean free path (MFP), they are being expected as interconnect materials. The semiconducting type is invested in making electrical devices. The band gap of this type scales approximately with the inverse of the diameter of the tubes.

Furthermore, MWCNT is many concentric shell of rolled graphene sheets. MWCNTs can be classified into two types; double-walled CNT (DWCNT) and MWCNT. Both DWCNT and MWCNT have two and many concentric shells, respectively. MWCNTs are always metallic form notwithstanding that SWCNTs can be either metallic or semiconducting. MWCNTs have similar current-carrying capacity (with the same as metallic SWCNTs) but are easy to synthesis than SWCNTs because the growth process is not complicated to control. Although MWCNTs exhibit high degree of uniformity of internal diameter of single tubes, they provided a broad pore-size distribution in the micropore and mesopore ranges. When considered CNTs as supporting material, the normal dimensions should be as follows: outer diameter 10–50 nm, inside diameter 3–15 nm, and length from 10 to 50 μm. Theoretically, SWCNTs could be either metallic or semiconducting; whereas MWCNTs should have a relatively high electrical conductivity as a result from the conductivity was mainly from the outer shell. Unfortunately, the surfaces of pristine CNTs are chemically inert with a hydrophobic surface, so it is very difficult for metal nanoparticles deposition. Thus, functionalization process for introducing anchoring sites; such as surface oxygen groups (using strong acids like HNO_3, H_2SO_4, etc.) and others (using ionic liquids, aromatic molecules, polymer, etc.), have been performed commonly for make the surface more hydrophilic and improve the catalyst support interaction.

2.6 CATALYST PREPARATION PROCEDURES

This topic covers the synthesis methods of electrocatalysts supported both on CBs and CNT. Several methods; for example, impregnation, colloidal, precipitation, emulsion, and polyol, can be used for the deposition of electrocatalyst nanoparticles on CNTs [7, 9, 12, 21].

2.6.1 IMPREGNATION METHOD

Because the impregnation method is easy to conduct and simple to scale-up, it has been a conventional method for electrocatalyst synthesis. However, the major

hindrance is that it is very difficult to control the particle size of catalyst. Additionally, it is hard to regulate the shape and structure of catalysts this method. In principle of impregnation, the supporting material is dispersed in a suitable solution containing the metal precursor which is generally dissolved in a water. Subsequently, the solution is slowly evaporated. During the evaporation step, the temperature or the pH may be controlled or the adjust simultaneously. The substrate is calcined or reduced with reducing agent; such as $Na_2S_2O_3$, $NaBH_4$, $Na_4S_2O_5$, N_2H_4, or formic acid, then it will get the desired catalyst. Unfortunately, the formation of particle growth is limited inside the pore of carbon material that directly affected to catalyst morphology. Additionally, the type of reducing agent that involved the reduction kinetic and mass transport of reducing agent should be considered. Thus, this method is difficult for controlling morphology.

2.6.2 CO-PRECIPITATION

The co-precipitation is simple that involved with the adding of metal precursors and reducing agent for bimetallic catalyst. Typically, the precursor is reduced by reducing agent to form metallic state and precipitated in solution. The advantage of this method is that the catalyst will have a uniform distribution of agitated areas at the molecular level, but there are some areas of agility embedded within the catalyst's non-reacting catalyst. This method is not suitable for expensive catalysts or metals. In addition, if the catalyst contains two or more active substances, the precautions to be taken are: Each metal salt can have different precipitation rates that will affect the structure of the catalyst. Precipitation control is achieved by selecting suitable salts, adjusting the pH and the temperature of the solution

2.6.3 COLLOID METHOD

The colloid method is used for nanocluster electrocatalyst preparation that is quite similar with precipitation method. This method is basically involved the metal precursor, reducing agent, and capping agent or surfactant. For preparation procedure, supporting

material was added into a mixture of metal source before or after nanoparticle formation. The reducing agent is played a key role for metal nanocluster formation; herein, if the reduction kinetic is fast, this step can be accomplished within a half hour. The advantage of this method is to able control size and distribution of nanoclusters. Meanwhile, the catalyst aggregation is prevented by surfactant. Among of colloid method, the Bönnemann method is a one of colloid method which consisted of chemical reduction of metal ions. In this case, the tetraalkylammonium triethyl borohydride was used as reducing agent by mixing tetra alkyl bromide and triethyl borohydrure in anhydrous tetrahydrofuran. Subsequently, KBr was crystallized and removed. The solution was kept at 0 $^{\circ}$C before the reduction of metal precursor. A colloid of metal source was growth and protected by a tetraalkyl chloride surfactant. Consequently, this method can prevent aggregation of nanoparticles.

a   b
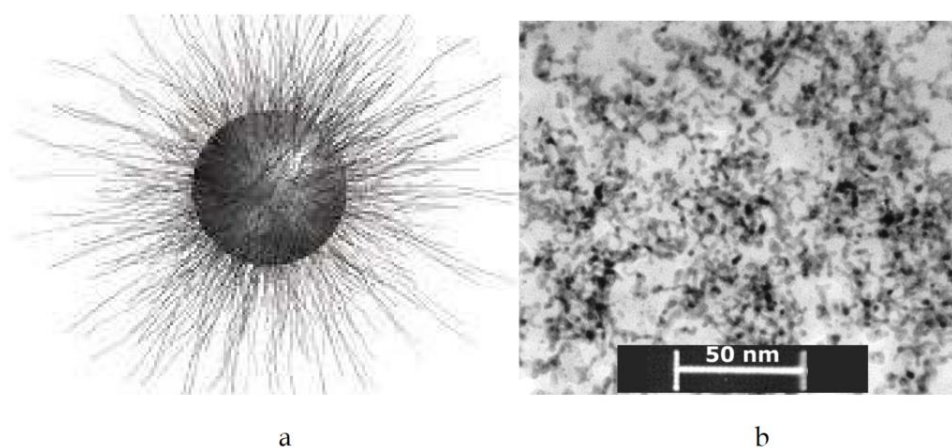
Figure 2.17 Illustration of metal particle protection with tetraalkyl chloride surfactant using Bönnemann method (a) and TEM image of Pt electrocatalyst prepared by Bönnemann (b). [21]

2.6.4 MICROEMULSION METHOD

The microemulsion or "water in oil" method is used for preparing metal alloy, catalyst, and semiconductor. This method involved oil droplets surrounded by surfactants in a continuous water phase at high water concentration or small water droplets

surrounded with surfactants in high oil concentration. Among of metal sources are an inorganic framework that can be soluble in water, so the emulsion with a high concentration of oil and low water concentration is exclusively used for catalyst preparation. The reverse micelle droplets were stabilized with some surfactant; for example, sodium 2 bis (2-ethylhexyl) sulfosuccinate (Na^+-AOT). Figure 2.18 illustrated the utilization of Na^+-AOT for stabilized metal micelle. The droplets are randomly dispersed in solution and exchanged their water content to reform into distinct micelles.
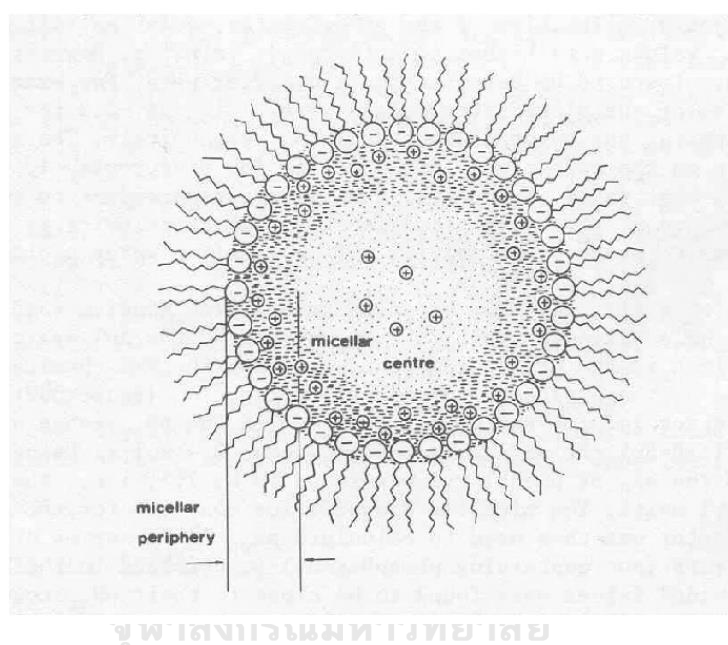
Figure 2.18 Illustration of reverse micelle droplet using Na^+-AOT as surfactant. [9]

The droplet size is most likely affected to particle size of metal due to the water content, as illustrated in Figure 2.19. Herein, if the water content is too high, the particles will larger. Meanwhile, reducing agent is necessary for the reduction step by adding or mixing in the emulsion system. Then, the nanoclusters are deposited on support and accomplished by adding solvent for destabilizing microemulsion. However, the size control for microemulsion process is very complicated since the reduction process is limited within only microemulsion droplets. Thus, it strongly believes that the nanoparticles

size is governed by the size of the water droplets in the microemulsion. In addition, the nature of reducing agent is a one of important factor for size control. The small particle can be obtained from rapidly reduction process.
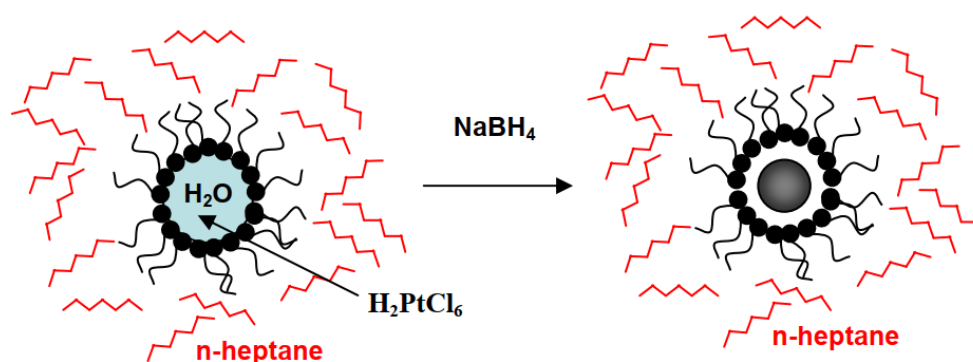
Figure 2.19 The schematic of water-in-oil microemulsion of platinum nanoparticle in hexane as solvent. [21]

2.6.5 POLYOL METHOD

The several polyol compounds, e.g. ethylene glycol, diethylene glycol or glycerol, were used as solvent, stabilizer and reducing agent. The polyol method is composed of metallic source that dispersed in polyol. The metallic salt was firstly dissolved to obtain metal ions in alkaline solution of polyol. The intermediates of metal oxides or hydroxides are generated. Subsequently, the acetaldehyde is produced polyol hydration to allow the metal reduction. The reaction mechanism for ethylene glycol as polyol source was displayed as following equations below

Dehydration step:	$CH_2OH - CH_2OH \rightarrow CH_3 - CHO + H_2O$	(2.27)
Acid-base	$CH_2OH - CH_2OH + 2OH^-$	(2.28)
reaction:	$\rightarrow CH_2O^- - CH_2O + 2H_2O$	
Reduction	$MO_2 + 4CH_3 - CHO$	(2.29)
reaction:	$\rightarrow M + 2CH_3COCOCH_3 + 2H_2O$	
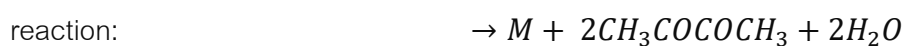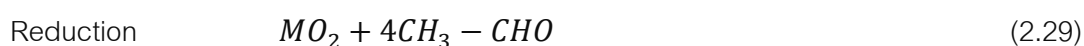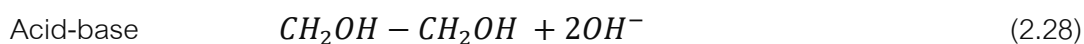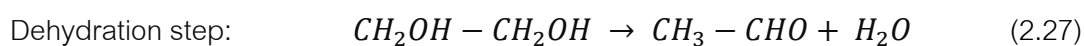
In the case of reduction step, the low particle growth kinetics cause from relative soft condition. The growth of grain was terminated by the adsorption of by-product on metal surfaces and/or from metal ions reduced to metal. The advantage of using polyol method is easy to scale-up because the procedure is simple and low-cost production. However, the soft reducing agent is obtained from polyol, as a result, it is needing to activate the polyol with increasing temperature by reflux or microwave irradiation.

2.7 SINGLE ATOM CATALYST

In fuel cell catalysis, the electrochemical reaction both anode and cathode are usually taken place at catalyst surfaces. Normally, the metal cluster or nanoparticles (NPs) supported on conducting materials was synthesized and served as active phase for electrocatalysis. Unfortunately, many obstacles; such as cost production, limitation of resources led to development for precious metal utilization. Moreover, the NPs is easy to aggregate during metal synthesis or catalytic reaction resulting in reduce the catalytic activity and durability. The heterogeneous single atom catalysts (SACs) was recognized to solve those problems. The utilization from SACs not only can enhance precious metal efficiency but also improve the catalytic activity and/or stability of metal atom. Figure 2.20 is illustrated the relation between specific activity and catalyst loading/size of metal. It obvious that the tiny particles in scale of single atom provided a good activity due to the free energy on active surfaces is enhanced when decreasing the particle size. Besides, using of SACs can prevent catalyst coalescence that not only improving catalytic activity but also creating metal durability. The SACs generally consisted of isolated atoms which dispersed on and/or incorporated with the appropriated surfaces of supporting materials. There is various type of SACs supported on supporting material. Figure 2.21 illustrated the SACs supported on different materials. Among of them, carbon-based material has been recognized as anchoring support for electrocatalysts because of high surfaces area, high electrical conductivity and potential for industrial scale [22].
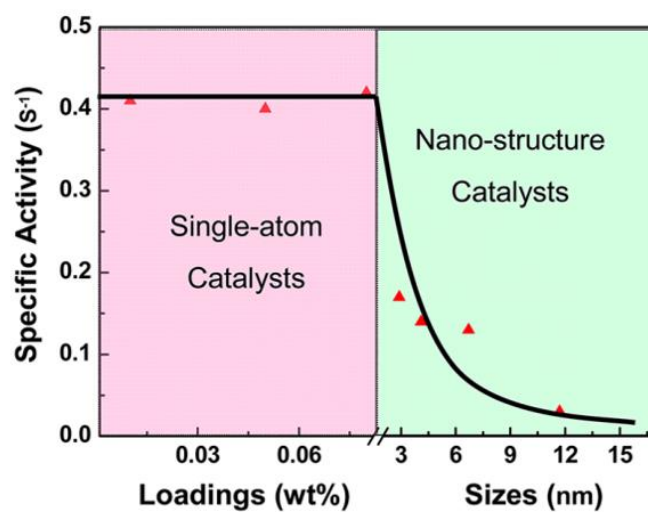
Figure 2.20 Schematic of specific activity with metal loadings or particle sizes. [23]
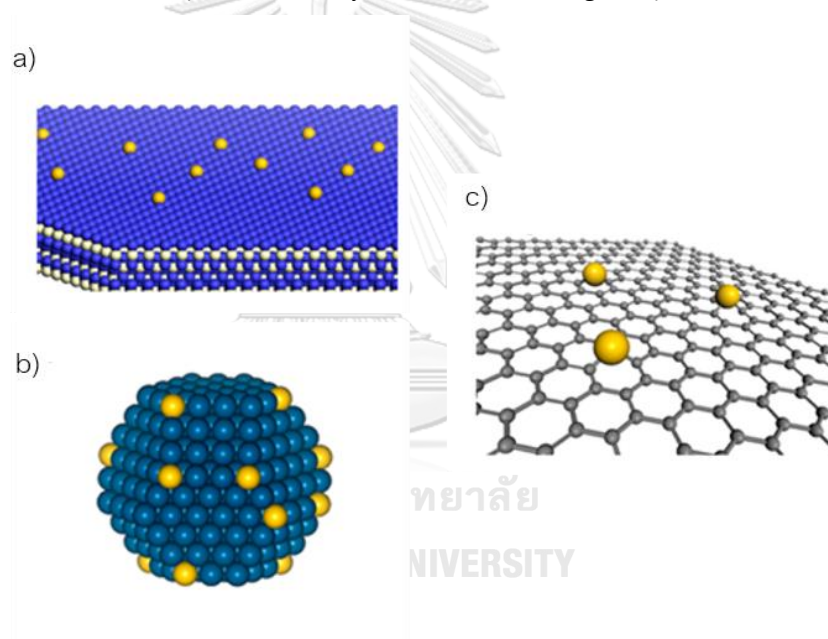
Figure 2.21 Different supports for metal single atom; (a) metal oxide, (b) metal surface, and (c) carbon material. [23]

2.7.1 DEFINITIONS AND CLASSIFICATIONS OF SINGLE ATOM CATALYST

As mention above, the SACs consisted of isolated metal dispersed on the surface of the supporting substrate. Most of them provided unique properties that were different from NPs system. This section will discuss into the three types of dispersed SACs as shown in Figure 2.22 and mention below [22, 24].

Single-Site Heterogeneous catalyst (SSHC)

From Figure 2.22 (a), the active single site included of one or more atoms that each site is locally isolated from another site without interconnection with each site. The interaction energy between each site and reactants has the same as every single site.

Single-Atom catalyst (SAC)

The SAC normally consists of only isolated single atom dispersed on substrate without interaction between another single metal atom, as represented in Figure 2.22 (b). The active single site has same or different properties that depended on the interaction between metal atom and adjacent atoms.

Atomically Dispersed Supported Metal Catalyst (ADSMC)

The ADSMC (illustrated by Figure 2.22 (c)) can be created as two-dimension rafts, metal atom cluster, or etc. that based on 100% metal dispersion. Some SAC could be categorized as subset of ADSMC depending upon their structure.

Among of single-atom types, not only the interaction between active single metal atom is a one of the important factor for governing the type of SACs and catalytic activity but also the preparation method will affect to their properties. Thus, the next topic will discuss the preparation method for synthesis SACs.
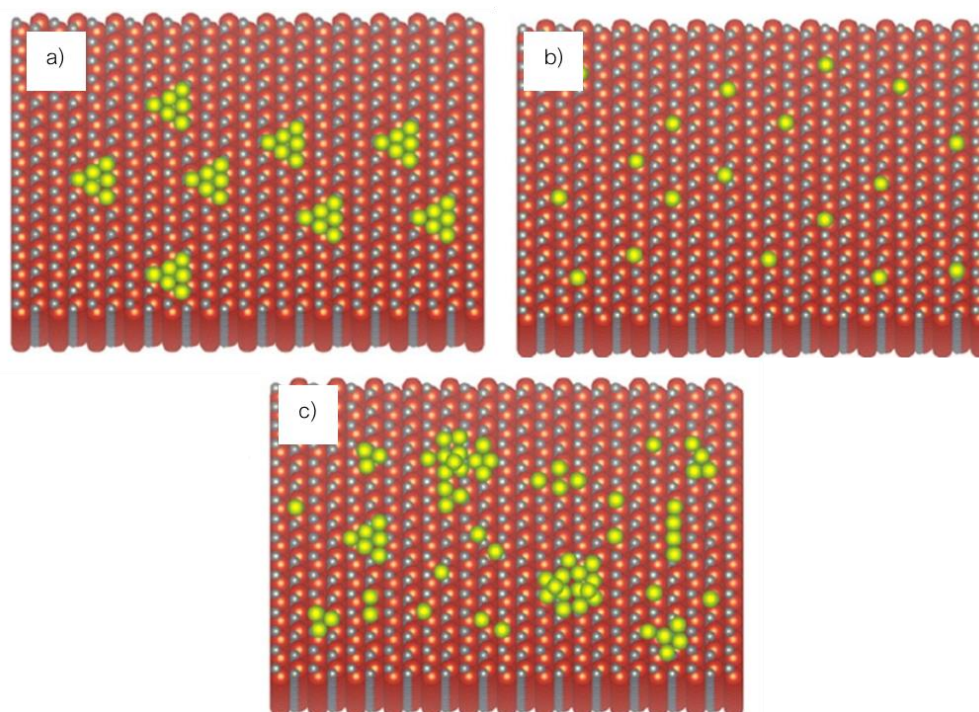
Figure 2.22 Illustration of single-site heterogeneous (a), single-atom catalyst (b), and atomically dispersed supported metal (c). [24]

2.7.2 PREPARATION METHODOLOGIES FOR SINGLE ATOM CATALYST

As mention above, the preparation procedure is played a key role in SACs catalyst. Before investigating the catalytic performance of SACs, it necessary to study the preparation methods of SACs. The challenging of SACs synthesis is to prevent the metal aggregation that probably due to preparation process or the subsequent treatments. In this account, some interesting method will be considered and discussed [23, 24].

O   Mass-selected Soft-landing method

The Mass-selected Soft-landing method is effectively synthesis method for supported NPs and SACs since this method provided controllable metal size with mass-selected atom beams and precise regulation of the surfaces integrated with ultrahigh vacuum procedures. The advantage of this method is the best model SACs on atomic

scale and excellent metal-support interaction. Nevertheless, the high cost and low yield are major obstruct for develop into commercialized scale.

○ Wet-Chemistry Method

Owning to the metal precursor contain single metal species, the key point of this method is to attach the metal atom and prevent their coalescence from synthesis procedure and post-treatment process. This general approach of this method was required many combination steps: (1) to introduce the metal precursor onto support by impregnation, ion-exchange or precipitation, (2) drying and calcination, and (3) reduction or activation step. This process was dispensed with special instrument. Moreover, this method is potential for commercial production.

○ Atomic Layer Deposition Method

The Atomic Layer Deposition process (ALD) can be served as SACs catalyst synthesis by using thin film growth technique. The selected supporting material is exposed to the pulsing vapor metal precursor and is self-limiting reaction to growth single atom layer. However, similar with mass-selected Soft-landing method problem, ALD method required the high-technique and complex instrument that led to scalability and cost problems.

○ Pyrolysis method

The Pyrolysis method has been intensively used for SACs supported on carbon-based materials, especially N-doped carbons. Prerequisite for pyrolysis, metal precursor is incorporated to porous carbon. Subsequently, the whole material is exposed into anaerobic condition; e.g. N_2, Ar, or H_2. This method provided a high single metal loading on porous carbon.

2.8 LITERATURE REVIEWS

Many researchers in this area attempt to enhance the performance of catalyst for EOR. The adding of tin (Sn) act on Pt to form alloyed metal was investigated by Lamy et

al. [25]. It was found that the ethanol oxidation of PtSn was greatly enhanced with respect to Pt content. Additionally, D'Urso et al. [26] studied the activity of three Pt-based anode catalysts supported on commercialized carbon (Vulcan XC-72R), which were prepared by using a modified polyol process. The results reveal that the adding of Sn, Ir and Rh may act as promoter of Pt enhancing ethanol electro-oxidation activity. De Souza et al. [27] investigated the ethanol electrooxidation activity of ternary Pt-Sn-Rh/C catalysts obtained either by substitution of tin (Sn) with rhodium (Rh) or by addition of Rh to a binary partially alloyed Pt_1Sn_1/C catalyst prepared by formic acid reduction method. The results reveal that the present of Rh, both addition and substitution in PtSn, can be increased the ethanol oxidation. The Pt-Sn-Rh/C catalysts obtained by Sn substitution, provide the best active for EOR. The effects of adding praseodymium (Pr) into alloyed PtSn on catalytic activity and stability for ethanol electrooxidation prepared by modified formic acid reduction method were conducted by Corradini et al. It can be observed that the added Pr can be enhanced both EOR activity and poisoning tolerance for ethanol oxidation intermediate product.

Furthermore, carbon nanotube (CNTs) is promising for supported electrocatalyst in fuel cell application since they provide better electrical properties and corrosion resistance than carbon Vulcan XC-72. Yang et al. [28] compared the methanol-electrooxidation activity of PtRu supported on carbon Vulcan and MWCNTs. The results showed that using MWCNTs as the supporting material provided a higher activity than Vulcan, attributed to good catalyst dispersion and high electrical property. Even though, MWCNTs provide higher activity than carbon Vulcan, the conventional acid treatment for promote anchor site is considered. The functionalization of MWCNTs by acid treatment method leads to physical and electrical damage because this procedure uses strong concentration mixture between nitric acid (HNO_3) and sulphuric acid (H_2SO_4) for functionalized anchor group. Moreover, the anchor site, which is obtained by this method, is difficult to control the sites distribution, so the active metals prefer to aggregate. Cheng et al. [29] investigated the methanol electrooxidation activity of nitrogen-contained species functionalized on MWCNTs as supporting material for PtRu catalyst, which were included of poly(diallyldimethylammonium chloride); PDDA, polyethylenimine; PEI, 1-aminopyrene; AP and tetrahydrofuran; THF. The results reveal that functionalization of non-covalent material did not only improve catalyst dispersion and distribution of PtRu nanoparticles but also enhance electrooxidation activity and stability. PEI functionalized

on MWCNTs gave the highest performance on methanol electrooxidation, ascribed that the functionalizing agents provide strong interaction of the electron rich nitrogen-containing group. Thus, Cheng and Jiang [30] continued to studied the PEI functionalization on MWCNTs, in comparison with typical acid treatment. Oxygenated species were functionalized, with a non-uniform pattern, on carbon support surface during acid treatment and they acted as anchoring sites for metal deposition. In contrast, the PEI on MWCNTs showed a higher methanol oxidation activity, attributed to the uniform and controllable anchor sites that can promote catalyst dispersion. Additionally, the CV of methanol oxidation displayed that 20% metal supported on PEI carbon nanotubes has the highest forward anodic peak current, which is 3 times of conventional carbon nanotubes. When increasing metal loading from 20% to 40%, the forward anodic current peak of 40% PtRu supported on PEI functionalized carbon nanotubes was increased by 6 times higher than the 40% PtRu conventional carbon nanotubes. In case of catalyst using PEI-nanotube as support, It was found that 40% PtRu supported on PEI functionalized carbon nanotubes gave a one half times higher activity than 20% metal supported on PEI carbon nanotubes, contrast with ESA results, attributed that the activity of electrocatalyst not only depends on the nanoparticles distribution, but also on the particle sizes and the connectivity between the particles. Recently, Graphene was introduced as a support for fuel cell electrocatalyst. Dong et al. [31] prepared platinum (Pt) and alloyed platinum ruthenium (PtRu) on graphene, carbon Vulcan and graphite and evaluated their methanol oxidation activities. The electrooxidative activity of methanol and ethanol showed that Pt and PtRu supported on graphene provided the highest activity, attributed to excellent electrical properties. Ye et al. [32] studied PtRuMo ternary alloy on different supports: CNTs, graphene and graphene-CNTs composite. It was clear that methanol electrooxidation activity of graphene-CNTs supported PtRuMo gave the highest activity, followed by graphene and CNTs, respectively. It was suggested that the addition of CNTs to form a composite support can inhibit re-stacking of graphene layers.

It is well known that Pt is very expensive and limited, so Palladium (Pd) is candidate for anode electrocatalyst instead of Pt in alkaline media because of highest EOR activity in high-pH media, more abundant on the Earth's crust and lower price than Pt [7]. The ethanol electrooxidation activity of Pt and Pd in basic solution was tested by Ma et al. [33], and results showed that Pd metal obtained higher performance than Pt. However, the sluggish kinetic for alcohol oxidation is still occurred. One of manner for enhance catalytic

electrooxidation is an adding secondary material in Pd system. Xu et al. [34] determined the effect of palladium-gold (Au) alloying on electrocatalytic stability for ethanol oxidation reaction. The alloyed catalysts were synthesized by co-reduction method using dimethylformamide as reducing agent under an ultrasonic condition. Although, the electrochemical activity test illustrated that Pd metal provided highest forward anodic current peak, the stability tests illustrated that alloyed PdAu provide the best performance. The impregnated palladium-ruthenium (PdRu) supported on carbon in different atomic ratio were prepared by Ma et al. [35]. The physical characterizations reveal that the bimetallic catalyst gave slightly small average particle size with respect to Pd single metal. The half-cell electrochemical testing indicated that Pd_xRu_y/C provide higher EOR activity, both lower onset potential and higher forward anodic current peak, than Pd/C. The Pd_xRu_y supported on commercialized carbon in various atomic ratios to study the relationship of the surface structure-composition-activity (synergetic effect) were synthesized and conducted by Monyoncho et al. [36]. The results demonstrated that the adding of Ru 1-10% to Pd can be improved EOR performances compared with Pd alone. Shen et al. [37] prepared and conducted the supported PdNi on Vulcan XC-72 which were synthesized by $NaBH_4$ reduction method. The cyclic voltammetry and short-term stability test displayed that the EOR activity and stability can be enhanced when Ni were formed alloying with Pd. Maiyalagan and Scott [38] investigated the performance of supported Pd–Ni nanoparticles on carbon nanofibers (CNF), which were used $NaBH_4$ as a reducing agent. The catalyst morphology results indicated to good uniformly distributed on the supporting material surface. Meanwhile, the EOR activity of Pd-Ni/CNF was higher than Pd/C. Wang et al. [39] synthesized binary alloyed of palladium–lead supported on carbon (PdPb/C) with different amounts of lead by co-reduction method. The electrochemical properties results revealed that PdPb (4:1)/C had a higher catalytic activity than the Pd/C catalyst.

From previous mention, MWCNTs is expected to use for supported electrocatalyst system. Singh et al. [40] investigated the ethanol electrooxidation activity in alkaline electrolyte of multicomponents of Pd, Pd–MWCNT and Pd–MWCNT–Ni prepared on glassy carbon electrodes. The results can be observed that the addition of small amount (1–5%) of MWCNTs to Pd gave higher ethanol oxidation activities, the increase being the greatest with 1%MWCNT. Furthermore, 1%Ni addition to the Pd–1%MWCNT composite electrode improves the apparent electrocatalytic activity by over 50%. Geraldes et al. [41]

explored the EOR activity in alkaline media of supported Pd and PdSn with atomic ratios 90:10 on multiwall carbon nanotubes (MWCNT) or Carbon Vulcan prepared by an electron beam irradiation reduction method. It was clear that the using of MWCNTs provide lower onset potential and higher anodic current peak than carbon Vulcan. Dong et al. [42] investigated the EOR activity of binary alloyed of PdCu supported on graphene. The catalyst morphology results exhibited to well-metal dispersion on graphene. The ethanol electrooxidation activity of Pd were improved by introducing Cu to form alloy.

Consequently, the challenges in direct ethanol fuel cells development are not only cost reduction but also enhancing catalyst activity of ethanol oxidation and clarifying its mechanism.

CHAPTER III
RESEARCH METHODOLOGY

3.1 CHEMICALS AND MATERIALS

1. Palladium (II) Chloride ($PdCl_2$), Sigma Aldrich

2. Ruthenium (III) chloride ($RuCl_3$), Sigma Aldrich

3. Gold (III) chloride trihydrate, ACROS Organics

4. Tungsten hexachloride (WCl_6), Sigma-Aldrich

5. Vulcan XC 72R carbon powder, Cabot Corporation

6. Multiwall carbon nanotube (NANOCYL® NC7000™ with $\varnothing_{average}$ = 9.5 nm.), Nanocyl.

7. Poly(ethyleneimine); PEI, 50 wt. % in H_2O with average M_w ~1300, Sigma Aldrich

8. Phosphotungstic acid hydrate ($H_3[PW_{12}O_{40}] \cdot xH_2O$), Sigma Aldrich

9. Sodium tungstate dihydrate ($Na_2WO_4 \cdot 2H_2O$), Sigma Aldrich

10. Nickel (II) acetylacetonate ($Ni(C_5H_7O_2)_2$), Sigma Aldrich

11. Dicyandiamide ($C_2H_4N_4$), Sigma Aldrich

12. Methanol (CH_3OH), 99.8% purity, Sigma Aldrich

13. Ethanol (C_2H_5OH), 99.9% purity, QReC and Sigma Aldrich

14. Glycerol ($C_3H_8O_3$), ≥ 99.5% purity, Sigma Aldrich

15. Sulfuric acid (H_2SO_4), 98% purity, QReC

16. Nitric acid (HNO_3), 65% purity, QReC

17. Isopropyl alcohol (C_3H_7OH), ≥ 99.7% purity, QReC

18. Nafion® 117 solution (5% in aliphatic alcohols and water), Sigma Aldrich

19. Deionized water

20. Potassium hydroxide (KOH) pellets, Qrec

21. Sodium hydroxide (NaOH) pellets, Carlo Erba

22. Nitrogen gas (N_2) 99.99% purity, Praxair

23. L-ascorbic acid, Sigma Aldrich

24. Ethylene glycol, QReC and Sigma Aldrich

3.2 LABORATORY INSTRUMENTS

1. Polytetrafluroethylene membrane filter, 0.1 µm pore size, Merk Millipore

2. Conventional oven,

3. Hotplate and stirrer

4. Ultrasonic bath

5. Vacuum tube furnace

6. Potentiostat/galvanostat interface 1000, Gamry

7. Potentiostat/galvanostat equipment (model PG STATO 30), AUTOLAB

3.3 SYNTHESIZATION OF PALLADIUM CATALYST AND FUNCTIONALIZATION METHODS OF CARBON MATERIAL
3.3.1 OXIDATION FUNCTIONALIZATION PROCEDURE

On Pristine multiwall carbon nanotubes (MWCNT), anchoring site were generated by conventional acid treatment method before using as the supporting material. The MWCNTs was added to a mixed acid solution of 1:1 (v/v) 12 M of sulfuric acid and 12 M of nitric acid with the ratio of carbon to acid mixture 70:30 (v/v). The slurry was shaken for 8 hours. Afterward, it was washed with deionized water for several times until the pH became 7, followed by filtration and drying overnight at 110 $^{\circ}$C in a conventional oven, denoted as AO-CNT.

3.3.2 NON-COVALENT FUNCTIONALIZATION WITH POLYETHYLENEIMINE AND SELF-ASSEMBLY OF PHOSPHOTUNGSTIC ACID

The schematic of self-assembly phosphotungstic acid (PWA) with polyethyleneimine (PEI) functionalized by multiwall carbon nanotube is illustrated in Figure 3.1. Briefly, 200 mg of Pristine MWCNT was dispersed in 400 ml of 0.5 wt.% PEI in deionized water for 1 h by ultrasonic technique. The dispersion was stirred for 12 h, after that it was filtered by PTFE membrane (Merk Millipore) and washed with deionized water

several times for remove the excess PEI, denoted as PEI-CNT. The PEI-CNT was dried in a conventional oven at 60 $^{\circ}$C for 12 h. Afterward, PEI-CNT was dispersed by ultrasonic bath for 1 h and stirred with a mixture of 0.48 g/ml of PWA in deionized water for 12 h. The as-prepared self -assembly with PWA (denoted as PWA-PEI-CNT) was washed with deionized water several times until neutral pH, then the PWA-PEI-CNT was dried at 60 $^{\circ}$C for 12 h.
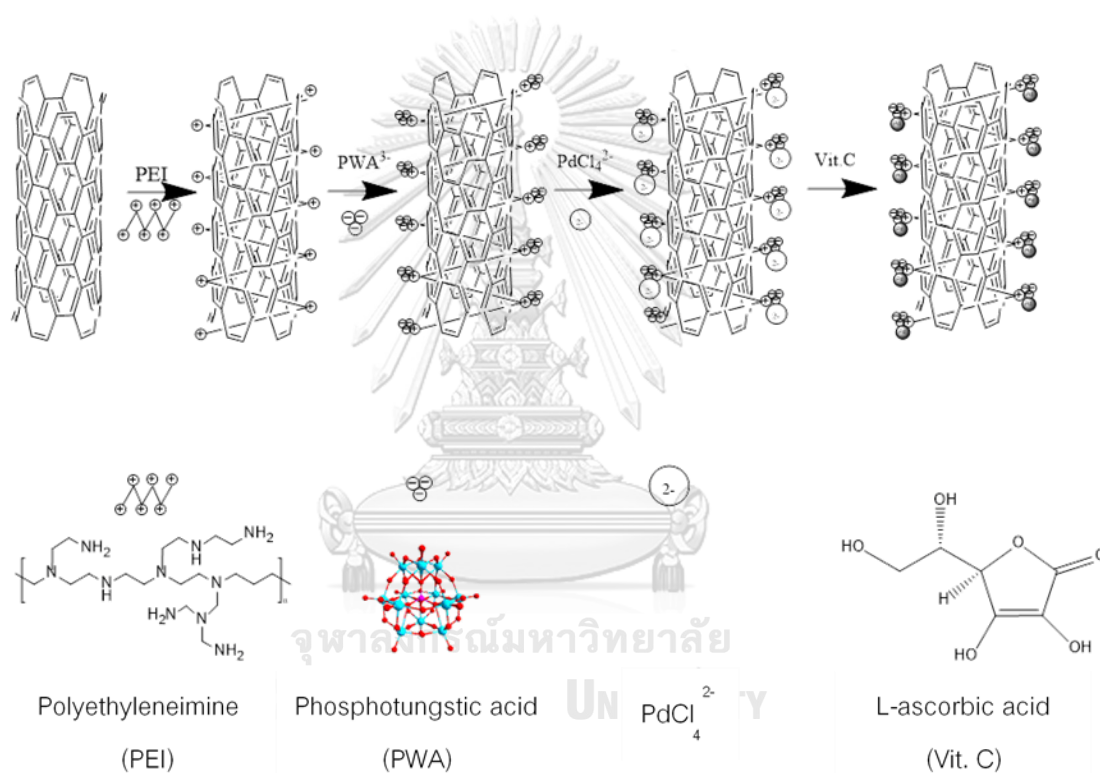
Figure 3.1 Self-assembly of MWCNTs and catalyst preparation procedure of Pd NPs in this work.

3.3.3   PREPARATION OF NITROGEN DOPED MWCNTS

The N-CNT was synthesized by multi-stage pyrolysis method. Firstly, AO-CNT was dispersed in ethanol assist with ultrasonic bath. The dispersion was added and grounded until uniformity with mass ratio 1:200 of DCM. The uniformed powder was dried at ambient

temperature for overnight, and then pyrolyzed in argon-rich condition at 800 $^{\circ}$C for 1 h. Finally, incorporated nitrogen with DCM onto O-CNT (denoted as N-CNT) was obtained.

3.3.4 PREPARATION OF NICKEL SINGLE ATOM SUPPORTED ON MWCNTS

The nickel single-atom catalyst doped multiwall carbon nanotube was synthesized as same as N-CNT using muti-step pyrolysis carbon-based method. Firstly, nickel (II) acetylacetonate, AO-CNT, and dicyandiamide (DCM) were grounded in order to promoted well-mixing. The powder was then pyrolyzed under 50 sccm of argon in a tube furnace following a heating procedure of 350 oC for 3 hours, 650 $^{\circ}$C for 3 hours and 900°C for one hours with a heating rate of 1 $^{\circ}$C/min. The nickel supported on MWCNT were denoted as NiSA-N-CNT.
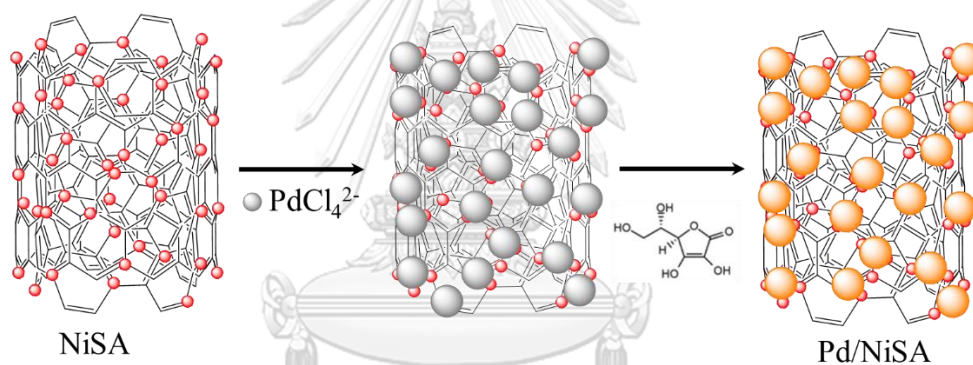
Figure 3.2 The scheme shows the procedure of supporting Pd NPs on NiSA.

3.3.5 PREPARATION OF PALLADIUM NANOPARTICLES

The Pd NPs supported on various support was synthesized by ethylene glycol method assistance with Vit-C as reducing agent. Briefly, 30 mg of supporting material were sonicated in ethylene glycol for 30 min. An appropriate amount of metal precursors was gradually dropped into the slurry and stirred for 3 hours, followed by adding 2M of NaOH in EG for pH adjustment to above 12. The slurry was stirred for 1 hour. Next, the pH was adjusted to 3 by adding 5 M HCl. An excess amount of 0.2 M ascorbic acid was dropped into the mixture and stirred overnight. The slurry was washed with deionized water and then dried at 100 $^{\circ}$C overnight.

3.4 SAMPLE CHARACTERIZATIONS

3.4.1 TRANSMISSION ELECTRON MICROSCOPY (TEM)

Catalyst morphology was carried out by FEI Talos FS200X. The tiny amount of sample powder was sonicated in high purity ethanol for a while, then dropped onto a 200-mesh copper grid coated with carbon film and dried in ambient condition. The Nano measure version 1.2.5 software was used for particles size and distribution calculation of as-prepared electrocatalysts.

3.4.2 X-RAY POWDER DIFFRACTION (XRD)

XRD patterns of electrocatalyst were performed by D8 advance from Bruker AXS using Cu Kα as X-ray source (λ=1.5406 Ao) and low background stuff holder. A small amount of catalyst powder was dispersed in ethanol by ultrasonication technique, subsequently dropped onto the holder. The patterns were reported with 2 theta in the range of 25° to 80° with step size of 0.02° at 40kV and 40mA.

3.4.3 X-RAY PHOTOELECTRON SPECTROSCOPY (XPS)

The X-ray photoelectron spectroscopy (XPS) measurements were performed on a Kratos Axis Ultra DLD spectrometer using a monochromatic AlKα (1486.6 eV) irradiation source operated at 225 W. The vacuum pressure of the analysis chamber of the spectrometer was maintained a 5×10^{-11} Torr or lower throughout the duration of the analyses.

3.4.4 THERMAL GRAVIMETRIC ANALYSIS (TGA)

For thermal gravimetric analysis (TGA) were carried out by PerkinElmer model pyris diamond under air environment. The sample was held at 100 $^{\circ}$C for 15 min, followed by rising to 800 $^{\circ}$C with ramping rate 10 $^{\circ}$Cmin^{-1}

3.4.5 ATTENUATED TOTAL REFLECTANCE-FOURIER TRANSFORM INFRARED SPECTROSCOPY (ATR-FTIR)

In the case of self-assembly CNT, the functional groups were analyzed by ATR-FTIR technique with Perkin Elmer, Spectrum One. The wavenumber was a range of 1,800 to 650 cm^{-1} with resolution 0.5 cm^{-1}.

3.4.6 ZETA POTENTIAL TESTING

The surface charge of CNT for self-assembly was investigated by zeta-potential technique using Zetasizer model ZSP from MALVERN. Before testing, the very small amount of sample was dispersed in D.I. water by ultrasonic bath. Subsequently, 2 ml of dispersion was added in cell curvetted.

3.4.7 ELECTROCHEMICAL MEASUREMENTS

The electrochemical characterization was accomplished by a conventional three-electrode technique using Gamry potentiostat/galvanostat interface 1000. Rotating glassy carbon disk electrode (RGCDE) with diameter 5 mm. was served as working electrode additionally Graphite rod and saturated calomel electrode (SCE) were applied to counter electrode and reference electrode, respectively. Normally before electrochemical measurement, thin film layer was fabricated, which was composed of 2

mg of catalyst powder was mixed together with a 0.5wt.% of Nafion solution (5wt.% Nafion solution in a mixture of aliphatic alcohol and water, from Sigma-Aldrich) and isopropyl alcohol in an ultrasonic bath for 1 hour afterward the catalyst ink was dropped onto RGCDE. For Electrochemical characterization techniques; Cyclic voltammetry (CV), Chronoamperometry (CA), and were determined for ethanol electrooxidation activity, microstructure-stability, and short-term with a mixture of 1M KOH + 1M alcohol under N_2-rich condition for deaeration. The potential window was defined from -0.8 to 0.3 vs. SCE and 50 mV/sec for scanning rate. In term of short-term stability was recorded at -0.3 V. with respect to SCE for 2 hours in a solution of 1M KOH + 1M alcohol. The electrochemical properties of 3 different fuels; which were included of methanol, ethanol, and glycerol, were measured under N_2-saturated 1M KOH + 1M alcohol.

CHAPTER IV

RESULTS AND DISCUSSION

4.1 EFFECT OF SECONDARY METAL FOR ENHANCE ELECTROOXIDATION TOWARD ETHANOL

4.1.1 CHARACTERIZATION OF AS-PREPARED CATALYSTS

The catalysts morphology was examined by TEM technique, represented in Figure 4.1. The most of electrocatalysts was spherical shape. For Pd/C (Figure 4.1 a), the nanoparticle aggregation was observed from this catalyst with averaged particle size 10.62 ± 3.18 nm. The NPs of $Pd_{99}Au_1$/C was smaller than Pd/C with average size 8.98 ± 3.29 nm. but larger than $Pd_{99}Ru_1$/C and $Pd_{99}W_1$/C with 7.97±3.12 nm. and 7.72±2.54 nm., respectively. The addition of secondary metal can be preventing for catalyst coalescence. Additionally, the metal composition of as-prepared catalysts was obtained by EDX technique, as shown in Figure 4.2. and Table 4.1. The EDS spectrums indicated that the electrocatalyst were contained with Pd, Au, Ru, and W supported on carbon Vulcan. In the case of elements composition from EDX measurement are displayed in Table 1. The element composition illustrated to successfully synthesis with designed atomic ratio. In accordance with TGA technique was tested for investigate total metal loading, as represented in Figure 4.3 and Table 4.1. The weight loss around 200°C to 300 ^{o}C can be ascribed to the absorbed water in the pore structure of carbon support [43, 44]. From among of TGA curves, the stabilized weight loss was PdO which can be observed. Thus, it can be confirmed that metal precursors were deposited onto carbon supported.
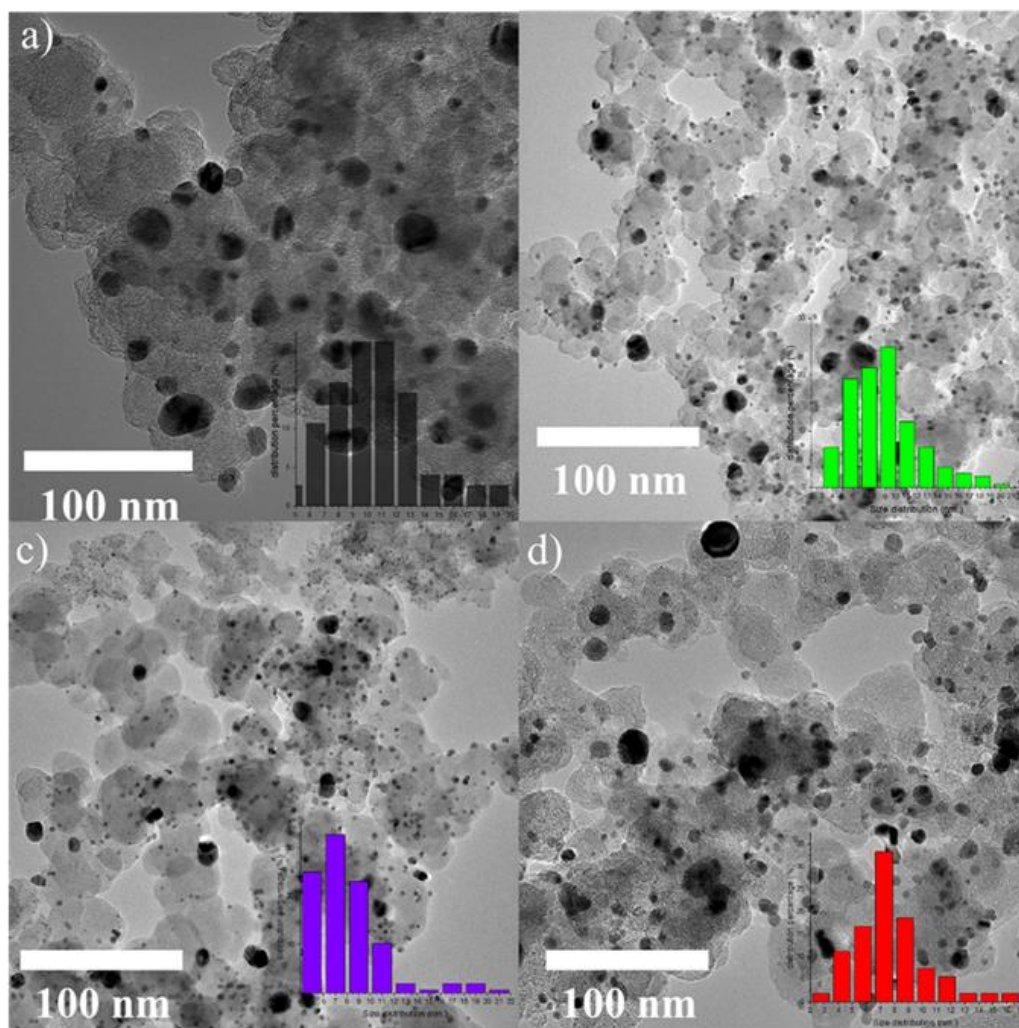
Figure 4.1 TEM images and of Pd/C (a), $Pd_{99}Au_1$/C (b), $Pd_{99}Ru_1$/C, and $Pd_{99}W_1$/C (d).
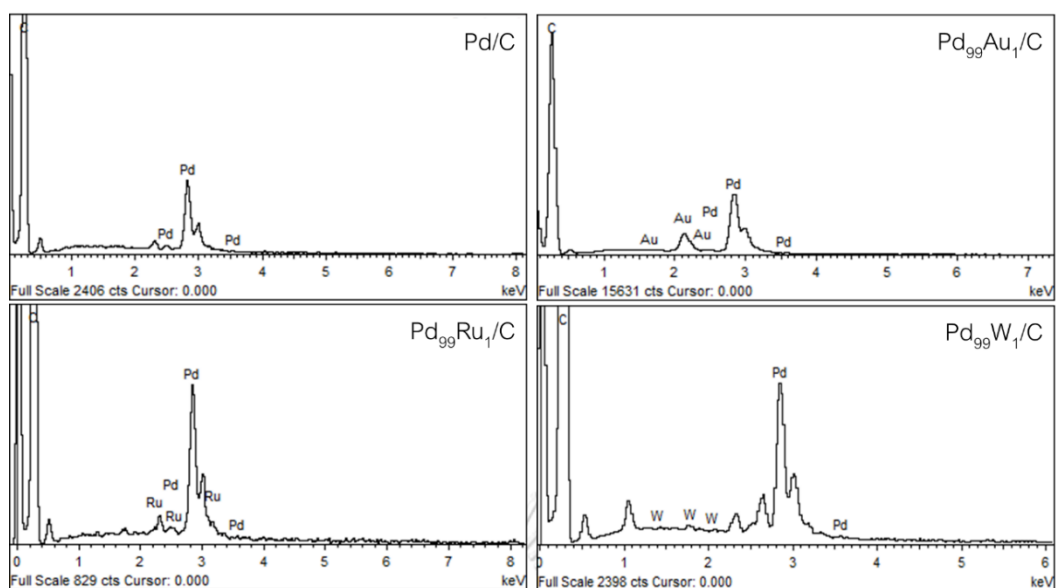
Figure 4.2 EDS spectrums of as-prepared palladium-based catalysts.
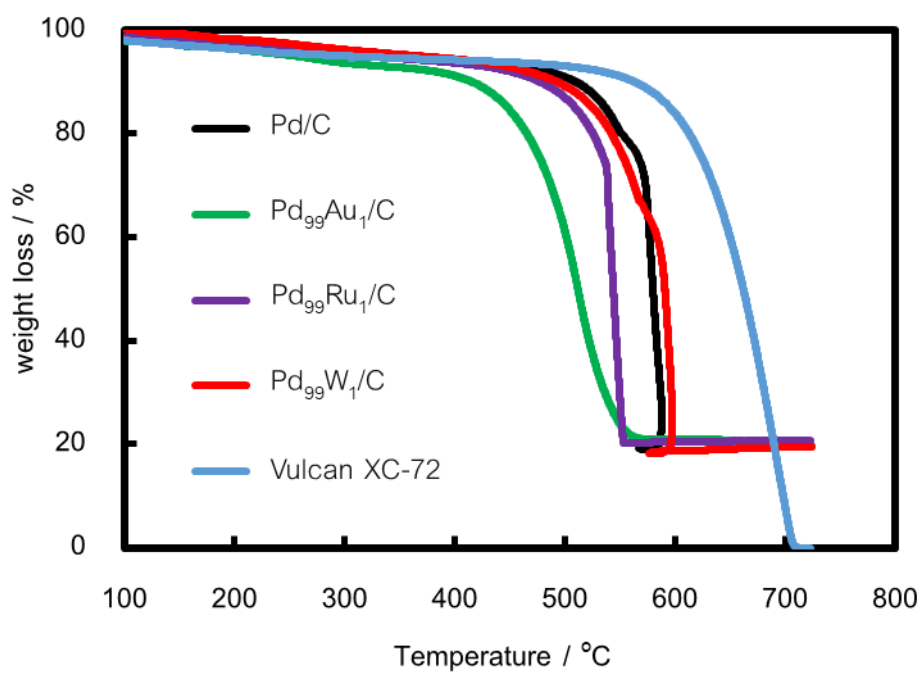
Figure 4.3 The TGA curves of as-prepared Pd catalysts.

Table 4.1 Elemental analysis results from EDS and TGA measurements for Pd-based

supported on Vulcan XC-72

Type of catalysts	EDX results			TGA
	Pd	2° metal	Total metal (wt.%)	Total metal (wt.%)
	(atomic %)	(atomic %)		
Pd/C	100	-	18	20
$Pd_{99}Au_1/C$	99	1	20	20
$Pd_{99}Ru_1/C$	99	1	20	21
$Pd_{99}W_1/C$	99	1	19	21

The XRD pattern of electrocatalysts is represented in Figure 4.4 and Table 4.2. The peak located around 25° revealed C (002) in graphite structure of carbon Vulcan XC-72. For Pd/C, the diffraction pattern was located around 40°, 46° and 68°, attributed to (111), (200) and (220) plane of faced center cubic (fcc) Pd crystal structure with respect to JCPDS card No. 03-065-2867. The diffraction pattern of $Pd_{99}Au_1/C$ represented a bulk phase as fcc of palladium and comparing with XRD pattern of gold from JCPDS card No. 01-004-0784 shown that no any separately peaks corresponded to Au, attributed to Au were merged together with palladium in this content (0.18 wt.%), which settled at 38.19^{o}, 44.39^{o}, 64.58^{o}, and 77.55^{o}, ascribed to (111), (200), (220) and (311) fcc crystal structure of Au. In case of $Pd_{99}Ru_1/C$, all diffraction peaks reveal that the bulk phases were palladium without peaks corresponded to ruthenium when considering with JCPDS card No. 01-073-7011. For XRD pattern of $Pd_{99}W_1/C$ exposed that the catalyst phases rich with Pd and without any peaks agree with pure tungsten when compared with JCPDS card No. 00-004-0806, which 2 theta were located at 40.3^{o}, 58.3^{o} and 73.2^{o}, ascribed to (110), (200) and (211) plane of W faced center cubic structure. Moreover, XRD pattern of $Pd_{99}W_1/C$ associated with the pattern of JCPDS card No. 01-074-0657 of $Pd_{0.6}W_{0.4}$ that provided 2 theta appeared around 39°, 46° and 67°, suggested to (111), (200) and (220) fcc crystal

structure of palladium. In this work can be observed that all diffraction peaks of palladium-based metal were settled around 40°, 46° and 68°, ascribed to (111), (200) and (220) plane of faced center cubic (fcc) Pd crystal structure and no peaks corresponding to Au, Ru, W and their oxides were found. Figure 4.5 are illustrated the Pd 3d XPS spectra of as-prepared catalysts. The binding energy located around 335 eV and 340 eV corresponded to Pd 3d5/2 and Pd 3d3/2, respectively. In the case with adding of secondary metal, the binding energy both Pd 3d5/2 and Pd 3d3/2 were a positively shift with respect to pure Pd, ascribed to alloy formation [45]. Moreover, the positive shift of the Pd 3d core level can be expressed by the d-band far away from valence band hence the poisoning agent; which come from non-complete alcohol electrooxidation, is much weaker absorbed on active surfaces [46].
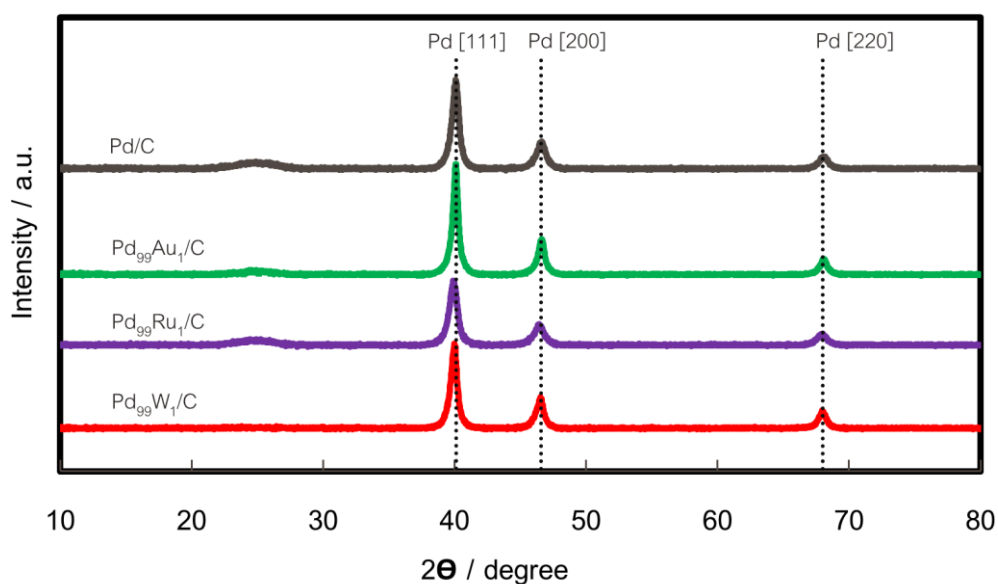
Figure 4.4 XRD pattern of electrocatalysts supporting material in 10° to 80° 2Θ.
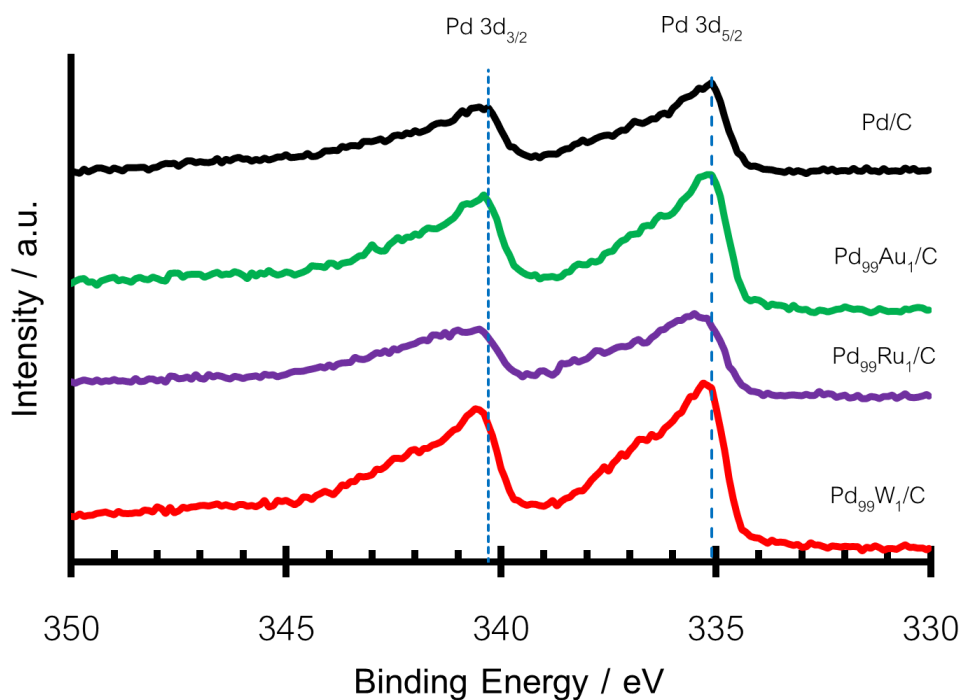
Figure 4.5 XPS Pd 3p spectra of Pd-based metals.

Table 4.2 XRD and binding energy (BE) values of Pd-based electrocatalysts.

Electrocatalysts	2 theta (degree)			Average crystalline size at [220 (nm.)	BE of Pd 3d (eV.)	
	[111]	[200]	[220]		Pd 3d$_{3/2}$	Pd 3d$_{5/2}$
Pd/C	40.09	46.64	68.12	16	340.05	335.05
Pd$_{99}$Au$_1$/C	40.09	46.64	68.06	12	340.36	335.19
Pd$_{99}$Ru$_1$/C	39.91	46.42	68.00	11	340.50	335.48
Pd$_{99}$W$_1$/C	39.99	46.52	67.96	8	340.56	335.25

4.1.2 ELECTROCHEMICAL PROPERTIES OF ETHANOL OXIDATION REACTION

Ethanol electrooxidation activity can be expressed by the magnitude of forward current peak (i_f) [47], which relative with the oxidation of freshly chemisorbed species which come from alcohol adsorption as well as The facility of alcohol molecule on electrocatalyst surfaces can be expressed by onset potential (E_s). The electrochemical properties of as-prepared catalysts toward ethanol was conducted in 1M KOH + 1M Ethanol and was illustrated in Figure 4.6 and their numerical data are represented in Table 4.3. In case of modified Pd with W, it can be observed that Pd catalyst modified with W provided a higher ethanol electrooxidation reaction (EOR) activity with 748.44 mA/mg$_{Pd}$, which considered from the forward current, than Pd/C with 209.32 mA/mg$_{Pd}$. Besides, the EOR activity can be significantly improved with the value of 548.02 mA/mg$_{Pd}$ for Pd$_{99}$Ru$_1$/C but lower than Pd$_{99}$W$_1$/C. Moreover, when consider with the onset potential value showed that PdW provided lower potential approximately 50 mV. vs SCE compared to Pd, indicated that the ethanol molecule can be facility oxidised on these surfaces. Unfortunately, adding of Au was not significantly improved electrooxidation activity of ethanol as well. The activity results of Pd$_{99}$Au$_1$/C was 252.62 mA/mg$_{Pd}$, which slightly a much higher than Pd. However, the onset potential of PdAu shown a lower than Pd, indicated that adsorbed ethanol molecules both catalysts gave an easier to electrooxidation than Pd/C. According to the binding energy of several metals for oxygen and hydroxide adsorption from Figure 4.7. it can be observed that the binding energy of tungsten for adsorbed OH$^-$ was higher than ruthenium and gold, indicated that the surfaces was strongly adsorbed and held OH$^-$ for oxidizing species from non-complete ethanol oxidation intermediates [48]. Consistency with XPS results, the Pd3d core level positively shifted with respect to Pd, attributed that the poisoning agents from non-complete ethanol oxidation were much easier to oxidize on Pd surfaces.
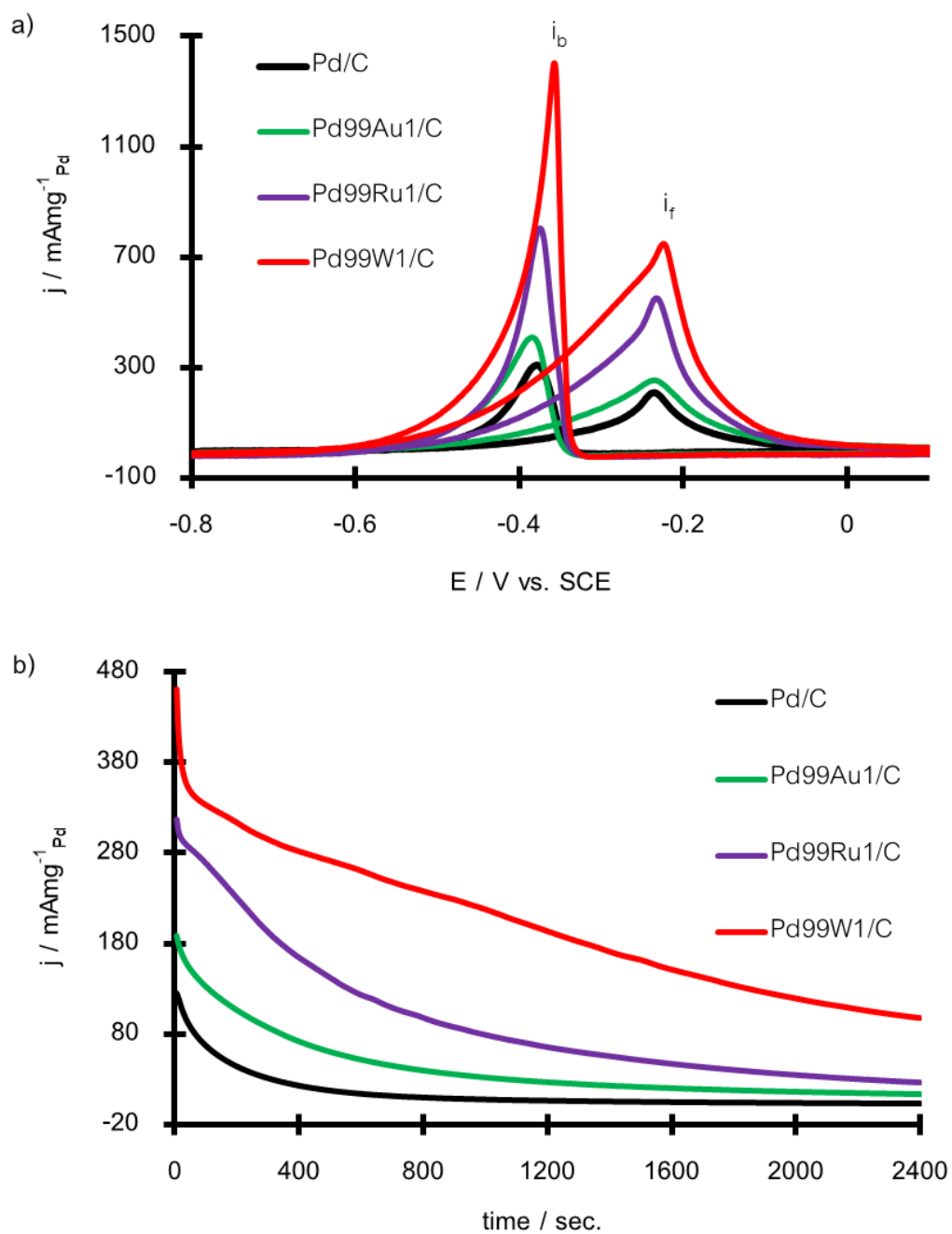
Figure 4.6 Cyclic voltammetry (a) and Chronoamperometry (CA) of EOR activity of as-prepared catalysts in a mixture of 1M KOH + 1M alcohol using 50 mVsec^{-1} as sweeping rate.
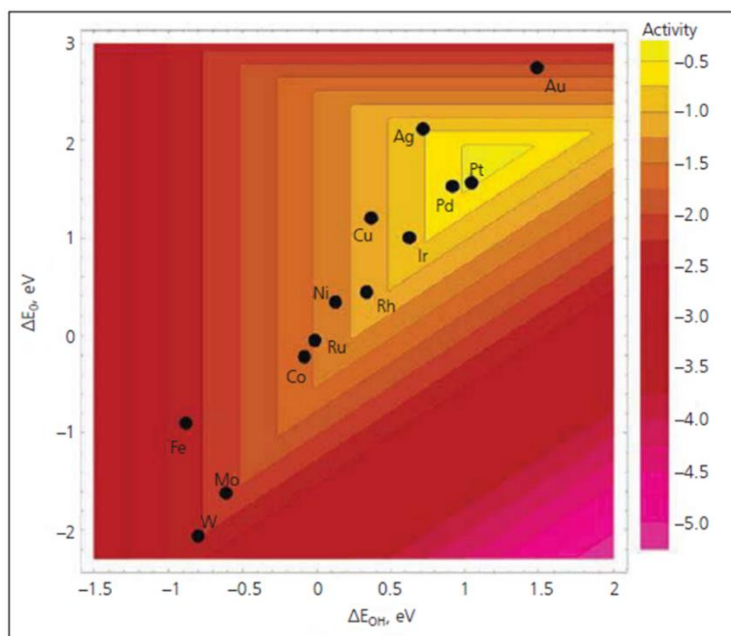
Figure 4.7 The oxygen reduction activity of various metals plotted as a function of both the oxygen and the hydroxyl group Binding energy. [48]

In order to investigate the potential to use as-prepared catalyst for other fuels, the electrocatalysts were conducted in both methanol and glycerol. The electrochemical activity and stability toward methanol (MOR) properties was displayed in Figure 4.8 (a) and (b). The mass activity of Pd/C exhibited a magnitude at 152.73 mAmg$^{-1}_{Pd}$ and onset potential as -0.46 V. Meanwhile the adding of Au and Ru displayed a similar mass activity with 238.58 mAmg$^{-1}_{Pd}$ and 235.67 mAmg$^{-1}_{Pd}$ for $Pd_{99}Au_1$/C and $Pd_{99}Ru_1$/C, respectively but still higher than Pd/C. In controversy with $Pd_{99}W_1$/C, both mass activity and Es provided significantly improved with a high value of 588.41 mAmg$^{-1}_{Pd}$ and a low value -0.48 V. vs SCE when compared with other catalysts. Furthermore, the stability with MOR with constant at -0.3 V. vs SCE of each catalyst were conducted and illustrated in Figure 4.8 (b). It was clear that $Pd_{99}W_1$/C shown a higher current after 2,400 second, indicating to high stability. In the case of $Pd_{99}Au_1$/C and $Pd_{99}Ru_1$/C, the stability testing results for those catalysts were equally that consistency with CV profile.
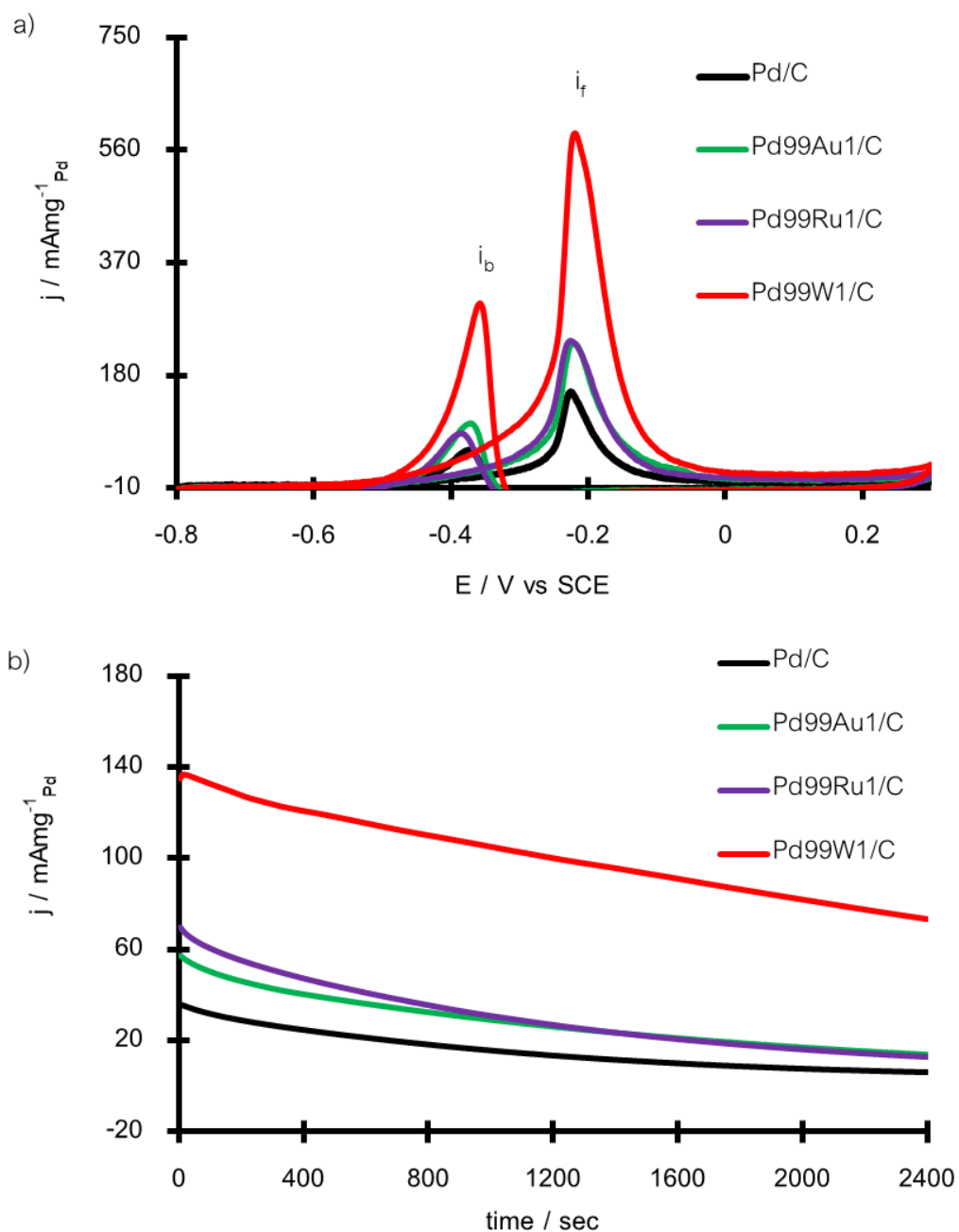
Figure 4.8 Cyclic voltammetry (a) and Chronoamperometry (CA) of MOR of as-prepared catalysts in a mixture of 1M KOH + 1M methanol using 50 mVsec^{-1} as sweeping rate.

In term of glycerol oxidation reaction (GOR) activity and stability were performed, as illustrated in Figure 4.9. The GOR activity of as-prepared catalysts were differently when compared with MOR and EOR. The GOR activity of $Pd_{99}Au_1$/C demonstrated a high

magnitude with a value of 552.13 $mAmg^{-1}_{Pd}$ with respect to 129.64 $mAmg^{-1}_{Pd}$ for Pd/C. In the case of adding Pd with Ru and W can be promoted GOR activity with 372.08 $mAmg^{-1}_{Pd}$ for $Pd_{99}Ru_1$/C and 239.27 $mAmg^{-1}_{Pd for}$ $Pd_{99}W_1$/C. Moreover, the low onset potential value can be observed from alloying of Pd with   -0.42 V. vs SCE for $Pd_{99}Au_1$/C where gave a significantly lower than 400 mV for Pd/C. Meanwhile alloyed Pd with Ru offered a lower E_s than Pd as -0.4 V. vs. SCE.

For comparison activity of three different fuels, the magnitude of forward current peak and onset potential were compared and displayed Table 4.3, respectively. In case of low-molecule alcohol (methanol and ethanol), it obvious that alloying with W metal can increase the activity of palladium metal compared with Ru and Au. From many literature claimed that Ru metal was a well-known promoter electrooxidation toward low molecule alcohol. In case of C_1-alcohol, PtRu is the best promoter for MOR, both acid and alkaline media [29, 30, 49-52]. Consistency with this work, the MOR activity of $Pd_{99}Ru_1$/C can be raised 1.56 times compared with Pd/C in alkaline environment. In addition to alloying with Au, the activity and stability results exposed a rather similarly with Ru. In contrast with $Pd_{99}W_1$/C displayed a significant higher activity 2.47 times than $Pd_{99}Ru_1$/C. In addition to C_2-alcohol, representative Ru in Pd catalyst is a fabulous for enhance EOR performance. According to Ma et al. [35], they explored PdRu/C for ethanol electrooxidation in alkaline media. From their results displayed PdRu gave a lower onset potential than Pd. It was consistency with Monyoncho et al. [36] studied the catalytic ethanol oxidation of Pd_xRu_{1-x} in alkaline solution. They observed that $Pd_{99}Ru_1$ gave significantly decrease onset potential. Likewise, $Pd_{99}Ru_1$ provided significant increase ethanol electrooxidation activity since the synergetic effect of Ru-oxide and Pd particles. The ethanol oxidation activity of modified Pd with Ru gave a good performance with respect to Pd/C, corresponded with previous work. Consistency with $Pd_{99}Ru_1$/C in this work, the EOR activity can be enhanced with Ru material. However, $Pd_{99}W_1$/C exhibited a better activity and stability for electrooxidation toward ethanol than $Pd_{99}Ru_1$/C, probably attributed to synergetic effect

between Pd and W. Consistence to the previous study by Liu et al. [53], they found that tungsten affected to promote electrocatalysis performance, both activity and stability, of palladium. PdW/C with atomic ratio 1:1 displayed that the lowest onset potential and the highest magnitude of forward anodic current peak. Consistency with this work, 1.37 times higher EOR activity than $Pd_{99}Ru_1$/C was obtained by modified Pd with W metal, due to the electronic effect of W to reduced onset potential [15]; which can be observed from XPS results. Unfortunately, adding of Au was not significantly improved electrooxidation activity of ethanol as well. For the GOR activity testing, it was in sharp contrast with MOR and EOR. Herein, $Pd_{99}Au_1$/C represented the superior activity; both the highest i_f and the lowest E_s, for GOR. Consistency with Zhang et al., they were to study the Au nanoparticle supported on carbon for AEM-DLFC [54]. They found that the GOR activity was a higher than methanol and ethylene glycol, attributed to deprotonation from Au material. Herein, $Pd_{99}Au_1$/C gave a significant enhance GOR activity, ascribed that Au can catalyzed for GOR reaction.

Table 4.3 Electrochemical properties from cyclic voltammetry of different fuels.

| Electrocatalysts	Methanol		Ethanol		Glycerol	
	E_s (V)	i_f (mAmg$^{-1}_{Pd}$)	E_s (V)	i_f (mAmg$^{-1}_{Pd}$)	E_s (V)	i_f (mAmg$^{-1}_{Pd}$)
Pd/C	-0.46	152.73	-0.49	209.32	-0.38	129.64
$Pd_{99}Au_1$/C	-0.46	235.67	-0.51	252.62	-0.42	552.13
$Pd_{99}Ru_1$/C	-0.46	238.58	-0.52	548.02	-0.40	372.08
$Pd_{99}W_1$/C	-0.48	588.41	-0.54	748.44	-0.39	239.27
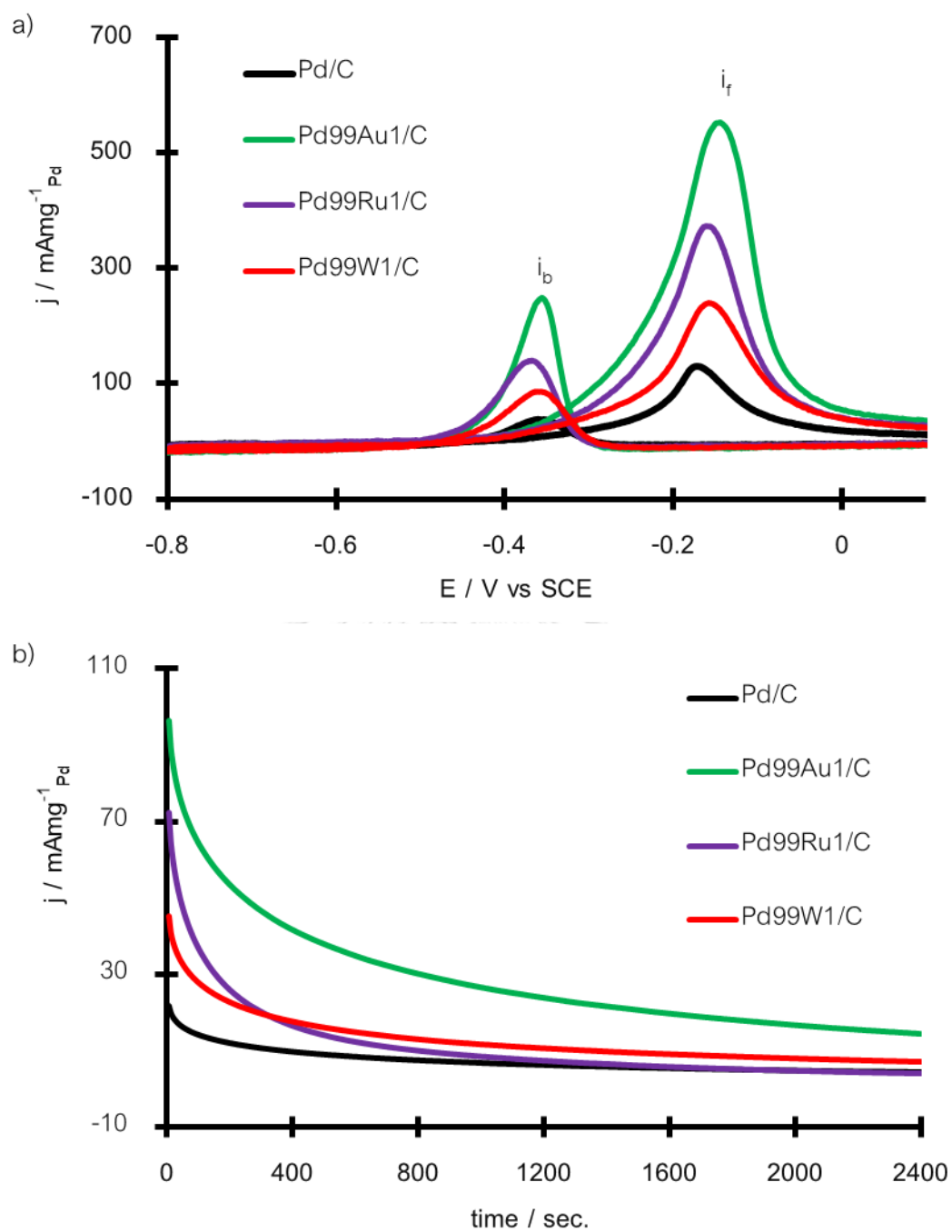
Figure 4.9 Cyclic voltammetry (a) and Chronoamperometry (CA) of GOR of as-prepared catalysts in a mixture of 1M KOH + 1M glycerol using 50 mVsec^{-1} as sweeping rate.

For all the results from Pd and Pd-based supported on Vulcan XC-72, It obvious that $Pd_{99}W_1$/C provided the best activity and stability results. In summary for first objective, the tungsten material should be selected for study in the next objective. Meanwhile, as-prepared Pd catalysts have potential for using in direct ethanol fuel cells.

4.2 THE EFFECT OF SUPPORTING MATERIAL AND FUNCTIONALIZATION METHODS ON ELECTROOXIDATION TOWARD ETHANOL

4.2.1 THE EFFECT OF FUNCTIONALIZATION METHOD FOR ETHANOL OXIDATION REACTION

According to Chapter 2, MWCNT has a significantly properties; e.g. high electrical conductivity, tolerant corrosive condition. Firstly, the effect of supporting material which composed of conventional CBs from (Vulcan XC-72) and MWCNTs (from Nanocyl®) was considered and conducted in a mixture of 1M KOH + 1M Ethanol. Before using these materials, the supporting materials were functionalized with acid-treatment by a mixture of 12M H_2SO_4 and 12M HNO_3 (as mention in Chapter 3, denoted as AO-CNT). For comparison with conventional acid treatment, non-covalent functionalization with poly(ethyleneimine); PEI, was prepared. The CV and CA profile of Pd supported on various support are displayed in Figure 4.10 (a), (b) for activity and stability measurements. The results reveal that functionalization with PEI provided an EOR activity with a value of 874 $mAmg^{-1}_{Pd}$ which was significant 2.6 times higher than conventional acid-functionalization with the value of 875 $mAmg^{-1}_{Pd}$, 334 $mAmg^{-1}_{Pd}$ for PEI-CNT and AO-CNT, respectively. According to Yang et al. [28], they studied the effect of different supporting material for MOR. They found that CNT exhibited a significant enhance MOR performance for Pt catalyst when compared with CB, ascribed to a good electrical conductivity of CNT. Nevertheless, some unique properties; e.g. electrical and mechanical properties, is demolished by using conventional acid functionalization. From many researches [29, 30,

55], they claimed that functionalization with mild condition with non-covalent method gave a better activity and stability results than conventional method. Among of functionalization agent, PEI can improve MOR activity and stability of Pt-based electrocatalyst. In this work, Pd supported on CNT functionalization with PEI was prepared and conducted for EOR in alkaline media, as shown in Figure 4.10 and Table 4.4. The results for comparison EOR activity and stability can be confirmed that the mild condition for CNT functionalization cannot damage intrinsic properties of CNT. Thus, the EOR performance can be improved when used this method.

Table 4.4 EOR activity of Pd supported on different functionalization method

Electrocatalysts	E_s (V)	i_f (mAmg$^{-1}_{Pd}$)
30Pd/AO-CNT	-0.56	334.20
30Pd/PEI-CNT	-0.57	874.58

However, the EOR performance should be developed by adding secondary material. From previous topic, the author found that tungsten material gave a significant improvement of EOR performance; both activity and stability. Unfortunately, the tungsten material is difficult to reduced [16], so It has been complicated to control the composition. It leads to utilizing phosphotungstic acid (PWA) as a tungsten source.
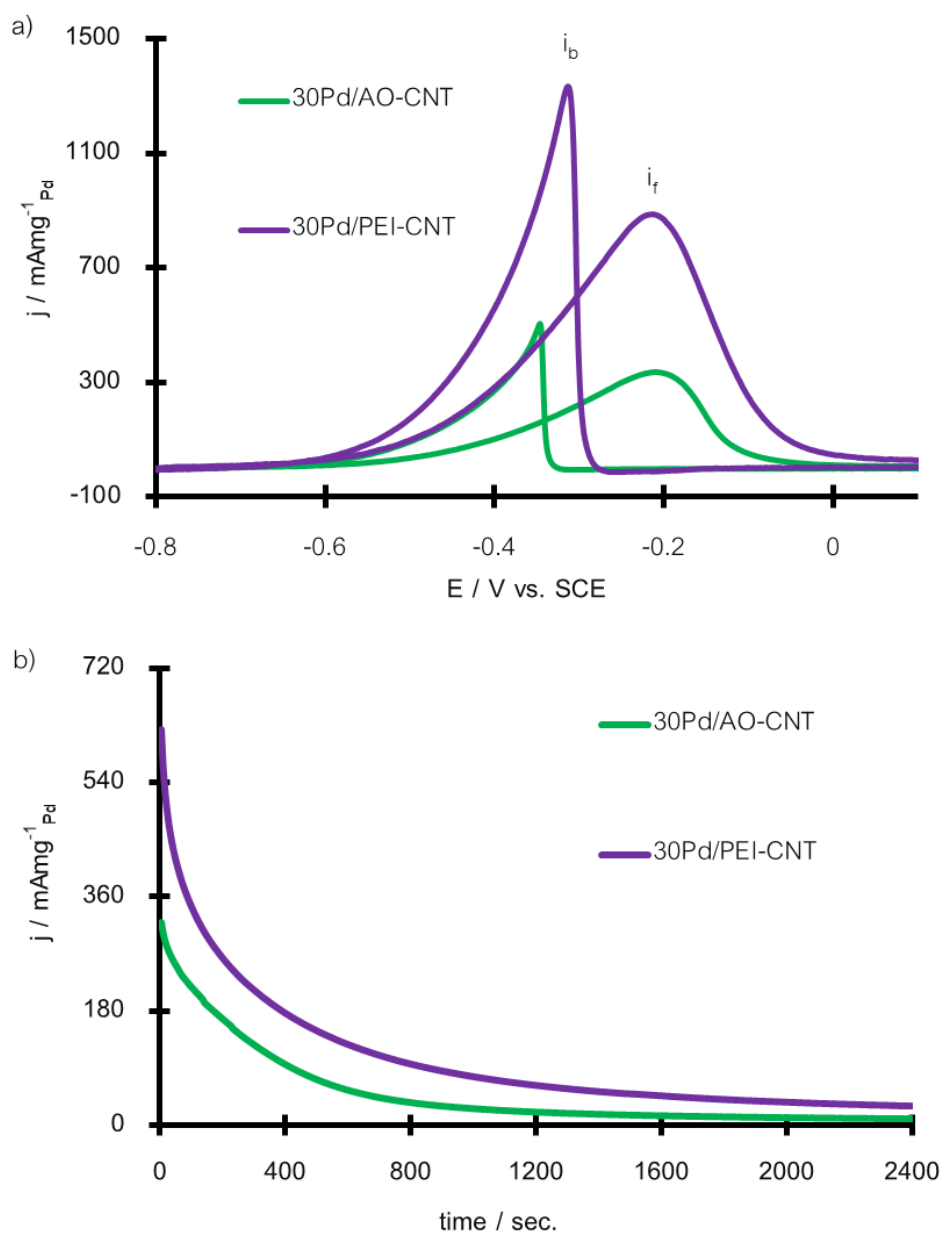
Figure 4.10 CV profile (a) and chronoamperometry at -0.3 V. vs. SCE (b) of ethanol oxidation reaction (EOR) of various functionalized CNTs in a mixture of 1M KOH + 1M ethanol with 50 mVsec^{-1} as sweeping rate.

4.2.2 SELF-ASSEMBLY POLYETHYLENEIMINE FUNCTIONALZATION ON MULTIWALL CARBON NANOTUBE WITH PHOSPHOTUNGSTIC ACID

In this topic, the palladium supported on PEI-CNT, which was assembled with PWA, was investigated for EOR, MOR, and GOR in alkaline media.

4.2.2.1 CHARACTERIZATIONS

The nanoparticle morphology was performed by TEM technique and displayed in Figure 4.11. A good metal cluster dispersion and low agglomeration were observed from 20Pd (Figure 4.11a) and 30Pd (Figure 4.11b) with mean particle 4.21 ± 0.95 nm., 4.32 ± 1.19 nm. for 20Pd and 30Pd, respectively. Unfortunately, the massive catalyst coalescence problem obvious when increasing Pd loading to 40%, as represented in Figure 4.11 c, with 12.33 ± 2.67 nm. Similar with 30Pd/AO-CNT from Figure 4.11 d, the huge problem for NPs aggregation still was observed with average particle size 18.51 ± 5.00 nm.

Figure 4.12 illustrated the XRD patterns of palladium nanoparticle supported in various CNT supporting. Among of them, the peaks settled approximately 25 $^{\circ}$ corresponded to [002] graphitic carbon structure from CNT support. In addition, the peaks at 2 theta settled around 40°, 46°, and 68° indicated to Pd FCC structure [111], [200], and [220], as reported by JCPDS card No. 03-065-2867.
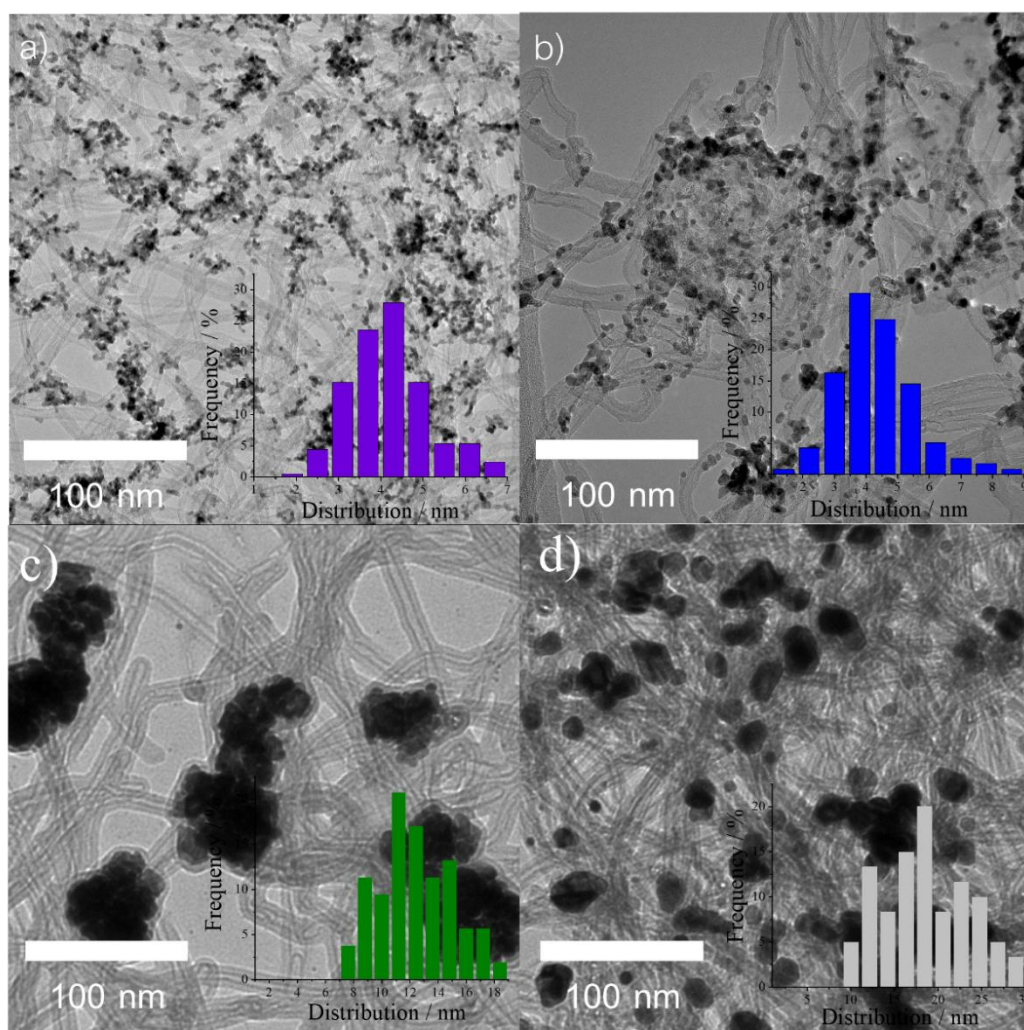
Figure 4.11 TEM images of 20Pd/PWA-PEI-CNT (a), 30Pd/PWA-PEI-CNT (b), 40Pd/PWA-PEI-CNT, and 30 Pd/AO-CNT (d).
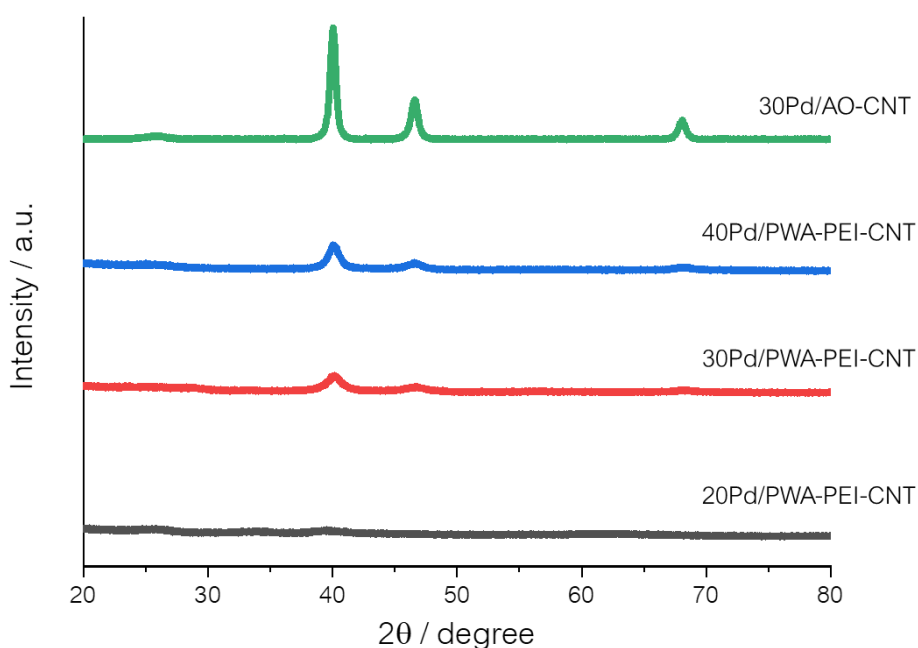
Figure 4.12 XRD pattern of as-prepared Pd NPs supported on self-assembly CNT with PWA and AO-CNT.

In the case of PEI, PWA, and Pd loading, TGA technique was conducted and displayed in Figure 4.13. The weight loss at 150 $^{\circ}$C to 500 $^{\circ}$C can be attributed to the weight loss of PEI and PWA with a loading of 7.58 wt.% and 9.19 wt.%, respectively [56]. For Pd-loading, after calculattion based on PWA-PEI-CNT which final residue was 21.52 wt.%, ascribed to tungsten oxide from PWA keggin structure [56]. The weight of Pd supported on PWA-PEI-CNT was 19.34 for 20Pd, 32.87 for 30Pd, and 41.41 for 40Pd. Moreover, the weight of Pd supported on AO-CNT was 28.35 wt.%. Among of this TGA results indicated to succuessfully deposite Pd on thoes supports using L-ascorbic acid as reducing agent.
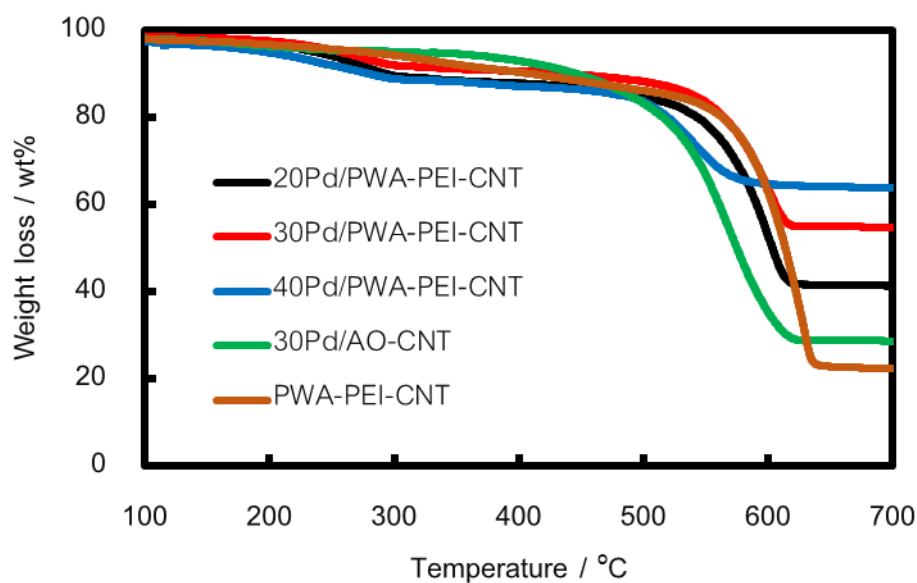
Figure 4.13 TGA curves of as-prepared catalyst and the supporting materials

The evidence for support represent of PWA assemble on PEI-CNT was analyzed by FTIR measurement and illustrated in Figure 4.14. The FTIR spectra revealed that the characteristic band of PWA corresponded to the interaction between oxygen atom in PWA kegging structure in a wavelength of 2400 cm^{-1} to 650 cm^{-1}. In case of pristine PWA and PWA-PEI-CNT, their spectra demonstrated the characteristic band of Keggin type heteropolyacid which located at 1079 cm^{-1}, 980 cm^{-1}, 898 cm^{-1} and 821 cm^{-1}, attributed to P-O_a, W-O_d, W-Ob-W and W-O_c-W, respectively [57, 58]. In contrast with pristine CNT, AO-CNT and PEI-CNT, no any peak corresponded to PWA. It indicated to successfully for functionalization with PWA on PEI-CNT.
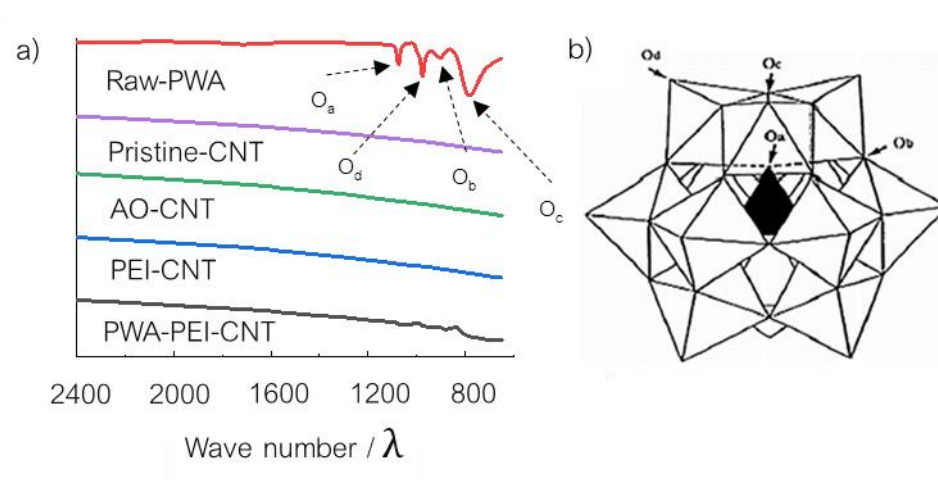
Figure 4.14 FTIR spectra of different support material (a) and illustration of Keggin structure of heteropoly acid (b). [58]
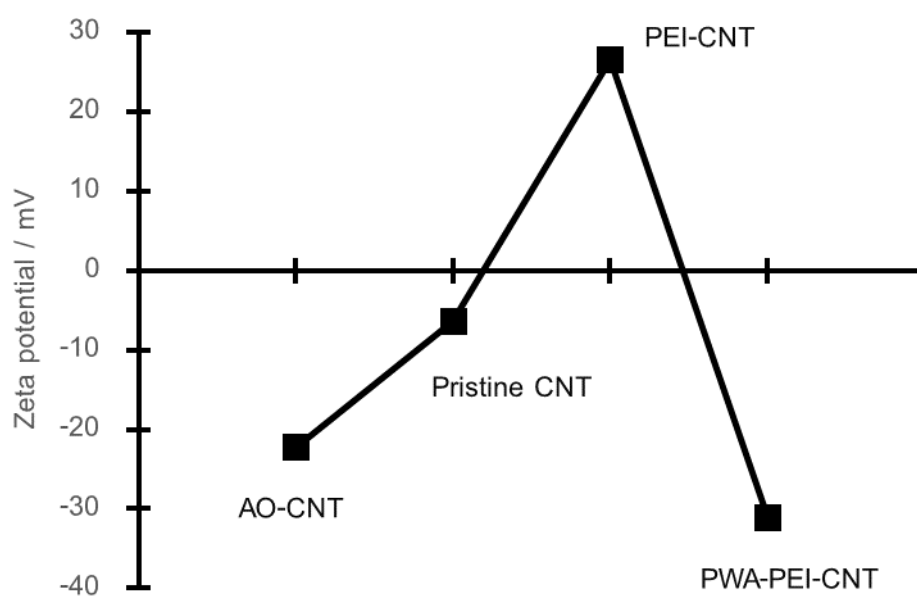
Figure 4.15 Zeta potential of supporting CNT in this experiment.

The zeta potential was conducted in order to observe the charge on CNT, as displayed in Figure 4.15. For comparison between pristine CNT and AO-CNT, the zeta

potential of AO-CNT was -22.23 mV higher than pristine CNT with a value of -6.37 mV, attributed that the negative species with carboxyl and/or hydroxyl group were introduced by acid functionalization [30]. Controversy with PEI functionalization, it obvious that the zeta value was positive with 26.53 mV, suggested to the represent of PEI on CNT surfaces. Meanwhile, when considering at PWA-PEI-CNT became negative again with -31.13 mV as zeta potential value, ascribed that PWA was introduced on PEI-CNT surfaces [56].

4.2.2.2 ELECTROCHEMICAL PROPERTIES OF AS-PREPARED CATALYST

The EOR activity (a) and short-term stability at -0.3 V vs SCE were carried out by CV and CA technique in a mixture of 1M KOH + 1M ethanol with N_2 environment, as shown in Figure 4.16. The activity of 30Pd/PWA-PEI-CNT gave a high mass activity with 3,313.87 $mAmg^{-1}_{Pd}$ and low onset potential with -0.57 V vs SCE which provided a significant 15.86 times higher mass activity and 40mV Es lower than 30Pd/AO-CNT with 208.89 $mAmg^{-1}_{Pd}$, -0.53 V vs SCE as mass activity, onset potential, respectively. In the case of 20Pd, the EOR activity was 1,343.36 $mAmg^{-1}_{Pd}$ and -0.56 V vs SCE for Es, which was 2.47 times lower activity and 10 mV higher Es than 30Pd. It was surprised when increasing Pd loading to 40%. The EOR activity significantly plummeted 394.07 $mAmg^{-1}_{Pd}$ while the onset potential was slightly high at -0.55 V vs SCE, attributed to the coalescence of Pd NPs. For CA results, it can be observed that 30Pd/PWA-PEI-CNT provided significantly sTable after polarization time at 2,400 sec with 314.23 $mAmg^{-1}_{Pd}$ when compared with 10.27 $mAmg^{-1}_{Pd}$ of 30Pd/AO-CNT. Meanwhile, the others Pd loading; both 20Pd and 40Pd, provided a similar current after polarization with 22.88, 25.05 and 10.27 $mAmg^{-1}_{Pd}$ for 20Pd and 40Pd. Consequently, the optimized Pd loading on PWA-PEI-CNT should be 30%.

a)

b)
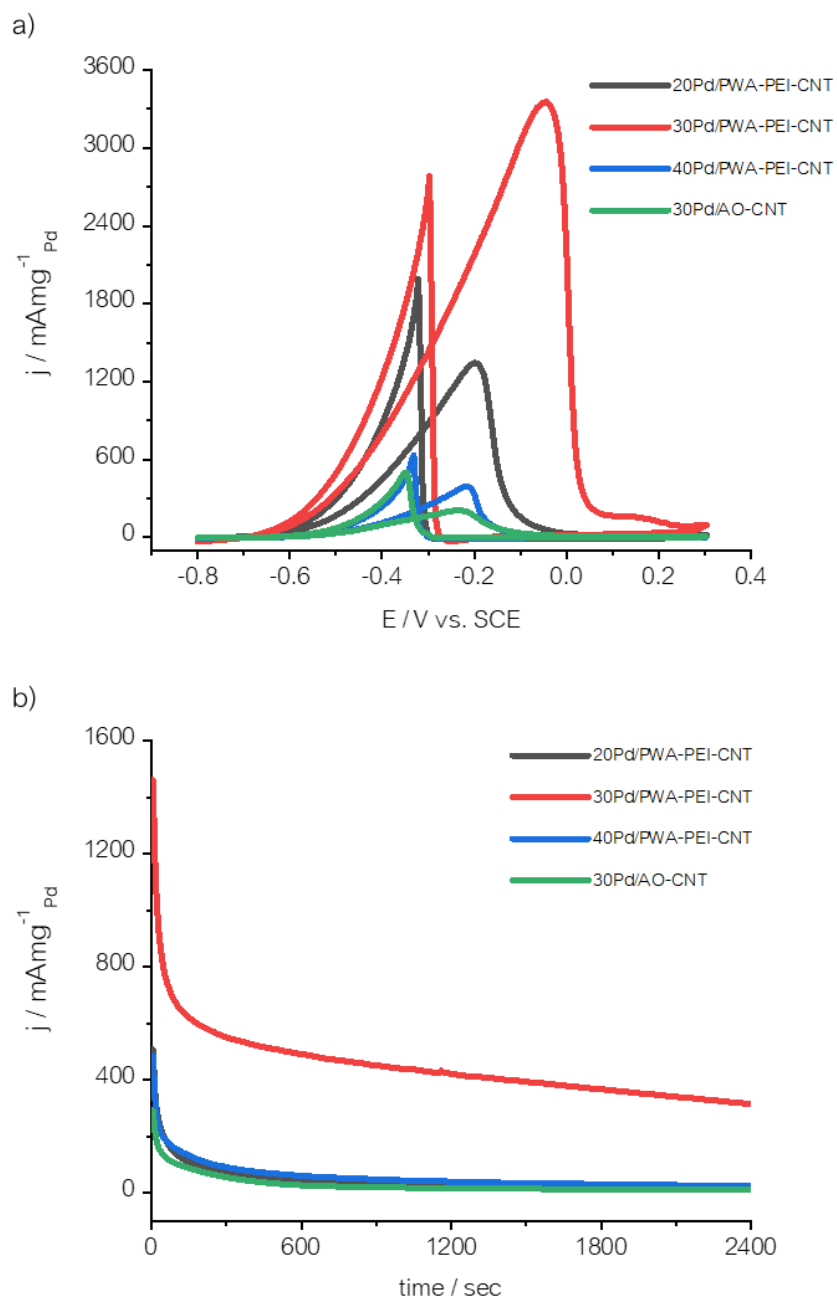
Figure 4.16 Cyclic voltammetry of EOR (a) and Chronoamperometry (b) of 20Pd, 30Pd, 40Pd supported on PWA-PEI-CNT compared with 30Pd/AO-CNT with N_2-saturated 1 M KOH + 1 M ethanol.

The electrooxidation toward methanol of self-assembly electrocatalysts series were measured in a mixture of 1M KOH + 1M methanol with saturated N_2 condition and illustrated in Figure 4.17. The MOR activity results reveal that 20Pd/PWA-PEI-CNT gave a

mass activity with 483.16 mAmg$^{-1}_{Pd}$ and -0.39 V vs SCE for Es. In case of increasing Pd loading to 30Pd, the MOR activity was greatly enhanced to 1,067.29 mAmg$^{-1}_{Pd}$ and -0.41 V vs SCE that significantly higher that 20Pd and 317.44 mAmg$^{-1}_{Pd}$, -0.32 vs SCE for 30Pd/AO-CNT. Again when increasing to 40Pd, the activity of MOR was dropped with 356.25 mAmg$^{-1}_{Pd}$ and -0.35 V vs SCE for mass activity and onset potential. Consistency with MOR activity, CA profile of as-prepared catalyst show the best stability after polarization 2,400 sec was achieved by 30Pd with 71.55 mAmg$^{-1}_{Pd}$ where was critical about 10 times higher than 30Pd/AO-CNT. Moreover, this loading gave a better stability than 20Pd and 40Pd after 2,400 sec with the current of 18.38, 14.33 mAmg$^{-1}_{Pd}$ for 20% and 40%, respectively.

Furthermore, GOR activity (Figure 4.18a) and stability (Figure 4.18b) were measured in 1 M KOH + 1 M glycerol. The GOR activity was enhanced by using self-assembly CNT supporting Pd NPs. The best activity was still obtained from 30Pd with mass activity 1,875.8 mAmg-1Pd and -0.4 V vs SCE as Es that gave a significant increase with respect to 30Pd/AO-CNT with -0.26 V vs SCE, 275.73 mAmg-1Pd for onset potential, mass activity. In the case of 20Pd, the activity was lower than 30Pd with 1,164 mAmg$^{-1}_{Pd}$ and Es = -0.31 but still higher than 30Pd/AO-CNT. Nevertheless, the increasing Pd loading to 40Pd did not provided enhance GOR activity which was 433.27 mAmg$^{-1}_{Pd}$ and -0.28 V vs SCE, similar to observe from MOR and GOR. Moreover, the CA measurement reveal that the utilization of self-assembly PEI-CNT with HPA support Pd NPs, especially 30% ,can be significantly improved stability for GOR. for instance, the initial current of 30Pd was 357.36 mAmg$^{-1}_{Pd}$, then decreasing until leach to sTable at 60.45 mAmg$^{-1}_{Pd}$ after 2,400 sec that was higher than 30Pd/AO-CNT with 2.82 mAmg$^{-1}_{Pd}$ after 2,400 sec. However, 20Pd and 40Pd supported on PWA self-assemble did not shown importantly improve stability compared with 30Pd.

a)

b)
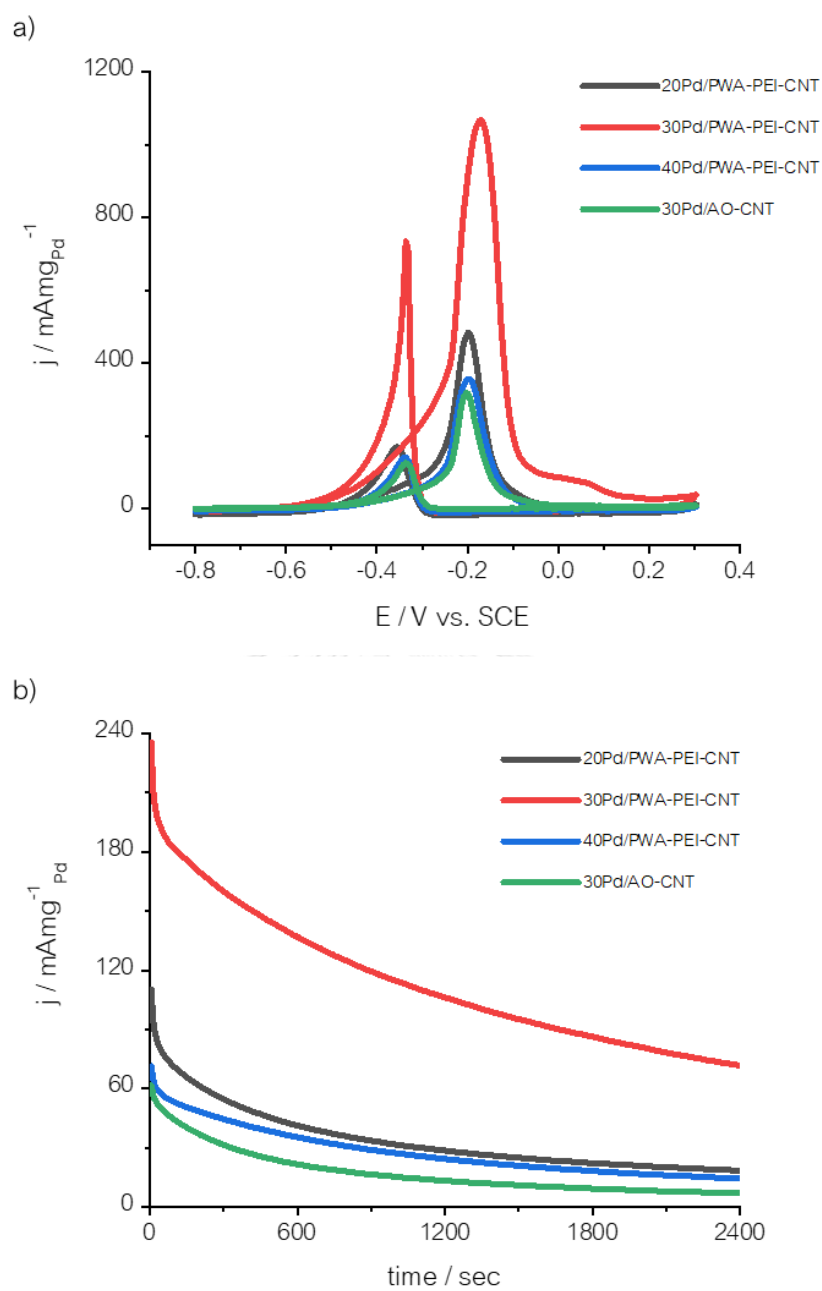
Figure 4.17 MOR activity (a) and CA (b) of various Pd NPs loading supported on PWA-PEI-CNT and 30Pd/AO-CNT in a mixture of 1 M KOH + 1 M methanol with saturated N_2.

a)

b)
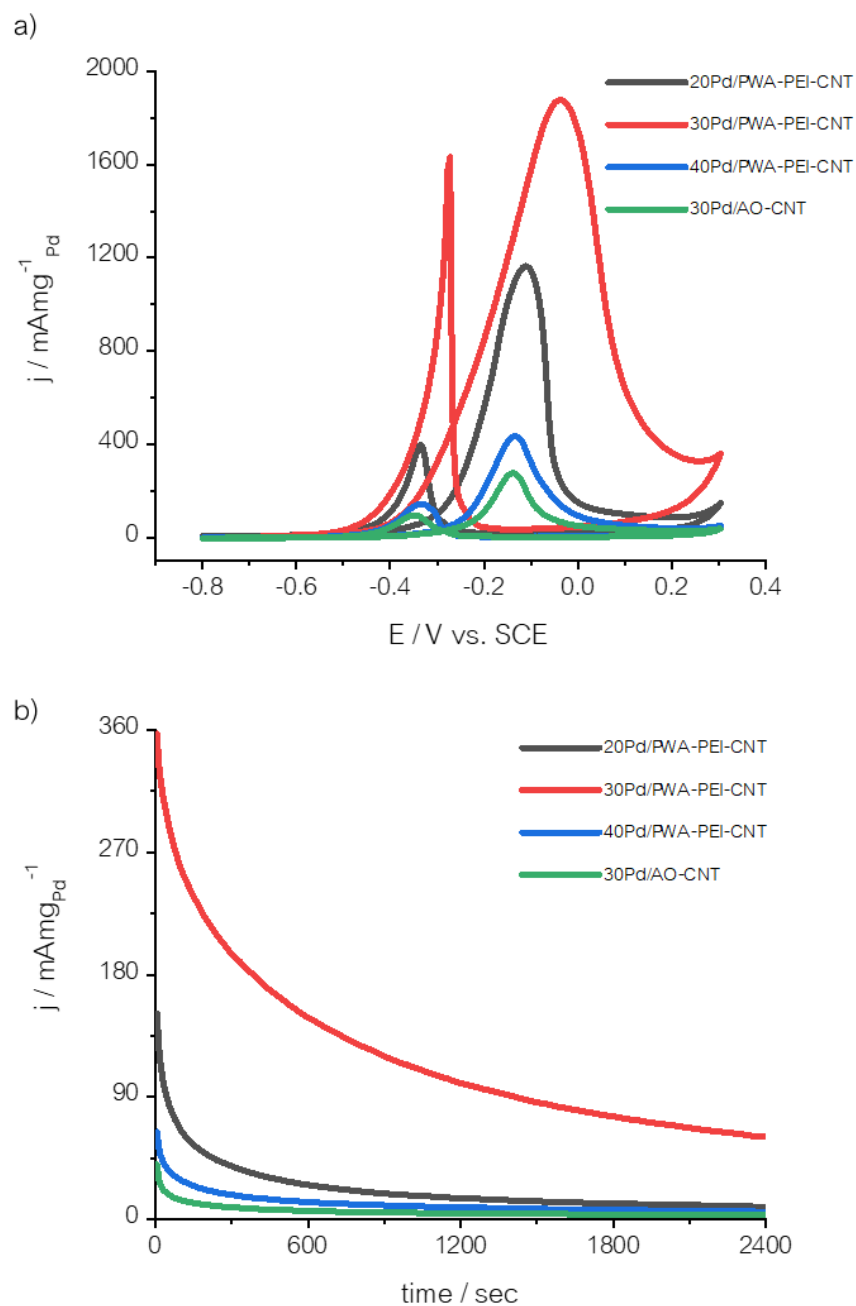
Figure 4.18 GOR activity (a) and stability (b) of Pd NPs supported on PWA-PEI-CNT with different loading and 30Pd/AO-CNT in a mixture of 1 M KOH and 1 M glycerol.

The Table 4.5 is illustrated for the comparison of the three different liquid fuels. It was obvious that the as-prepared Pd NPs was potentially used as electrocatalyst for EOR reaction that observed from a high mass activity and low onset potential. In the case of

Pd NPs loading, 30Pd loading was the best optimized loading for the electrooxidation toward alcohol that MOR, EOR, and GOR shown the highest i_f for each any fuels.

Table 4.5 Electrochemical properties of alcohol oxidation for self-assembly CNT series compared with conventional acid functionalization.

Electrocatalysts	Methanol		Ethanol		Glycerol	
	E_s (V)	i_f (mAmg$^{-1}_{Pd}$)	E_s (V)	i_f (mAmg$^{-1}_{Pd}$)	E_s (V)	i_f (mAmg$^{-1}_{Pd}$)
20Pd/PWA-PEI-CNT	-0.39	483.16	-0.56	1,343.36	-0.31	1,164.68
30Pd/PWA-PEI-CNT	-0.41	1,067.29	-0.57	3,313.87	-0.40	1,875.80
40Pd/PWA-PEI-CNT	-0.35	356.25	-0.55	394.07	-0.28	433.27
30Pd/AO-CNT	-0.32	317.44	-0.53	208.89	-0.26	275.73

4.2.3 EFFECT OF NEW-CLASS OF SUPPORTING MATERIAL, NICKEL SINGLE ATOM SUPPORTED ON MWCNT (NISA-N-CNT)

Recently, Prof. Jiang's group successfully synthesized a new class of transition-metal and nitrogen co-doped carbon nanotubes (NiSA-N-CNT), and these nanotubes are composites of atomically dispersed Ni-N$_x$ species with high metal content up to 6 at% and 20 wt% [59]. These single atoms doped homogenously doped carbon nanotubes showed outstanding activity, selectivity, and stability for electrochemical CO_2-to-CO conversion. However, its demonstrated poor catalysts for other catalytic reactions. Here we deposited the Ni SAC doped carbon nanotubes with Pd nanoparticles, the results showed that the Ni SACs could significantly promote the activity of methanol, ethanol, and ethylene glycol oxidation.

4.2.3.1 CHARACTERIZATION OF PALLADIUM SUPPORTED ON NISA-N-CNT

Figure 4.19 illustrates catalyst morphology and size-distribution of decorated NiSA-N-CNT surfaces with palladium nanoparticles. In the case of 20% Pd loading, the TEM images reveal that Pd nanoparticles with average size of 8.1±2.2 nm nm were uniformity supported on NiSA-CNT. When increasing the Pd loading, the Pd nanoparticle increases as well. The particle size of 30Pd/NiSA-CNT was slightly bigger than 20 Pd/NiSA-CNT with an average size of 9.2 ± 2.9 nm. In addition, 40Pd loading, average particle size was 11.8 ± 3.4 nm. The average particle size of Pd NPs in Pd/N-CNT was 7.45 ± 1.4 nm.
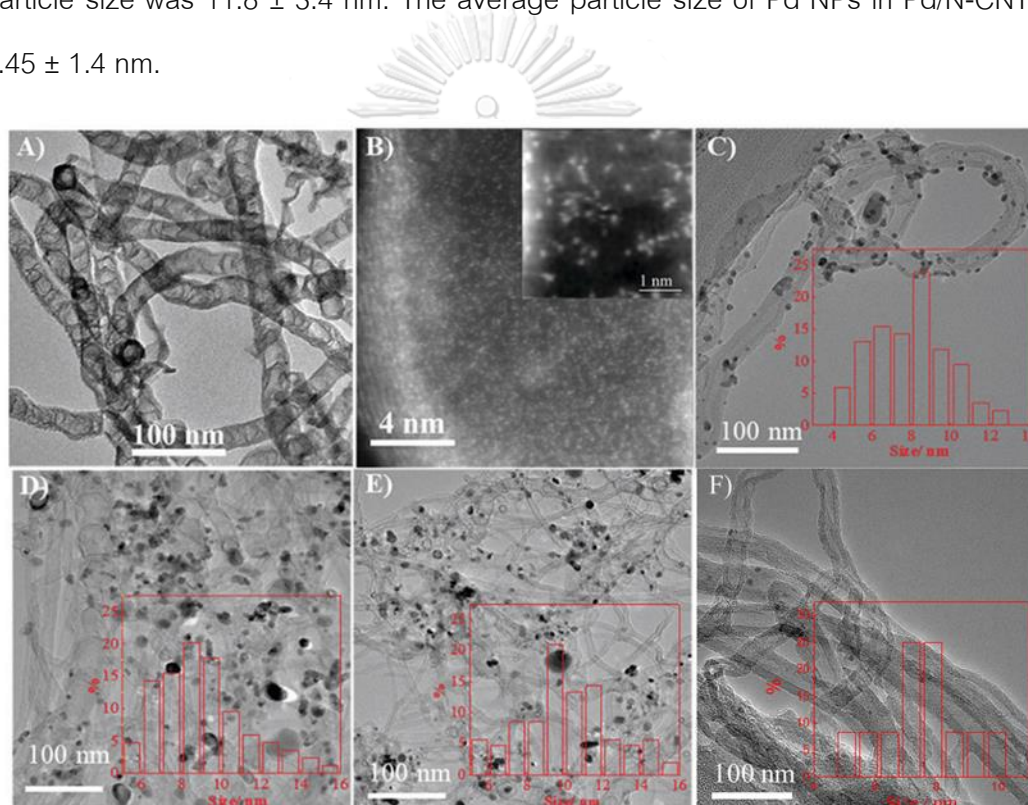
Figure 4.19 TEM images of as-prepared Pd NPs supported on NiSA of NiSA (A), and AC-STEM of NiSA (B); TEM images of 20Pd/NiSA (C); 30Pd/NiSA (D); 40Pd/NiSA (E); and 30Pd/N-CNTs (F.)

Addiotionally, the catalyst loading was confirmed by TGA technique in a range of 100 ^{o}C to 800 ^{o}C with 50 ml/min of air, as represented in Figure 4.20. For undecorated NiSA-N-CNT was initially decomposed around 400 ^{o}C and fully decomposed approximately 500

$^{\circ}$C with the weight of sample Table at 16.86 wt.%. In case of decorated nickel atomically and Pd supported on N-CNT, the weight loss around 250 $^{\circ}$C to 400 $^{\circ}$C should be assigned to PdO formation [44]. For the reaction of carbon decomposition to form CO_2 occurred at 450 $^{\circ}$C and complete around 600 $^{\circ}$C after that the catalysts weight loss was represented at 35.22%, 45.51% and 54.6% for 20%, 30% and 40% of decorated nickel atomically with palladium. It was found after deducted with weight loss from NiSA-N-CNT that Pd loading of each catalyst was 18.36%, 28.29%, and 37.74%. In addition, the Pd loading on N-CNT was 32.16%. Consequently, Pd metal was successfully supported on both NiSA-N-CNT and N-CNT.
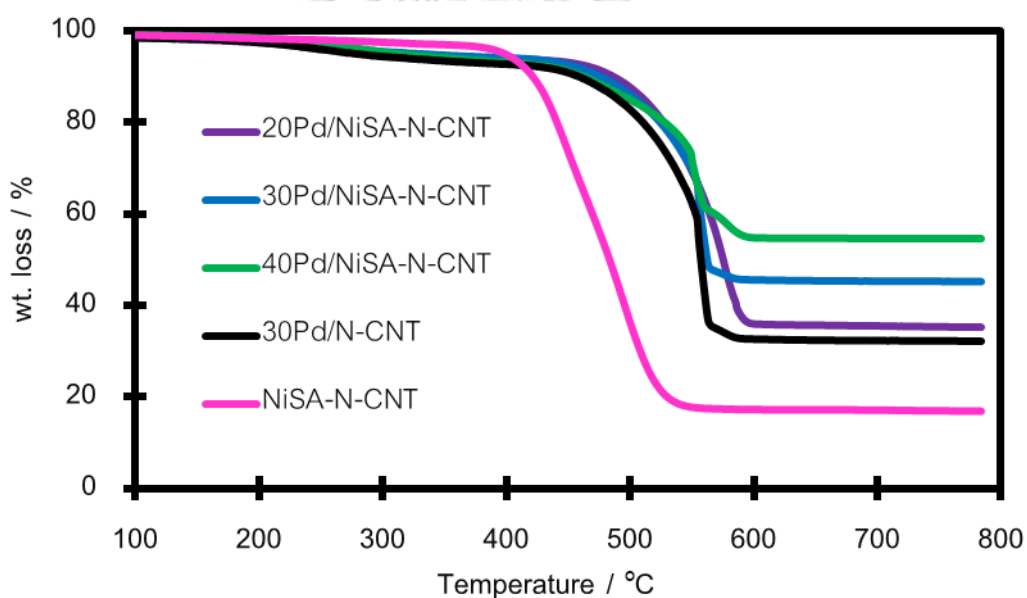
Figure 4.20 TGA curve of as-synthesized catalysts.
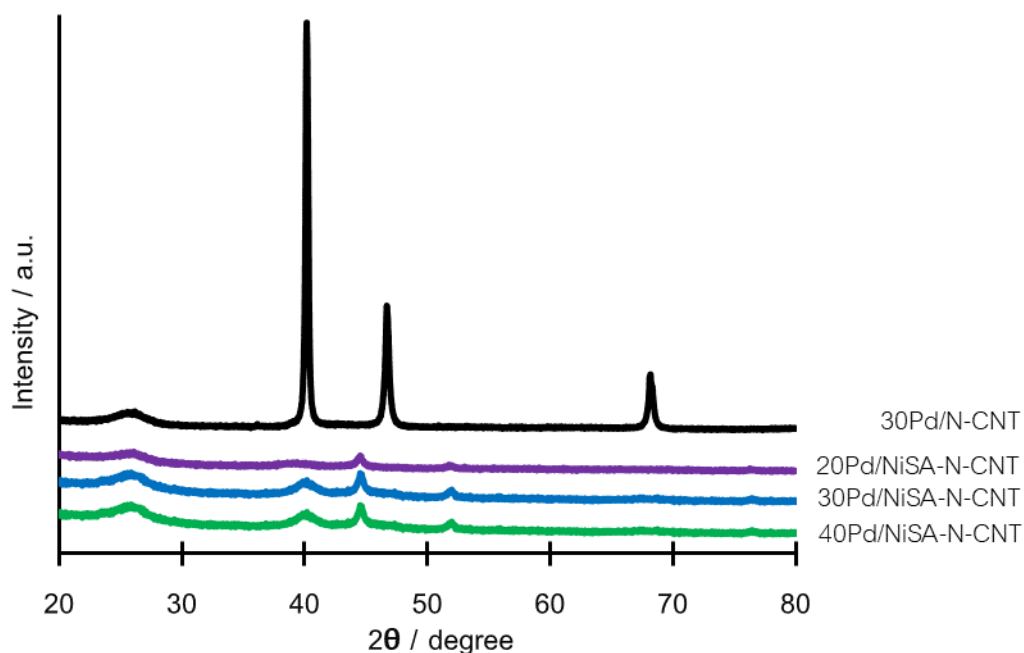
Figure 4.21 XRD pattern of Palladium supported on atomically disperse nickel onto MWCNTs and supported on nitrogen-doped MWCNTs, respectively.

The XRD technique was conducted to confirm crystal structure of the materials (Figure 4.21). The first peak of all patterns located around 25° indicated to 002 plane of graphite material. In case of various loading of palladium supported NiSA-CNT appeared the peak around $40^{\circ}, 45^{\circ}$ and 68° indicated that palladium [111], [200] and [220] faced-center cubic (FCC) crystal structure (JCPDS 00-005-0681). In addition, there were observed that the peak corresponded to FCC crystal structure of nickel nearly $45^{\circ}, 53^{\circ}$, and 76°, ascribed to [111], [200], and [220] FCC with (JCPDS 00-004-0850).

The XPS measurement was performed to understand the elemental surfaces and interaction of Pd with NiSA-N-CNT (Figure 4.22.a-d, Table 2). For survey scan (Figure 4.22 a), the spectra illustrated the peaks corresponded to C 1s, N 1s, O 1s, Pd 3d and Ni 2p which located around 285 eV, 400 eV, 531 eV, 340 eV, and 870 eV, respectively. In the case of high resolution for the N1s peak of NiSA-N-CNT, their decorated and 30Pd/N-CNT is located around 399 eV, confirmed the represent of nitrogen-doped on CNT surfaces.

Furthermore, the XPS spectra of high resolution from 890 eV. to 840 eV. of decorated nickel atomically with palladium and NiSA-N-CNT have been observed the two peaks which were located at 872.4 eV and 854.9 eV ascribed to Ni2p3/2 and Ni2p1/2, respectively. While the Pd 3d3/2 and 3d5/2 for Pd/N-CNT were located at 340.6 and 355.3 eV, which was 0.3-0.6 eV lower than that of 20Pd/NiSA-N-CNT with a number of 341.0 and 355.7 eV, respectively. The huge positive shift of the Pd 3d peaks revealed the electron donation from a donation from the Pd nanoparticles to NiSA-N-CNT making the Pd more likely in an oxide form rather than metallic form. Further increase the Pd loading will lead to a decrease of binding energy, probably attributed to the formation of larger Pd particles with leads to a delocalization of the electrons [60].
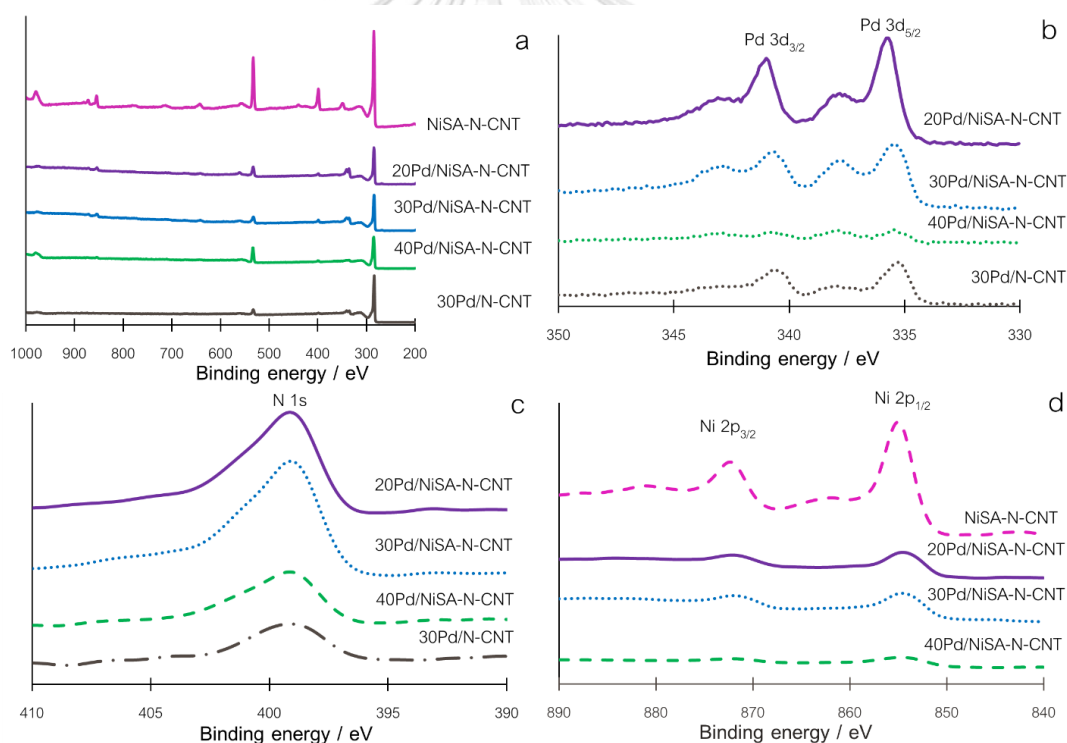
Figure 4.22 XPS spectra of as-synthesized electrocatalysts; survey scan (a), Pd 3d (b), N 1s (c), and Ni 2p (d).

4.2.3.2 ELECTROCHEMICAL PROPERTIES OF PALLADIUM NANOPARTICLES SUPPORTED ON ATOMMICALLY NICKEL TOWARD ETHANOL

Firstly, Nickel single atom supported on carbon nanotube (NiSA-N-CNT) was conducted in different liquid alcohols, as represented in Figure 4.23. It observed that no any peak corresponded to alcohol electrooxidation. Thus, NiSA-N-CNT is not active for methanol, ethanol, and glycerol electrooxidation.
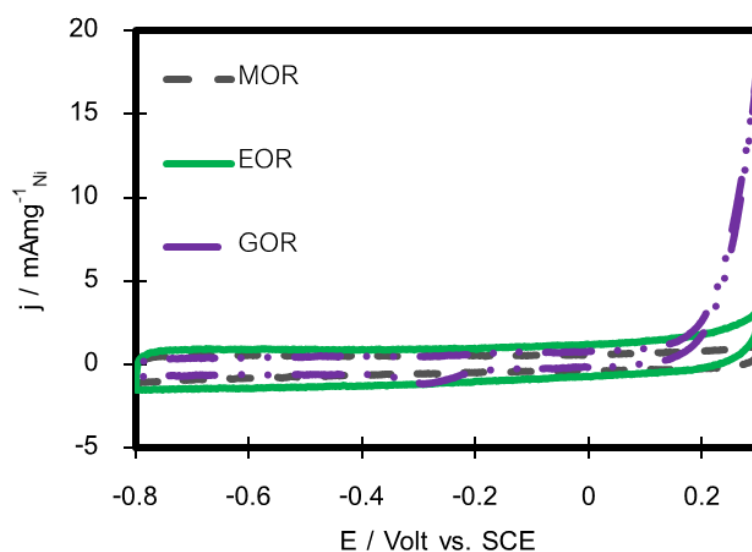
Figure 4.23 Electrooxidation toward alcohols of NiSA-N-CNT in a mixture of 1M KOH + 1M alcohol under N_2-rich environment.

The Pd material is investigated for ethanol electrooxidation in N_2-saturated 1M KOH + 1M Ethanol (Figure 4.24a and b). Both the activity and stability for ethanol oxidation is significantly improved after the Pd nanoparticles supported on NiSA-N-CNT. For instance, the onset potential and forward current density of Pd/N-CNT is -0.52 V and 22.53 mAmg$^{-1}_{Pd}$. While the onset potential for 20Pd/NiSA-CNT is -0.57 V, which was lower than that of Pd/N-CNT. And the increase of Pd loading will resulted in a decrease of mass activity with a onset potential of -0.57 V and mass current density of ~1,200 mAmg$^{-1}_{Pd}$, and the onset potential and current density decrease to 20 mV and 753.63 mAmg$^{-1}_{Pd}$ for 30Pd/NiSA-N-CNT, and -0.53 V and 85.87 mAmg$^{-1}_{Pd}$ for 40Pd/NiSA-N-CNT. The

chronoamperometry is investigated in N_2-saturated 1M KOH + 1M Ethanol at -0.3 V, the rapidly current drop dramatically indicated that blocking of the active surface by intermediate species. Pd supported on NiSA-CNT slightly higher than supported Pd on N-CNT. For example, the initial current density is 645 mAmg$^{-1}_{Pd}$ for 20Pd/NiSA-CNT, decrease to 16 mAmg$^{-1}_{Pd}$ after 2,400 sec., while this current density is still higher 3.74 and 10 times of 30Pd/NiSA-N-CNT and 40Pd/NiSA-N-CNT.

The Pd nanoparticles were investigated for methanol oxidation in N_2-saturated 1 M KOH + 1M methanol, as displayed in Figure 4.25. Pd nanoparticles supported on N-CNT exhibits an onset potential of -0.40 V, and a forward peak current density of 35.84 mAmg$^{-1}_{Pd}$. Supporting the Pd nanoparticles could significantly enhance the methanol oxidation activity. The 20Pd/NiSA-CNT shows an onset potential of -0.47 V, and 60 mV higher than that of Pd/N-CNT as well as the current density for methanol oxidation was 335.91 mAmg$^{-1}_{Pd}$, which was approximately 10 times of Pd/N-CNT. When increasing the loading actually will lead to a decrease of mass activity from 335.91 for 20Pd/NiSA-CNT to 123.23 for 30Pd/NiSA-CNT and 72.35 for 40Pd/NiSA-CNT. The decrease of mass current density is due to the increase of the Pd nanoparticle size which leads to the poor synergistic between the Pd nanoparticles with NiSA-CNT. This is consistent with the XPS results where shows the shift of the Pd 3p, N 1s and Ni 2p peaks are more significantly in the case of 20Pd/NiSA-CNT compared with that of 30Pd/NiSA-CNT and 40Pd/NiSA-CNT. These results reveal the NiSA-CNT could significantly enhance the methanol oxidation activity of Pd nanoparticles. Furthermore, short-term stability of each catalyst was carried out by chronoamperometry technique, as displayed in Figure 4.25 b. It was obvioused that decorated Ni-SA-CNT with 20% Pd loading provided the best stable than others catalyst, the initial current density is around 110 mAmg$^{-1}_{Pd}$ for 20Pd/NiSA-CNT, and after 2400 s, the current density decrease to 22 mAmg$^{-1}_{Pd}$, which is significantly higher than that of 2.67 and 0.82 mAmg$^{-1}_{Pd}$ for 30Pd/NiSA-CNT and 40Pd/NiSA-CNT, respectively. The improved stability likely due to the enhancement of the resistance of the Pd

nanoparticle for intermediate such as CO or HCO etc. poisoning on the Pd surface. These results revealed that the interaction between Pd nanoparticle and NiSA-CNT could improve the activity and stability for methanol oxidation.
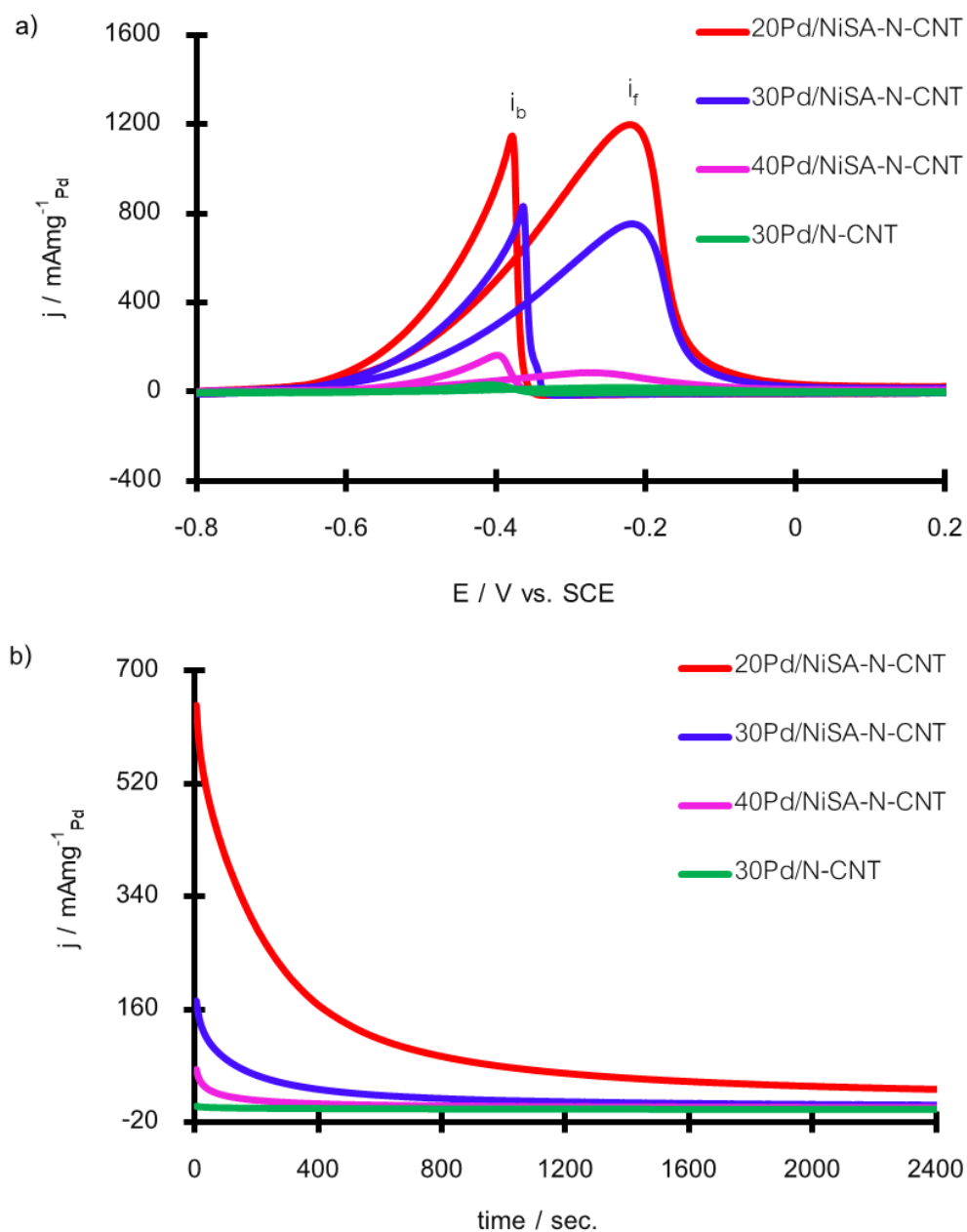
Figure 4.24 EOR activity (a) and CA result (b) at -0.3 V. vs. SCE of various loading Pd /Ni-SA-CNT and N-doped CNT in a mixture of 1M KOH + 1M Ethanol under N_2-saturated condition.
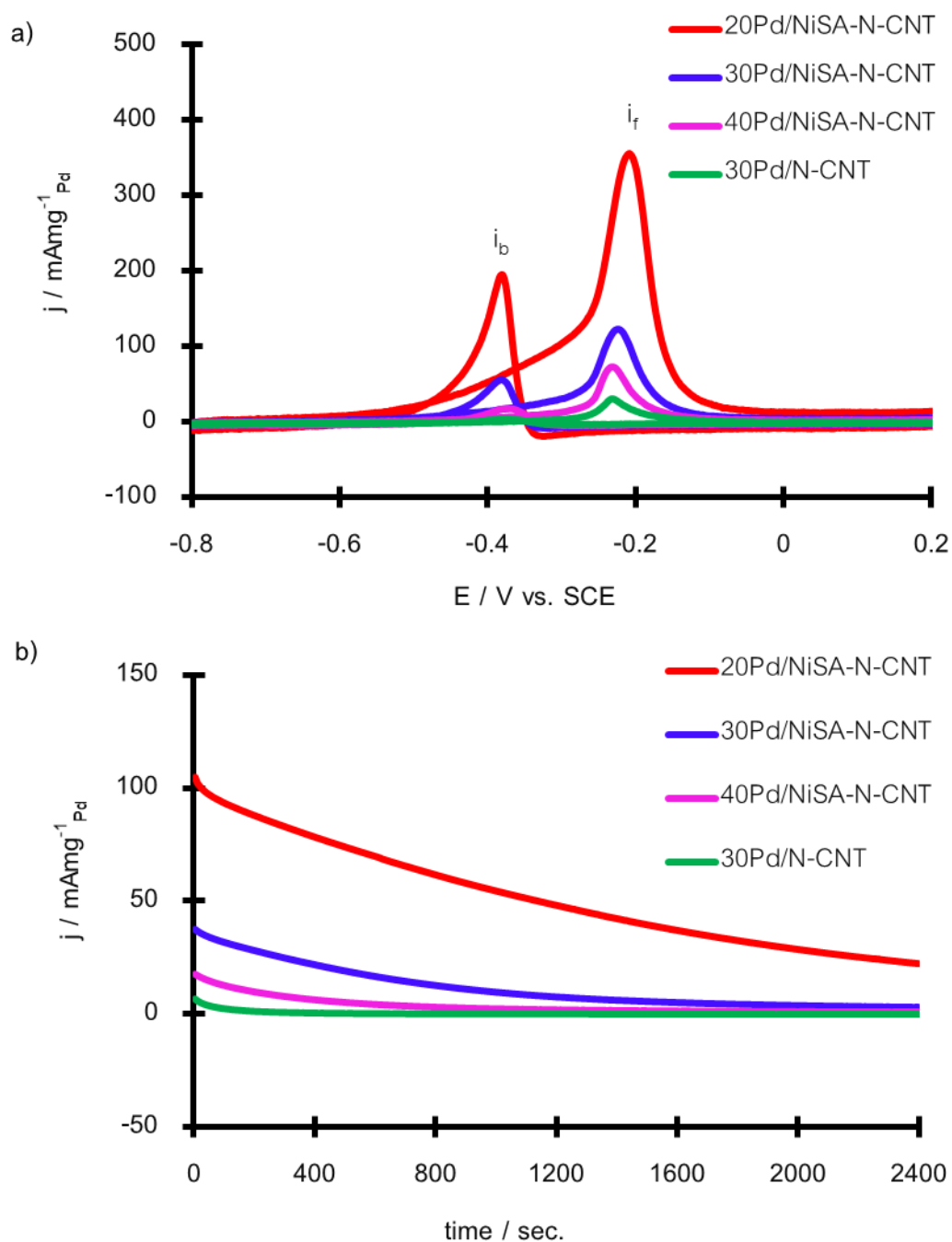
Figure 4.25 MOR activity (a) and chronoamperometry profile (b) of decorated Ni-SA-CNT with Pd NPs in N_2-saturated 1M KOH + 1M methanol at -0.3 V. vs. SCE.

In the case of GOR, the Pd/NiSA-N-CNT is further investigated in a N_2-saturated 1M KOH + 1M glycerol with sweeping rate 50mVsec^{-1} (Figure 4.26). The mass activity for 20Pd/NiSA-CNT was ~ 777 mAmg$^{-1}_{Pd}$ with a onset potential of -0.35 V. The current density

is more than 5 times of 30Pd/N-CNT with mass activity of 50.14 mAmg$^{-1}_{Pd}$, suggested that NiSA-N-CNT could also significantly improve the activity of Pd for glycerol oxidation. In this case 30Pd/NiSA-CNT, the mass current density (246.46 mAmg$^{-1}_{Pd}$) is 3 times lower than 20Pd/NiSA-CNT. The current density further decreases to 137.43 mAmg$^{-1}_{Pd}$ for 40Pd/NiSA-CNT. Similarly, the stability of Pd/NiSA-CNT is also significantly improved, 20Pd/NiSA-CNT shows significantly higher stability compared with 30Pd/NiSA-CNT, 40Pd/NiSA-CNT and 30Pd/N-CNT, further disclose the improved stability after the Pd nanoparticles incorporated with NiSA-N-CNT.

In comparison alcohol oxidation activity of Pd NPs supported on NiSA-N-CNT, the results are shown in Table 4.6. For non-decorative NiSA-N-CNT displayed none active for methanol, ethanol and glycerol oxidation, as reported from Figure 4.23. Pd nanoparticles supported on N-CNT also show extremely poor activity for methanol, ethanol and glycerol oxidation. On the other hand, supporting Pd nanoparticles on NiSA-N-CNT will significantly promote the electrochemical activity of these organic molecules oxidation. The enhanced activity probably attributed that the NiSA-N-CNT could draw electron from the Pd nanoparticles which make the Pd is more positively charged to form Pd oxide species. These Pd oxide species could improve the desorption of the carbonaceous intermediates which has been evidenced by the enhanced stability of Pd/NiSA-N-CNT. These results demonstrated NiSA-N-CNT is an outstanding catalysts support for electrochemical oxidation of C$_2$-alcohol molecules.
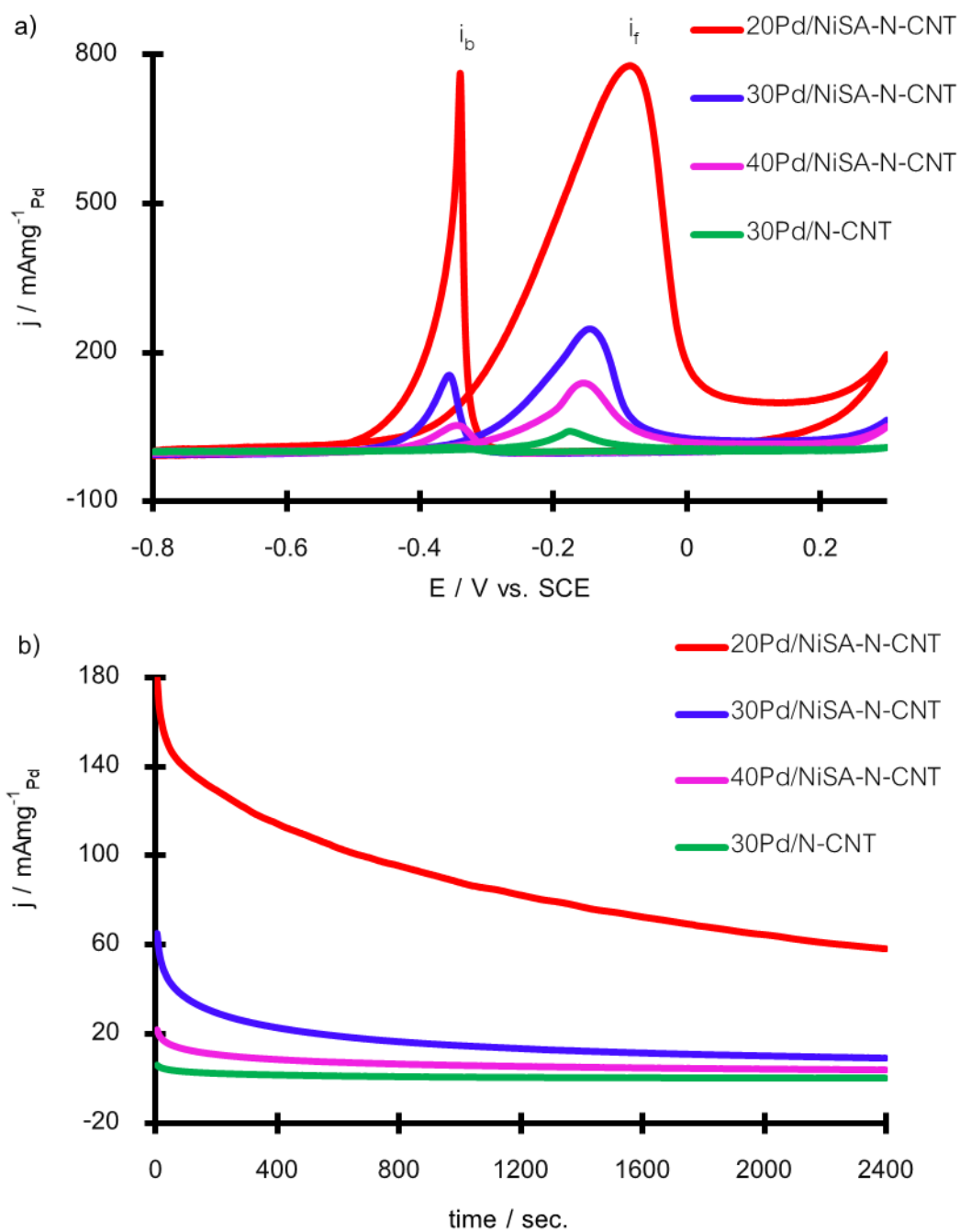
Figure 4.26 Electrooxidation activity toward glycerol (a) of various Pd loading decorated on Ni-SA-CNT and CA profile (b) at -0.3 V. vs SCE. in N_2-riched with 1M KOH + 1M glycerol.

Table 4.6 Alcohol electrooxidation property of Pd NPs supported on NiSA-N-CNT.

Electrocatalysts	Methanol		Ethanol		Glycerol	
	E_s (V)	i_f (mAmg^{-1}$_{Pd}$)	E_s (V)	i_f (mAmg^{-1}$_{Pd}$)	E_s (V)	i_f (mAmg^{-1}$_{Pd}$)
20Pd/NiSA-N-CNT	-0.47	355.91	-0.74	1,199.76	-0.35	777.79
30Pd/NiSA-N-CNT	-0.45	123.23	-0.73	753.63	-0.31	246.46
40Pd/NiSA-N-CNT	-0.43	72.35	-0.53	85.87	-0.27	137.43
30Pd/N-CNT	-0.40	35.84	-0.52	22.53	-0.26	50.14

4.3 EOR MECHANISM OF AS-PREPARED PALLADIUM CATALYST

Theoretically of ethanol electrooxidation mechanism, dual-pathway is always well-known for express phenomena on Pd surfaces, which are involved with and without C-C breaking in ethanol molecule. In case of Pd, the ethanol oxidation mechanism are followed by equation (4.1) to (4.5) [14, 61]

$$Pd + OH^- \leftrightarrow Pd - (OH)_{ads} + e^- \tag{4.1}$$

$$Pd + C_2H_5OH \leftrightarrow Pd - C_2H_5OH_{ads} \tag{4.2}$$

$$Pd - C_2H_5OH_{ads} + 3OH^- \rightarrow Pd - (C_2H_3O)_{ads} + 3H_2O + 3e^- \tag{4.3}$$

$$Pd - (C_2H_3O)_{ads} + Pd - (OH)_{ads} \xrightarrow{r.d.s.} Pd - (CH_3COOH)_{ads} + Pd \tag{4.4}$$

$$Pd - (CH_3COOH)_{ads} + OH^- \xrightarrow{fast} Pd + CH_3COO^- + H_2O \tag{4.5}$$
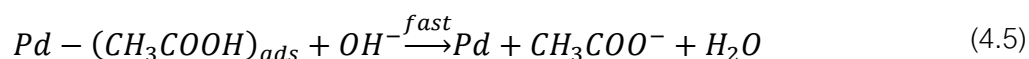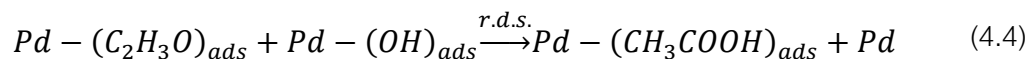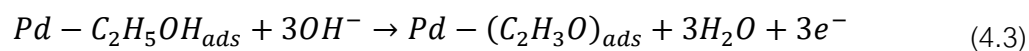
The reaction (4.4) is a slowest step as well as the reaction (4.5) is very fast. In reaction (4), ethoxy species is strongly adsorbed on Pd surfaces. Accordingly, the criteria

of design electrocatalyst in order to improving electrooxidation activity toward ethanol should be promoted oxidation of ethoxy species. So as to analyze the final product for EOR mechanism, as-prepared catalyst; which provided the best activity with each series, were conducted with 1M KOH + 1M potassium acetate and 1 M acetaldehyde, represented in Figure 4.27 and 4.28, respectively. From CV profile of potassium acetate from Figure 4.27, the peak settled around -0.8 to -0.5 V. vs SCE corresponded to adsorbed and desorbed of hydrogen. For shoulder peak located approximately -0.1 to 0.2 V. vs. SCE in anodic scan may be attributed to either oxide layer or adsorbed OH⁻ on Pd surfaces. Meanwhile, the palladium (II) oxide (Pd-O) was wildly accepted in a range of -0.6 to -0.2 V. vs. SCE in cathodic direction. According to Liang et al [14], they proposed that ethoxy species was be spitted to obtain acetate for the major product. In this work, CV profile of potassium acetate (Figure 4.27) reveal that no any oxidation peak peaks, both forward and backward, indicated that the acetate species is the final product.

Additionally, the electrooxidation of acetaldehyde was observed from Figure 4.28. From this CV profile displayed that acetaldehyde specie is still active intermediate which observed from forward and backward oxidation peak. In this case, the first oxidation peak initially oxidized around -0.2 V. vs. SCE, likely due to carbonaceous electrooxidation; herein, attributed to acetaldehyde electrooxidation. Meanwhile, the tiny backward oxidation peal can be detected in a range of -0.4 V. to -0.2 V. vs SCE for all of catalysts except Pd supported on NiSA-CNT and PWA-PEI-CNT. Consistency with the CO stripping in alkaline media from [62, 63], they found that the CO oxidation peak can be observed in the range of -0.1 V. to 0.3 V. vs Hg/HgO. Nevertheless, this experimental result was observed the tiny reverse oxidation peak that settled around -0.4 to -0.2 V. vs. SCE, most likely ascribed to the oxidation of intermediate products from non-complete acetaldehyde electrooxidation. Notwithstanding, the CV for 30Pd/PWA-PEI-CNT and 20Pd/NiSA-N-CNT was not shown oxidation cathodic (backward) peak where located around -0.4 to -0.2 V vs SCE compared with the other catalyst. The peak located at those potential range

probably ascribed to Pd-O. Besides, the CV of those catalysts are similarly with CO stripping voltammetry of Pd in acid media, as reported by [64, 65]. From this results maybe indicated that the Pd NPs supported on both NiSA-N-CNT and PWA-PEI-CNT can be promoted the C-C cleavage of EOR. Unfortunately, it is very difficult to obtain exactly species from electrochemical technique without mass spectroscopy technique, e.g. FTIR, GC-MS, etc., for confirm C_1-session. Normally, C-C cleavage of ethanol molecules on Pd surface is rather difficult than Pt [66-68]. Consequently, it cannot be confirmed that both 20Pd/NiSA-N-CNT and 30Pd/PWA-PEI-CNT can be promoted C_1-session for EOR mechanism.
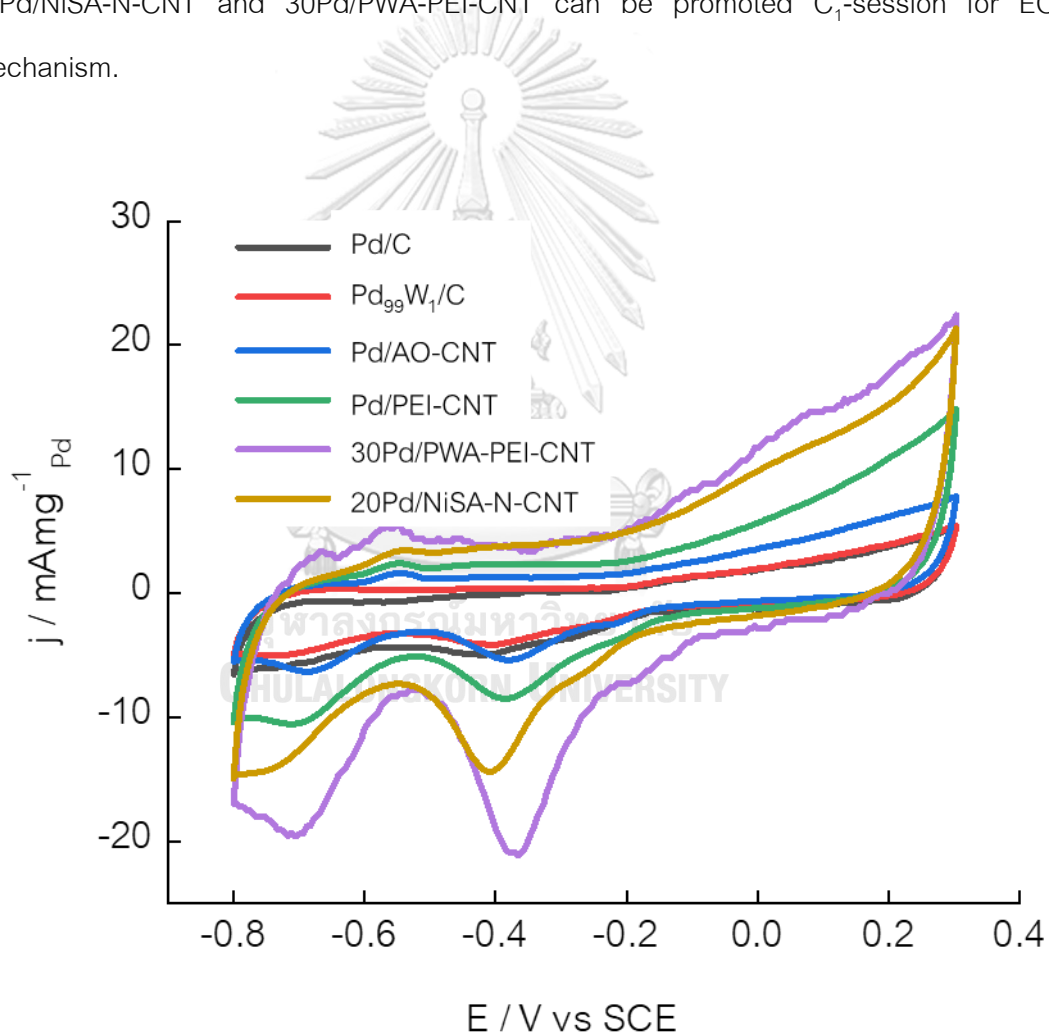
Figure 4.27 Cyclic voltammetry of Pd Nps supported on different types carbon in a mixture of 1 M KOH + 1 M potassium acetate with 50 mVsec^{-1} for scanning rate.
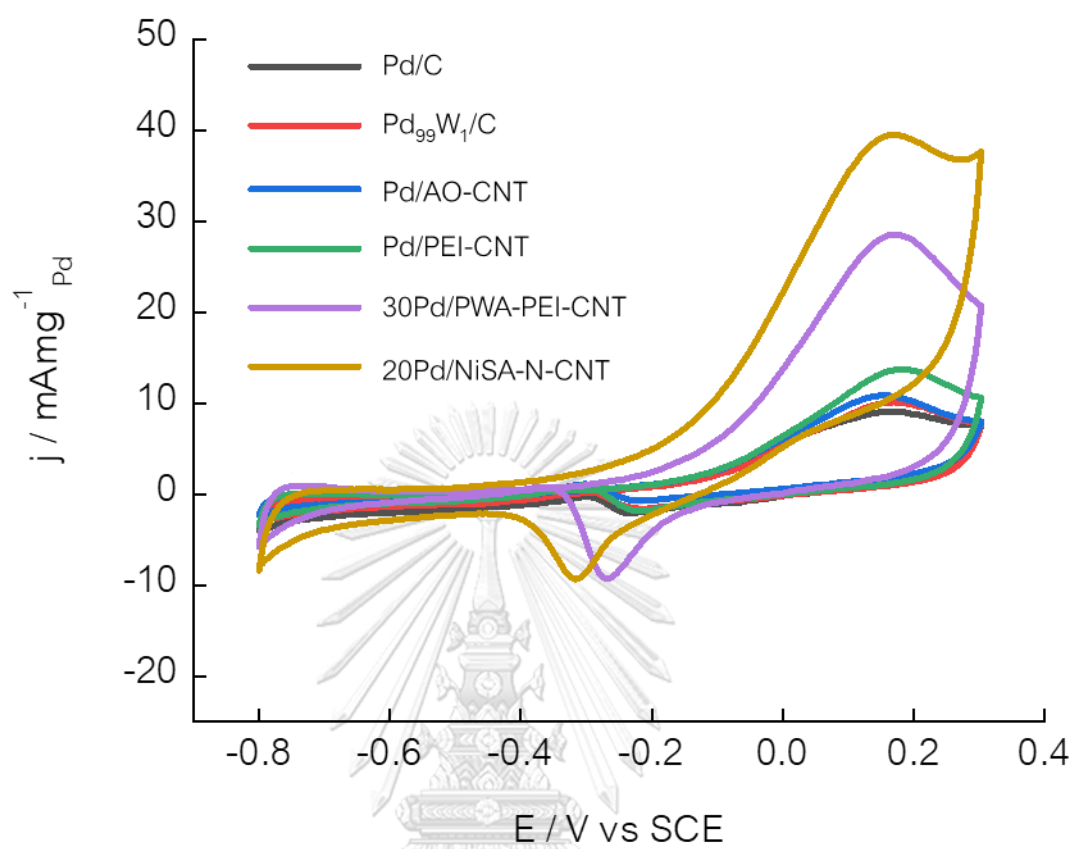
Figure 4.28 Cyclic voltammetry of as-prepared in a mixture of 1M KOH + 0.25 Acetaldehyde with 50 mVsec^{-1} for sweeping rate.

CHAPTER V

CONCLUSION AND RECCOMMENDATIONS

5.1 CONCLUSIONS

5.1.1 THE EFFECT OF SECONDARY METAL ON ELECTROOXIDATION TOWARD ALCOHOLS

In the case of first objectively, the effect of alloying Au, Ru and W on the electrocatalytic activity of Pd for electrooxidation reactions of methanol, ethanol and glycerol in 1M KOH solution was studied. The addition of Au, Ru and W substantially increases the electrocatalytic activity and stability of Pd but behaves differently in different alcohols. In case of methanol and ethanol, $Pd_{99}W_1/C$ exhibits a significantly higher activity than other catalyst. On the other hand, $Pd_{99}Au_1/C$ shows the best activity and stability for GOR.

5.1.2 THE EFFECT OF SUPPORTING MATERIAL AND FUNCTIONALIZATION METHOD ON AOR PERFORMANCE.

Firstly, oxidation functionalization and non-covalent functionalization with PEI of CNT was investigated for EOR. It obvious that the EOR activity and stability of PEI-CNT provided a better performance compared with AO-CNT. In the case of self-assembly with PWA, the MOR, EOR, and GOR performance was significantly increased with respect to AO-CNT, expressed by electrochemical properties, forward anodic mass activity (i_f), onset potential (E_s), and current density after polarization time from chronoamperometry profile. The optimized Pd NPs loading for alcohol oxidation was 30Pd.

5.1.3 THE EFFECT OF NEW-CLASS TYPE OF SUPPORTING MATERIAL USING NISA-N-CNT FOR PALLADIUM NANOPARTICLES.

In this section, the authors developed a NiSA-N-CNT with Ni single atom homogeneously anchored on the CNT. Decoratived Pd nanoparticles onto NiSA-N-CNT could leads to a significant enhancement of the activity for methanol, ethanol and glycerol oxidations. The 20Pd/NiSA-CNT shows optimized activities with the mass current density

several times high than Pd/N-CNTs. The 20Pd/NiSA-CNT also shows significantly enhance stability due to the enhanced activity for the oxidation of the carbonaceous intermediates that produced during the electrochemical oxidation of methanol, ethanol and glycerol. The NiSA-CNT could draw the electrons from the Pd nanoparticles, leads to the formation of Pd oxides which facilitate the oxidation of the carbonaceous intermediates. Our results provide a new type of supported to develop efficient catalysts.

5.1.4 INVESTIGATION ETHANOL ELECTROOXIDATION REACTION (EOR) MECHANISM USING ELECTROCHEMICAL CHARACTERIZATION

The EOR mechanism was carried out by cyclic voltammetry technique in a mixture of 1M KOH + 0.25 M acetaldehyde and 1M KOH + 1M potassium acetate. For analyzing final product, it was observed that no any peaks of electrooxidation toward potassium acetate, thus the terminal intermediate product should be acetate species. Meanwhile, the acetaldehyde was used as fuel for EOR mechanism testing. According to their CV profile, the oxidation peaks of acetaldehyde were found, indicated that acetaldehyde was an active product. Among of this section, the EOR mechanism should be involved C_1-session mechanism.

5.2 RECCOMMENDATIONS

Further research on Pd electrocatalyst for ethanol electrooxidation should be concerned with following aspects:

1. In the case of secondary metal, it was clear that tungsten provided a significant result for EOR and MOR activity and stability in alkaline media. Consequently, the atomic ratio should be optimized for further study.

2. For non-covalent functionalization with PEI, Pd NPs supported on this material illustrated a high activity and stability over AO-CNT. The alloy Pd with other metal would be considered for further research.

3. It was worth noting that the new-class supporting material; NiSA-N-CNT, was provided a better activity and stability. However, adding of secondary material for enhance AOR performance should be develop. Therefore, the further study on this material should be focused on alloy form or deal with the shape of Pd.

REFERENCES

1. Laramie, J. and A. Dicks, *Fuel cell systems explained.* John Wiley and Sons, New York, 2003.

2. Hoogers, G., *Fuel cell technology handbook*. 2002: CRC press.

3. Handbook, F.C., *EG&G Technical Services, Inc. Under Contract No.* DEAM26-99FT40575, US Department of Energy, Office of Fossil Energy, National Energy Technology Laboratory, Morgantown, West Virginia, USA, 2004.

4. Revankar, S.T. and P. Majumdar, *Fuel cells: principles, design, and analysis*. 2014: CRC press.

5. Zhang, J., J. Wu, and H. Zhang, *PEM fuel cell testing and diagnosis*. 2013: Newnes.

6. An, L. and T. Zhao, *Anion Exchange Membrane Fuel Cells: Principles, Materials and Systems*. Vol. 63. 2018: Springer.

7. Lu, M., et al., *Materials for Low-Temperature Fuel Cells*, ed. G.Q.M. Lu. 2014: John Wiley & Sons.

8. Mukherjee, A. and S. Basu, *Anode Catalyst for Direct Hydrocarbon Alkaline Fuel Cell*, in *Anion Exchange Membrane Fuel Cells*. 2018, Springer. p. 105-140.

9. Zhang, J., *PEM fuel cell electrocatalysts and catalyst layers: fundamentals and applications*. 2008: Springer Science & Business Media.

10. Maiyalagan, T. and V.S. Saji, *Electrocatalysts for Low Temperature Fuel Cells: Fundamentals and Recent Trends*. 2017: John Wiley & Sons.

11. Teng, X., *Anodic catalyst design for the ethanol oxidation fuel cell reactions.* Materials and Processes for Energy: Communicating Current Research and Technological Developments, Formatex Research Center, 2013: p. 473-484.

12. Jacob, T. and C. Lamy, *Catalysts for alcohol-fuelled direct oxidation fuel cells*. 2012: Royal Society of Chemistry.

13. Shao, M., *Electrocatalysis in fuel cells: a non-and low-platinum approach*. Vol. 9. 2013: Springer Science & Business Media.

14. Liang, Z.X., et al., *Mechanism study of the ethanol oxidation reaction on palladium in alkaline media.* Electrochimica Acta, 2009. **54**(8): p. 2203-2208.

15. Wang, Y., S. Zou, and W.-B. Cai, *Recent Advances on Electro-Oxidation of Ethanol on Pt- and Pd-Based Catalysts: From Reaction Mechanisms to Catalytic Materials.* Catalysts, 2015. **5**(3): p. 1507-1534.

16. Pereira, L.G.S., V.A. Paganin, and E.A. Ticianelli, *Investigation of the CO tolerance mechanism at several Pt-based bimetallic anode electrocatalysts in a PEM fuel cell.* Electrochimica Acta, 2009. **54**(7): p. 1992-1998.

17. Hajbolouri, F., et al., *CO Tolerance of Commercial Pt and PtRu Gas Diffusion Electrodes in Polymer Electrolyte Fuel Cells.* Fuel Cells, 2004. **4**(3): p. 160-168.

18. Simões, F.C., et al., *Electroactivity of tin modified platinum electrodes for ethanol electrooxidation.* Journal of Power Sources, 2007. **167**(1): p. 1-10.

19. Wang, Y., *Nanomaterials for Direct Alcohol Fuel Cell*. 2015: Pan Stanford.

20. Das, D. and H. Rahaman, *Carbon nanotube and graphene nanoribbon interconnects*. 2014: Crc Press.

21. Hashim, A.A., *The delivery of nanoparticles*. 2012: InTech.

22. Li, H., et al., *Carbon-supported metal single atom catalysts.* New Carbon Materials, 2018. **33**(1): p. 1-11.

23. Yang, X.-F., et al., *Single-atom catalysts: a new frontier in heterogeneous catalysis.* Accounts of chemical research, 2013. **46**(8): p. 1740-1748.

24. Liu, J., *Catalysis by supported single metal atoms.* Acs Catalysis, 2016. **7**(1): p. 34-59.

25. C. Lamy, E.M.B., J-M. Léger, *Electrocatalytic oxidation of aliphatic alcohols: Application to the direct alcohol fuel cell (DAFC).* Journal of Applied Electrochemistry, 2001. **31**(7): p. 799-809.

26. D'Urso, C.B., A.; Triaca, W. E.; Luna, A. M. Castro; Baglio, V.; Aricò, A. S., *Synthesis, Characterization and Electrocatalytic Activity of Bi and Tri-metallic Pt-Based Anode Catalysts for Direct Ethanol Fuel Cells.* International Journal of Electrochemical Science, 2012. **7**(10): p. 9909 - 9919.

27.   de Souza, E.A., et al., *Ethanol electro-oxidation on partially alloyed Pt-Sn-Rh/C catalysts.* Electrochimica Acta, 2014. **147**: p. 483-489.

28.   Yang, C., et al., *Preparation and characterization of multi-walled carbon nanotube (MWCNTs)-supported Pt-Ru catalyst for methanol electrooxidation.* Journal of Alloys and Compounds, 2008. **448**(1-2): p. 109-115.

29.   Cheng, Y., et al., *Effect of nitrogen-containing functionalization on the electrocatalytic activity of PtRu nanoparticles supported on carbon nanotubes for direct methanol fuel cells.* Applied Catalysis B: Environmental, 2014. **158-159**: p. 140-149.

30.   Cheng, Y. and S.P. Jiang, *Highly effective and CO-tolerant PtRu electrocatalysts supported on poly(ethyleneimine) functionalized carbon nanotubes for direct methanol fuel cells.* Electrochimica Acta, 2013. **99**: p. 124-132.

31.   Dong, L., et al., *Graphene-supported platinum and platinum–ruthenium nanoparticles with high electrocatalytic activity for methanol and ethanol oxidation.* Carbon, 2010. **48**(3): p. 781-787.

32.   F. Ye, X.C., L. Yu, S. Chen, W. Lin, *Synthesis and catalytic performance of PtRuMo nanoparticles supported on graphene-carbon nanotubes nanocomposites for methanol electro-oxidation.* Journal of Electrochemical Science, 2012.

33.   Ma, L., D. Chu, and R. Chen, *Comparison of ethanol electro-oxidation on Pt/C and Pd/C catalysts in alkaline media.* International Journal of Hydrogen Energy, 2012. **37**(15): p. 11185-11194.

34.   Xu, J.B., et al., *Stabilization of the palladium electrocatalyst with alloyed gold for ethanol oxidation.* International Journal of Hydrogen Energy, 2010. **35**(13): p. 6490-6500.

35.   Ma, L., et al., *PdRu/C catalysts for ethanol oxidation in anion-exchange membrane direct ethanol fuel cells.* Journal of Power Sources, 2013. **241**: p. 696-702.

36.   Monyoncho, E.A., et al., *Synergetic effect of palladium–ruthenium nanostructures for ethanol electrooxidation in alkaline media.* Journal of Power Sources, 2015. **287**: p. 139-149.

37. Shen, S.Y., et al., *Synthesis of PdNi catalysts for the oxidation of ethanol in alkaline direct ethanol fuel cells.* Journal of Power Sources, 2010. **195**(4): p. 1001-1006.

38. Maiyalagan, T. and K. Scott, *Performance of carbon nanofiber supported Pd–Ni catalysts for electro-oxidation of ethanol in alkaline medium.* Journal of Power Sources, 2010. **195**(16): p. 5246-5251.

39. Wang, Y., et al., *Novel palladium–lead (Pd–Pb/C) bimetallic catalysts for electrooxidation of ethanol in alkaline media.* Journal of Power Sources, 2010. **195**(9): p. 2619-2622.

40. Singh, R.N., A. Singh, and Anindita, *Electrocatalytic activity of binary and ternary composite films of Pd, MWCNT, and Ni for ethanol electro-oxidation in alkaline solutions.* Carbon, 2009. **47**(1): p. 271-278.

41. Geraldes, A.N., et al., *Palladium and palladium–tin supported on multi wall carbon nanotubes or carbon for alkaline direct ethanol fuel cell.* Journal of Power Sources, 2015. **275**: p. 189-199.

42. Dong, Q., et al., *Pd/Cu bimetallic nanoparticles supported on graphene nanosheets: Facile synthesis and application as novel electrocatalyst for ethanol oxidation in alkaline media.* International Journal of Hydrogen Energy, 2014. **39**(27): p. 14669-14679.

43. Jiang, T., et al., *Glucose electrooxidation in alkaline medium: Performance enhancement of PdAu/C synthesized by NH 3 modified pulse microwave assisted polyol method.* Applied Catalysis B: Environmental, 2015. **162**: p. 275-281.

44. Moraes, L.P.R., et al., *Synthesis and performance of palladium-based electrocatalysts in alkaline direct ethanol fuel cell.* International Journal of Hydrogen Energy, 2016. **41**(15): p. 6457-6468.

45. Sun, D., et al., *Monodisperse AgPd alloy nanoparticles as a highly active catalyst towards the methanolysis of ammonia borane for hydrogen generation.* RSC Advances, 2016. **6**(107): p. 105940-105947.

46.   Wu, D., K. Kusada, and H. Kitagawa, *Recent progress in the structure control of Pd-Ru bimetallic nanomaterials.* Sci Technol Adv Mater, 2016. **17**(1): p. 583-596.

47.   Wang, D., et al., *Electrooxidation of methanol, ethanol and 1-propanol on pd electrode in alkaline Medium.* Int. J. Electrochem. Sci, 2009. **4**: p. 1672-1678.

48.   Holton, O.T. and J.W. Stevenson, *The Role of Platinum in Proton Exchange Membrane Fuel Cells.* Platinum Metals Review, 2013. **57**(4): p. 259-271.

49.   He, Q., et al., *Carbon-supported PdM (M=Au and Sn) nanocatalysts for the electrooxidation of ethanol in high pH media.* Journal of Power Sources, 2009. **187**(2): p. 298-304.

50.   Jha, N., et al., *Pt–Ru/multi-walled carbon nanotubes as electrocatalysts for direct methanol fuel cell.* International Journal of Hydrogen Energy, 2008. **33**(1): p. 427-433.

51.   Guo, J.W., et al., *Preparation and characterization of a PtRu/C nanocatalyst for direct methanol fuel cells.* Electrochimica Acta, 2005. **51**(4): p. 754-763.

52.   Choi, J.-H., et al., *Methanol electro-oxidation and direct methanol fuel cell using Pt/Rh and Pt/Ru/Rh alloy catalysts.* Electrochimica Acta, 2004. **50**(2-3): p. 787-790.

53.   Liu, Q., et al., *Preparation and Electrocatalytic Characteristics of PdW/C Catalyst for Ethanol Oxidation.* Catalysts, 2015. **5**(3): p. 1068-1078.

54.   Zhang, Z., L. Xin, and W. Li, *Supported gold nanoparticles as anode catalyst for anion-exchange membrane-direct glycerol fuel cell (AEM-DGFC).* International Journal of Hydrogen Energy, 2012. **37**(11): p. 9393-9401.

55.   Yuan, W., et al., *Pt-based nanoparticles on non-covalent functionalized carbon nanotubes as effective electrocatalysts for proton exchange membrane fuel cells.* RSC Adv., 2014. **4**(86): p. 46265-46284.

56.   Wang, D., et al., *Enhanced oxygen reduction at Pd catalytic nanoparticles dispersed onto heteropolytungstate-assembled poly (diallyldimethylammonium)-functionalized carbon nanotubes.* Physical Chemistry Chemical Physics, 2011. **13**(10): p. 4400-4410.

57. Kim, H.-J., Y.-G. Shul, and H. Han, *Synthesis of heteropolyacid (H3PW12O40)/SiO2 nanoparticles and their catalytic properties.* Applied catalysis A: general, 2006. **299**: p. 46-51.

58. Vu, T.H.T., et al., *Esterification of 2-keto-L-gulonic acid catalyzed by a solid heteropoly acid.* Catalysis Science & Technology, 2013. **3**(3): p. 699-705.

59. Cheng, Y., et al., *Atomically Dispersed Transition Metals on Carbon Nanotubes with Ultrahigh Loading for Selective Electrochemical Carbon Dioxide Reduction.* Adv Mater, 2018. **30**(13): p. e1706287.

60. Chen, L., A. Yelon, and E. Sacher, *X-ray Photoelectron Spectroscopic Studies of Pd Nanoparticles Deposited onto Highly Oriented Pyrolytic Graphite: Interfacial Interaction, Spectral Asymmetry, and Size Determination.* The Journal of Physical Chemistry C, 2011. **115**(16): p. 7896-7905.

61. Mahapatra, S.S., A. Dutta, and J. Datta, *Temperature effect on the electrode kinetics of ethanol oxidation on Pd modified Pt electrodes and the estimation of intermediates formed in alkali medium.* Electrochimica Acta, 2010. **55**(28): p. 9097-9104.

62. Wei, Y., et al., *Nitrogen-Doped Carbon Nanotube-Supported Pd Catalyst for Improved Electrocatalytic Performance toward Ethanol Electrooxidation.* Nanomicro Lett, 2017. **9**(3): p. 28.

63. Chen, L., et al., *Improved ethanol electrooxidation performance by shortening Pd-Ni active site distance in Pd-Ni-P nanocatalysts.* Nat Commun, 2017. **8**: p. 14136.

64. Vafaei, M., et al., *Facile synthesis of a highly active Pd/Co bimetallic nanocatalyst on carbon fiber cloth via a two-step electrodeposition for formic acid electrooxidation.* Journal of Solid State Electrochemistry, 2015. **19**(1): p. 289-298.

65. Wang, R., et al., *Effect of the structure of Ni nanoparticles on the electrocatalytic activity of Ni@ Pd/C for formic acid oxidation.* International journal of hydrogen energy, 2013. **38**(29): p. 13125-13131.

66. Shen, P.K. and C. Xu, *Alcohol oxidation on nanocrystalline oxide Pd/C promoted electrocatalysts.* Electrochemistry Communications, 2006. **8**(1): p. 184-188.

67.   Xu, C., et al., *Methanol and ethanol electrooxidation on Pt and Pd supported on carbon microspheres in alkaline media.* Electrochemistry Communications, 2007. **9**(5): p. 997-1001.

68.   Bambagioni, V., et al., *Pd and Pt–Ru anode electrocatalysts supported on multi-walled carbon nanotubes and their use in passive and active direct alcohol fuel cells with an anion-exchange membrane (alcohol=methanol, ethanol, glycerol).* Journal of Power Sources, 2009. **190**(2): p. 241-251.

จุฬาลงกรณ์มหาวิทยาลัย
CHULALONGKORN UNIVERSITY

VITA

NAME   Thantakorn Nitayua

DATE OF BIRTH   20 October 1986

PLACE OF BIRTH   Bangkok

INSTITUTIONS ATTENDED

HOME ADDRESS   49/1, Village No.3, Bang Phli Yai Sub-distinct, Bang Phli
                        Distinct, Samut Prakarn Province, 10540

PUBLICATION   Unusual synergetic effect of nickel single atoms on the
                        electrocatalytic activity of palladium for alcohol oxidation
                        reactions in alkaline media